e - ISSN 2586-9396

Current Applied Science and Technology

Vol. 19 No. 2

May - August 2019

KING MONGKUT'S INSTITUTE OF TECHNOLOGY LADKRABANG

Advisory Board

Current Applied Science and Technology or CAST, formerly KMITL Science and Technology Journal, has been established since its inception as KMITL Science Journal published by King Mongkut's Institute of Technology Ladkrabang (KMITL) in 2001. The journal has been dedicated to publishing advanced and applied knowledge in the form of high-quality research and review articles covering the main areas of Biotechnology, Environmental Science, Agricultural Technology, and other fields related to Applied Science and Technology. Special issues devoted to important topics in advanced science and technology will occasionally be published.

The journal is an open access peer-reviewed and double blinded journal using Online Journal System (OJS) publishing online academic research and review articles. Previously, articles were published in print on a regular basis (two issues per year) since 2001 and since 2010 onward the articles have been published both in print and electronic forms starting from volume 10. In 2017, the journal title has been changed from *KMITL Science and Technology Journal* to *Current Applied Science and Technology* (CAST) (e-ISSN 2586-9396) to be more identifiable to the international scientific community according to the suggestion of Thai-Journal Citation Index Centre. The journal has been published online only since volume 17(2) (July-December, 2017). In addition, the journal has attracted researchers from other countries more than 22% according to the data. Because of more demands on publication in CAST, the editorial board has decided to publish online original academic research and review articles three issues per year (April, August and December) from 2018 onward.

Furthermore, the advisory board and editorial board comprises honorable and well-known members from around the world in which 50% of editorial board members are from various countries like U.K., Norway, Japan, India, China, Singapore and Egypt. Only 25% of Thai editorial board members are from the publisher organization and 25% from other publisher organizations. Most of advisory and editorial board members have high H-index according to SCOPUS.

The journal is also committed to maintaining the high level of integrity in the content published and has a Conflict of Interest policy in place. The journal uses plagiarism detection software to screen the submissions. The journal has been working closely with Thai-Journal Citation Index Centre to ensure that the journal complies with international standard of SCOPUS.

Current Applied Science and Technology (CAST)

(formerly KMITL Science and Technology Journal)

Editor

Dusanee Thanaboripat
King Mongkut's Institute of Technology Ladkrabang, Thailand

Editorial Board

CONTENTS

Diversity and Plant Growth Promoting Activities of Rice Epiphytic Bacteria

Suchitra Aphimeteetamrong and Chokchai Kittiwongwattana*

Department of Biology, Faculty of Science, King Mongkut's Institute of Technology Ladkrabang, Bangkok, Thailand

Received: 19 November 2018, Revised: 20 February 2019, Accepted: 13 March 2019

Abstract

Plant-associated bacteria have been known for their direct and indirect abilities to promote plant growth. Because of their benefits on plants, they are generally recognized as plant growth promoting bacteria (PGPB). In the present study, epiphytic bacteria were isolated from surfaces of roots, stems and leaves of rice plants that were grown in organic farms. Of 113 bacterial isolates, 68 and 45 isolates were stained Gram-positive and Gram-negative, respectively. Based on their cell shapes, 106 isolates were bacilli while seven isolates were cocci. The use of the 16S rRNA gene sequence analysis indicated that they were members of phyla *Fimicutes* (54.87%), *Proteobacteria* (38.05%) and *Bacteroidetes* (7.08%). All isolates were assessed for their abilities in nitrogen fixation, phosphate solubilization, siderophore production, auxin production and 1-aminocyclopropane-1-caboxylic acid (ACC) deaminase activity. The result showed that 91 isolates were tested positives for at least one activity. The antagonistic activity against the pathogenic fungus *Pyricularia oryzae* was also tested. Twenty-three isolates inhibited the growth of the fungal mycelia. The percentage of growth inhibition of these isolates against *P. oryzae* ranged from 73.10±3.24% to 100.00±0.00%. The protease and chitinase activities were found in 19 and 2 isolates, respectively. However, crude preparation of bioactive compounds from bacterial cultures yielded negative results. Based on the results obtained in this study, the surfaces of rice plants were colonized by various bacteria with potentials in plant growth promotion.

Keywords: epiphytic bacteria, plant growth promoting bacteria, *Pyricularia oryzae*, rice
DOI 10.14456/cast.2019.7

1. Introduction

Diverse groups of bacteria were found associated with plants. They may colonize either plant rhizosphere as rhizobacteria, outer surfaces of plant organs as epiphytic bacteria or plant intercellular spaces as endophytic bacteria. A number of these bacteria were found to provide various direct benefits for plant growth as well as indirectly protect plants from phytopathogens. They are recognized as plant growth promoting bacteria (PGPB). Much research effort has been dedicated to study these bacteria for their application in agriculture in order to decrease our dependence on excessive use of chemicals that has led to the contamination of toxic compounds in environments [1].

*Corresponding author. Tel.: +662-327-8400 Fax: +662-329-8412
E-mail: chokchai.ki@kmitl.ac.th

One of the direct mechanisms by PGPB is the increase of bioavailability of plant nutrients. Nitrogen is the most important nutrient for plant growth. However, it is mostly found as the diatomic gas that is not readily available for plants. It has to be converted into ammonia by either physical or biological nitrogen fixation. Several nitrogen- fixing bacteria in various genera including *Azosprillum*, *Herbasipirillum*, *Bacillus*, *Burkholderia* and *Pseudomonas* were found to provide fixed nitrogen to their plant hosts [2]. Phosphorus is considered the second- most important macronutrient for plants. However, a large amount of phosphorus is fixed or trapped in organic and inorganic compounds [3]. Phosphate- solubilizing bacteria are able to release phosphorus from its insoluble forms for plant absorption and utilization during growth and development. PGPB of genera *Bacillus*, *Pseudomonas* and *Burkholderia* are examples of phosphate- solubilizing bacteria [4]. Iron is one of the macronutrients required for plant growth. However, it is generally found as insoluble ferric (Fe^{3+}) hydroxides. This limits the uptake of iron by plants. Many PGPB were able to increase the availability of iron by secreting iron-chelating siderophores. Subsequently, the iron-bound form of siderophores is imported into the plant cells [5]. Members of the genus *Pseudomonas* were well known for their siderophore production [6]. Modulation of phytohormones is another direct mechanism found in PGPB. Auxin is an important hormone that regulates virtually all aspects of plant growth and development. The most common form of auxin in plants is Indole-3-acetic acid (IAA) that is also produced by many bacteria [7]. Examples of IAA- producing PGPB are *Azospirillum brasilense*, *Pseudomonas putida* and *Pantoea agglomerans* [8]. Ethylene is a phytohormone that is required for plant stress responses. The precursor of ethylene biosynthesis is 1-aminocyclopropane-1-carboxylic acid (ACC) that is converted into ethylene by the activity of the ACC synthase enzyme [9]. However, overproduction of ethylene induced by stress conditions could lead to growth reduction and senescence [10]. Previous studies showed that a number of PGPB were able to lower the ethylene level by producing ACC deaminase that converts ACC into α-ketobutyrate and ammonia. This resulted in the decrease of the ethylene levels and the increase of stress tolerance in plant hosts [11-13]. PGPB may indirectly confer disease resistance on the plant host through their antagonistic activities against phytopathogenic fungi. These activities may be derived from their ability to produce hydrolytic enzymes that disrupt cell wall components of the pathogens. Protease and chitinase degrade proteins and chitin that are components of the fungal cell wall [14]. Alternatively, many PGPB were shown to produce antifungal compounds that inhibited growth of the pathogens. Members of genera *Bacillus* and *Pseudomonas* were prominent PGPB in this regard because of their ability to synthesize various groups of antibiotics including ribosomal and non-ribosomal peptides and polyketides [5].

The aim of the present study was to investigate diversity and plant growth promoting activities of epiphytic bacteria of rice plants grown in organic farms that did not permit the use of chemical fertilizers and pesticides. We isolated epiphytic bacteria from the surfaces of roots, stems and leaves of rice plants collected from Bangkok, Chonburi, Saraburi and Suphanburi provinces, Thailand. Characterization of culturable isolates was determined based on their morphological characteristics and 16S rRNA gene sequences. Both direct and indirect plant growth promoting activities were examined. The result provided basic information of potential epiphytic PGPB for further *in planta* analysis and their application as biofertilizers and biocontrol agents.

2. Materials and Methods

2.1 Rice samples and isolation of epiphytic bacteria

Whole rice plants grown in organic farms were collected from Bangkok (13°52'56. 8" N 100°53'05.1"E), Chonburi (13°12'37.9"N 101°26'20.8"E), Saraburi (14°21'14.7"N 100°54'20.1"E)

and Suphanburi (14°32'35. 2" N 100°03'25. 6" E) provinces, Thailand. Samples from Bangkok location was of Hom-Nil variety while those from other locations were of Rice-Berry variety. Roots, stems and leaves were rinsed under running water and cut into small pieces.

2.2 Isolation of epiphytic bacteria

Samples were separately put in glass bottles containing 100 ml of sterilized distilled water. The bottles were shaken on a rotary shaker at 180 rpm for 30 min. Bacterial cell suspension was serially diluted and plated on nutrient agar (NA; HiMedia, India) plates and tryptone soya agar (TSA; HiMedia, India) plates. All plates were incubated at 30°C. Bacterial colonies were picked once they appeared on the surface of the media. This process was continued for seven days. Bacterial colonies were purified by repeatedly streaking on NA plates.

2.3 Morphological characterization

Pure isolates were examined for morphological characteristics including Gram-staining and cell shapes. The procedure was as follows: bacterial cells were smeared on a glass slide and fixed by passing through flame for a few times, crystal violet was used as the primary stain and removed after 1 min of staining. This was followed by addition of Gram's iodine on the smear for 1 min. The primary stain was removed by 95% ethanol within 20 s. The washing step was stopped by rinsing the slide with water. Safranin was used for staining the smear for 1 min and subsequently removed by rinsing with water. Bacterial cells were observed under a light microscope.

2.4 Identification of bacterial isolates using 16S rRNA gene sequences

Genomic DNA of all isolates was prepared using a commercial kit (Presto^{TM} Mini gDNA Bacteria Kit, Geneaid, Taiwan). Nearly complete 16S rRNA gene fragments were amplified using universal primers 41F (5'-GCTCAGATTGAACGCTGGCG-3') and 1492R (5'- TACGGYTACCTTGTTA CGACTT-3') [15-16]. Amplified products were cleaned using a commercial kit (Gel/PCR Purification Kit, Favorgen Biotech Corp, Taiwan) and sequenced using 41F and 1492R primers. Pairwise alignment of the 16S rRNA gene sequences was performed on the EzBioCloud database [17].

2.5 Plant growth promoting activities

For nitrogen fixation, bacterial cells were washed in glucose-nitrogen-free broth [18] and centrifuged at 5,000 rpm for 15 min with a Minispin microcentrifuge (Eppendorf, Germany). The rotor diameter was 12 cm. The supernatant was discarded, and the same liquid medium was used for cell suspension. Two µl of the suspension were placed on glucose-nitrogen-free agar. Plates were incubated at 30°C for 4 days. The ability to grow on the same solid medium supplemented with 3 mM $(NH_4)_2SO_4$ was used as the indication of a positive result. To determine the phosphate solubilizing activity, bacterial colonies were spotted on Pikovskaya's (PVK) medium and National Botanical Research Institute's phosphate growth medium [19]. Bacteria were grown at 30°C for 4 days and checked for phosphate solubilization on both media. Chrome azurol S (CAS) agar medium [20] was used to examine the production of siderophores. Bacterial colonies were streaked on the medium and grown at 30°C for 48 h.

To determine IAA production, bacterial cells were inoculated in 50 ml of nutrient broth (NB; Himedia, India) containing 1% (w/v) L-tryptophan and grown at 30°C for 48 h on a rotary shaker at 160 rpm. Bacterial cells were separated from the culture by centrifugation at 2,500 rpm

for 5 min with a Minispin microcentrifuge (Eppendorf, Germany). The rotor diameter was 12 cm. One-hundred µl of the supernatant were tested for the presence of IAA by mixing with an equal volume of Salkowski's reagent [21]. For ACC deaminase activity, bacterial cells were washed in 1 ml of Dworkin and Foster (DF) salt minimal broth [22] once by resuspension and centrifugation. Harvested bacterial cells were then resuspended in 1 ml of fresh DF salt minimal broth and 2 µl of the cell suspension were inoculated on DF salt minimal agar supplemented with 2mM ACC as the sole nitrogen source. Bacteria were incubated at 30ºC for 4 days. Negative and positive control groups were bacteria grown on DF salt minimal agar and DF salt minimal agar containing 2 mM $(NH_4)_2SO_4$, respectively.

2.6 Indirect plant growth promoting activities

The antagonistic activity against *P. oryzae* was determined using the dual culture test. Epiphytic bacteria were streaked on potato dextrose agar (PDA; SRL, India). A mycelium plug of *P. oryzae* was placed 2 cm away from the bacteria. Plates were incubated at 30ºC for 14 days. Control plates were prepared by inoculating *P. oryzae* without epiphytic bacteria. The inhibition zone was the indicator of a positive result. To determine the percentage of growth inhibition, the experiment was repeated with all antagonistic isolates. Three replicates were performed for each isolate. Control plates were prepared by placing the mycelium plug on the medium only. The percentage of growth inhibition in each replicate was calculated as shown in below equation.

$$\text{Percentage of growth inhibition} = [(R_c-R_e)/R_c] \times 100$$

R_c is the radius of the fungal colony in control plates. R_e is the radius of the fungal colony in experimental plates. For statistical analysis, one-way ANOVA was performed and followed by the Tukey test. $P<0.05$ was considered statistically significant.

To test for their protease and chitinase activities, epiphytic bacteria were inoculated on skim-milk agar medium and NA medium that was supplemented with 1% colloidal chitin, respectively [23]. All plates were incubated at 30ºC for 48 h.

For extraction of extracellular antifungal compounds, antagonistic isolates were cultured in 50 ml NB at 30ºC for 7 days on a rotary shaker with 160 rpm. Subsequently, cultures were subjected to liquid-liquid extraction using an equal volume of ethyl acetate as the organic solvent. Each culture was extracted three times and the exhausted supernatant was collected. The solvent was evaporated using a rotary evaporator at 40˚C under 240 bars. Remaining crude extracts were washed off the bottle using methanol and left in a desiccator until methanol completely evaporated. The extracts were weighed and resuspended in methanol at 150 mg/µl and 300 mg/µl concentrations. The suspension was placed on sterilized paper discs No. 1 (GE Healthcare, USA). The discs were left to dry and tested for growth inhibition on *P. oryzae* in place of epiphytic bacteria as described in the dual culture test.

3. Results and Discussion

A total number of 113 epiphytic bacterial isolates were obtained from the rice plants. Forty-seven isolates were obtained from root surfaces. Thirty-one and thirty-five isolates were from stem and leaf surfaces, respectively. Gram-staining of these isolates showed that 68 and 45 isolates were Gram-stained positive and Gram-stained negative, respectively. Based on their cell shapes, 106 isolates were bacilli while the remaining seven isolates were cocci.

For molecular characterization, partial 16S rRNA gene sequences of all isolates were amplified and sequenced. The sequences were used for the pairwise alignment analysis on the EzBiocloud database. Details of the result are provided in Table1. The result showed that 34 isolates displayed 100% sequence similarity with the sequences on the database. The sequence similarity of the remaining 79 isolates ranged from 98.50% to 99.99% when compared with the database. Sixty-two isolates (54.87%) of the isolates belonged to the phylum *Firmicutes* and represented the largest group of the population. They were classified into four different genera including *Bacillus* (51 isolates), *Staphylococcus* (6 isolates), *Fictibacillus* (4 isolates) and *Exiguobacterium* (1 isolate). The second-largest group comprised of 43 isolates (38.05%) that were determined as members in the phylum *Proteobacteria*. They were divided into seventeen genera. Seven genera were found with more than one isolates. These included *Pseudomonas* (12 isolates), *Acinetobacter* (6 isolates), *Burkholderia* (4 isolates), *Enterobacter* (4 isolates), *Klebsiella* (3 isolates), *Aeromonas* (2 isolates) and *Chromobacterium* (2 isolates). One isolate was recorded for each of the following genera: *Aquitalea*, *Brevundimonas*, *Citrobacter*, *Kinneretia*, *Pandoraea*, *Rahnella*, *Roseateles*, *Serratia*, *Vogesella* and *Xanthomonas*. The smallest group contained eight isolates (7.08%) and belonged to phylum *Bacteroidetes*. They were divided into three genera including *Chryseobacterium* (4 isolates), *Chitinophaga* (3 isolates) and *Sphingobacterium* (1 isolate). Based on the isolation sources, the bacterial communities were relatively different (Table 1). On root surfaces, members of *Firmicutes* constituted 53.19% of the population. This was followed by *Proteobacteria* (34.04%) and *Bacteroidetes* (12.77%). In contrast, the dominant group (54.84%) on stem surfaces consisted of members in phylum *Proteobacteria* and was followed by *Firmicutes* (38.719%) and *Bacteroidetes* (6.45%). On the other hand, only those of phyla *Firmicutes* (71.43%) and *Proteobacteria* (28.57%) were recovered from leaf surfaces. At the genus level, 18, 12 and 7 different genera were found on roots, stems and leaves, respectively. This result indicated that root-surface colonizing bacteria were likely the most diverse group.

The diversity of culturable bacteria observed in the present study was consistent with previous reports. Members of phyla *Firmicutes*, *Proteobacteria* and *Bacteroidetes* were commonly isolated from rhizosphere, organ surfaces and internal tissues of various plant species. For example, a previous study investigated the diversity of bacteria on grape plants that were grown in two different vineyards. Despite the locations, *Firmicutes* and *Proteobacteria* were two of the three largest groups that colonized berries, leaves and barks of the plants. Another group of isolated bacteria belonged to the phylum *Actinobacteria* [24]. Similarly, our previous study showed that endophytic bacteria isolated from rice plants were members of *Firmicutes*, *Proteobacteria*, *Bacteroidetes* and *Actinobacteria* [25]. The culture-dependent approach had a limitation for the study of bacterial diversity since not all bacteria could grow on synthetic media. It could only reveal small fractions of an actual bacterial population. To overcome this limitation, several studies employed next-generation sequencing technologies and the metagenomic approach to obtain more inclusive information regarding the bacterial diversity. A recent study used Illumina MiSeq sequencing for identifying bacterial operational taxonomic units (OTUs) that were endophytes of rice sprouts, roots and stems. Although members of the common phyla mentioned above still represented the dominant groups, OTUs of other phyla including *Fusobacteria*, *Acidobacteria*, *Deinococcus-Thermus* and *Verrucomicrobia* were also detected. Additionally, the study observed a high level of bacterial diversity at the genus level [26]. In the present study, the level of diversity observed in root-colonizing bacteria was relatively higher than that found in stem- and leaf-colonizing bacteria. Roots and other plant underground organs were well known for their richness in bacterial compositions. An important contributing factor was derived from the secretion of root exudates that provided various types of organic compounds which may act as either nutritional resources that support bacterial growth and signaling molecules for bacterial chemotaxis [2].

All epiphytic bacteria were examined for their direct plant growth promoting activities including nitrogen fixation, phosphate solubilization, siderophore production, IAA production and

ACC deaminase activity. Ninety-one isolates displayed at least one positive activity (Table 2). Forty-nine isolates (43.36%) showed one activity. The second largest group of 33 isolates (29.20%) was tested positive for two activities. Only eight (7.08%) and one (0.88%) isolates displayed three and

Table 1. Characterization of 113 epiphytic bacteria from rice plants based on the analysis of the 16S rRNA gene sequences. Numbers in parentheses indicate the number of isolates that were affiliated with each genus.

Phylum	Genus		
	Roots	Stems	Leaves
Firmicutes	*Bacillus* (20), *Exiguobacterium* (1), *Fictibacillus* (3), *Staphylococcus* (1),	*Bacillus* (10), *Staphylococcus* (2),	*Bacillus* (21), *Fictibacillus* (1), *Staphylococcus* (3)
Proteobacteria	*Acinetobacter* (1), *Aeromonas* (2), *Aquitalea* (1), *Burkholderia* (2), *Enterobacter* (1), *Klebsiella* (1), *Padoraea* (1), *Pseudomonas* (3), *Rahnella* (1), *Serratia* (1), *Vogesella* (1), *Xanthomonas* (1)	*Acinetobacter* (4), *Burkholderia* (2), *Chromobacterium* (2), *Citrobacter* (1), *Enterobacter* (3), *Kinneretia* (1), *Klebsiella* (2), *Pseudomonas* (2)	*Acinetobacter* (1) *Brevundimonas* (1), *Pseudomonas* (7), *Roseateles* (1)
Bacteroidetes	*Chitinophaga* (3), *Chryseobacterium* (3)	*Chryseobacterium* (1), *Sphingobacterium* (1)	–

Table 2. Distribution of plant growth promoting activities among isolated epiphytic bacteria. N: nitrogen fixation, P: phosphate solubilization, S: Siderophore production, I: IAA production, A: ACC deaminase activity.

Activities	Number of isolates
N	17
P	3
S	21
I	4
A	4
N+P	2
N+S	6
N+A	5
N+I	1
P+A	2
S+A	8
I+A	4
I+S	5
N+P+A	1
N+S+I	1
N+S+A	3
P+S+A	1
S+I+A	2
P+S+I+A	1

four activities, respectively. Twenty-two isolates (19.47%) were tested negative for all activities. None of the isolates displayed all five activities.

Details of bacterial groups that displayed the positive activities are provided in Table 3. For nitrogen fixation, 36 positive isolates were able to grow on the glucose-nitrogen-free agar. Members of the phylum *Firmicutes* represented the dominant group (23 isolates) and were classified as *Bacillus*, *Exiguobacterium*, *Fictibacillus* and *Staphylococcus*. The second-largest group was *Proteobacteria* with 11 isolates that belonged to genera *Acinetobacter*, *Aeromonas*, *Brevundimonas*, *Klebsiella*, *Pandoraea* and *Pseudomonas*. Two isolates were affiliated with genera *Chitinophaga* and *Chryseobacterium* of phylum *Bacteroidetes*. For phosphate solubilization, the positive result was determined based on the presence of the clear zone around bacterial colonies on PVK and NBRIP media. Among 113 isolates, we found 9 isolates that displayed the phosphate solubilization activity. They were members of genera *Bacillus*, *Burkholderia*, *Pseudomonas* and *Roseateles*. Forty-nine isolates were able to produce siderophores as indicated by the presence of the orange halo around the colonies that were grown on CAS agar medium. Thirty-one isolates that belonged to the phylum *Firmicutes* were members of genera *Bacillus*, *Exiguobacterium*, *Fictibacillus* and *Staphylococcus*. Fifteen isolates were of the phylum *Proteobacteria*. They included isolates of genera *Acinetobacter*, *Aeromonas*, *Burkholderia*, *Kinneretia*, *Klebsiella*, *Pandoraea*, *Pseudomonas* and *Serratia*. The remaining three isolates were of the phylum *Bacteroidetes*. They were classified as members of genera *Chitinophaga*, *Chryseobacterium* and *Sphingobacterium*.

The results on bacterial activities involved in the increase of plant nutrients were relatively consistent with previous reports. Except for *Fictibacillus*, *Staphylococcus* and *Chitinophaga*, strains of the other nine genera were described for their nitrogen-fixing capability on the basis of either growth on nitrogen-free medium or the ability to reduce ethylene by nitrogenase or the presence of the *nifH* gene which codes for a nitrogenase subunit [27-32]. For phosphate-solubilizing activity, positive genera found in the present study were also previously reported as phosphate solubilizers [31-33]. The only exception was genus *Roseateles*. For siderophore production, other strains of most genera found in the present study were capable of producing siderophores [25, 34-41]. In contrast, up to the date of manuscript preparation, there were no reports of plant-associated bacteria in genera *Fictibacillus*, *Kinneretia* and *Chitinophaga* that displayed siderophore production.

The test for IAA production was performed by mixing culture supernatant with Salkowski's reagent. The pink color is the indicator of the presence of IAA. The positive result was obtained from the supernatant of 19 bacterial isolates. The predominant group consisted of 16 isolates of the phylum *Proteobacteria*. They were classified into genera *Acinetobacter*, *Burkholderia*, *Enterobacter*, *Klebsiella*, *Pandoraea*, *Pseudomonas* and *Rahnella*. Three other isolates were all members of the phylum *Firmicutes* and belonged to genera *Bacillus* and *Staphylococcus*. Determination of ACC deaminase was based on the utilization of ACC as the sole nitrogen source in DF minimal agar. Thirty-one isolates were able to produce ACC deaminase. Among these, seventeen isolates belonged to the phylum *Firmicutes* and were classified as members of genera *Bacillus* and *Exiguobacterium*. Fourteen positive isolates of the phylum *Proteobacteria* consisted of members in genera *Acinetobacter*, *Burkholderia*, *Enterobacter*, *Pseudomonas*, *Roseateles* and *Serratia*. Other bacterial strains in the corresponding genera previously demonstrated for IAA production [25, 33, 37, 42-46] and ACC deaminase activity [27, 47-51] were consistent with our observation. One exception was found with the genus *Roseateles* whose members, thus far, were not known for producing the ACC deaminase enzyme.

All 113 epiphytic bacterial isolates were screened for the antagonistic activity against *P. oryzae*, the causal agent of the leaf blast disease, on the basis of the inhibition zone formation in the dual culture test (Figure 1). Twenty-three isolates were found as the antagonists of the fungal pathogen. They were members of four different genera including *Bacillus* (16 isolates), *Burkholderia* (4 isolates), *Chitinophaga* (2 isolates) and *Pseudomonas* (1 isolate). The percentage

Table 3. Affiliation and the number of isolates of epiphytic bacteria that were tested positive.

Activities	Affiliation		
	Firmicutes	***Proteobacteria***	***Bacteroidetes***
Nitrogen fixation	4 genera, 23 isolates	6 genera, 11 isolates	2 genera, 2 isolates
Phosphate solubilization	10 genera, 3 isolates	2 genera, 6 isolates	-
Siderophore production	4 genera, 31 isolates	8 genera, 15 isolates	3 genera, 3 isolates
IAA production	2 genera, 3 isolates	7 genera, 16 isolates	-
ACC deaminase	2 genera, 17 isolates	6 genera, 14 isolates	-
Antagonism against *P. oryzae*	1 genera, 16 isolates	2 genera, 5 isolates	1 genus, 2 isolates

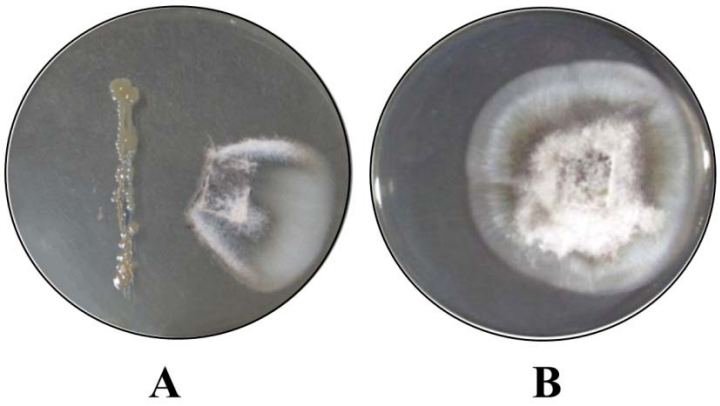

Figure 1. Formation of the inhibition zone between *Bacillus* sp. 1110 and *P. oryzae* (A) indicated the antagonistic activity of the isolate as opposed to the control plate (B) that was inoculated with the fungal pathogen only.

of growth inhibition was determined in each of the antagonistic isolate (Figure 2). The highest level (100% growth inhibition) was observed in *Bacillus* sp.1021, *Bacillus* sp. 1110, *Bacillus* sp. 2211, *Bacillus* sp. 2306, *Bacillus* sp. 3210, *Bacillus* sp. 3308, *Bacillus* sp. 3310 and *Pseudomonas* sp. 2302. The remaining isolates displayed the percentage of growth inhibition that ranged from 73.10% to 98.12%. Enzymatic protease and chitinase activities were tested on all 23 antagonistic isolates. The formation of the clear zone around bacterial colonies on skim-milk agar and NA supplemented with 1% colloidal chitin indicated the positive results of protease and chitinase, respectively. The result showed that 17 isolates produced proteases only. There were no isolates that only showed chitinase activity. Two isolates including *Burkholderia* spp. 1208 and 2208 displayed both protease and chitinase activities. To investigate the production of antifungal compounds, crude ethyl-acetate extracts of the antagonistic isolates were prepared. Although these isolates displayed relatively high levels of *P. oryzae* growth inhibition in the dual culture test, the crude extracts were unable to inhibit the mycelial growth of the fungal pathogen.

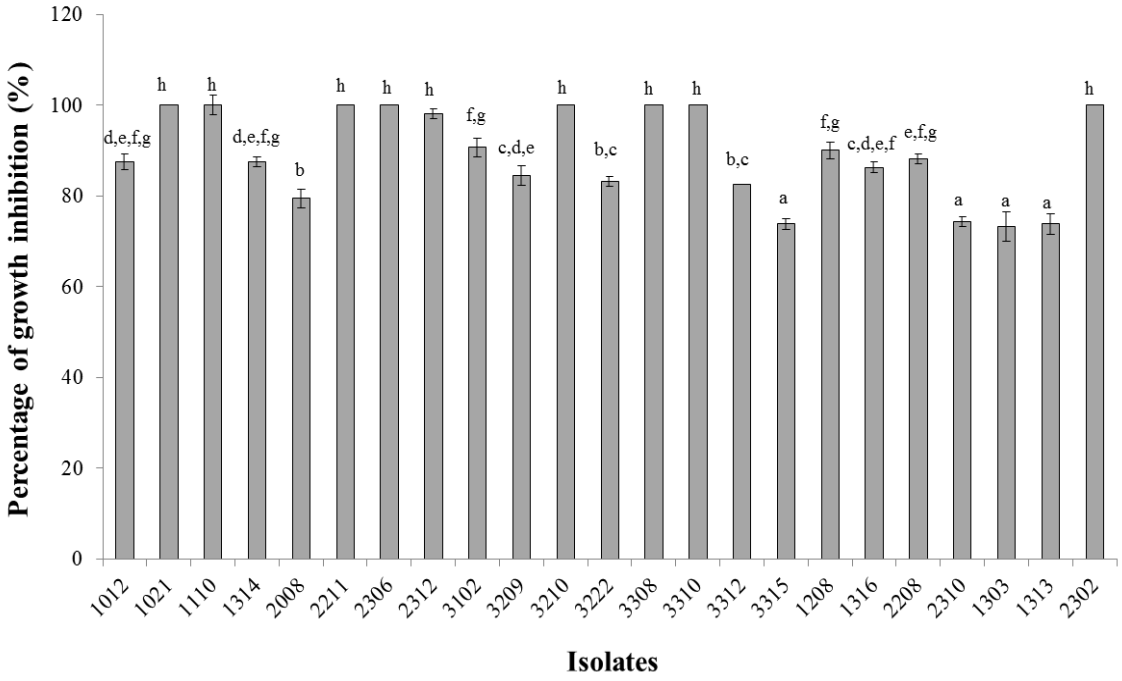

Figure 2. The percentage of growth inhibition of 19 antagonistic isolates against *P. oryzae*. Values represent mean ± standard deviation (n = 3). Different letters indicate statistically significant differences between the percentage of growth inhibition of the isolates (P<0.05).

The antagonistic isolates obtained in our study belonged to four different genera including *Bacillus*, *Pseudomonas*, *Burkholderia* and *Chitnophaga*. This was somewhat in agreement with previous reports. Strains of genera *Bacillus* and *Pseudomonas* were shown for their capability to inhibit the mycelial growth of *P. oryzae* [52-53]. In contrast, *Burkholderia glumae* 411 gr-6 was the only strain of the genus *Burkholderia* that was characterized and reported for its inhibitory effect on the fungus [54]. However, because of its pathogenicity in causing the panicle blight disease [55], its direct application as the biocontrol agent may be limited. Members of the genus *Chitinophaga* were scarcely associated with inhibition of phytopathogen growth. An isolate of the genus was able to reduce the severity of the damping off disease in potato that was caused by *Rhizoctonia solani* [56]. Inhibition and suppression of pathogen growth and colonization by PGPB occur through various mechanisms. One of them is the production of cell-wall degrading enzymes. Protease and chitinase were important for the disruption of proteins and chitin of the fungal cell wall, respectively [5]. In our study, protease was likely more involved in the inhibition of *P. oryzae* growth than chitinase. This was because 17 out of 23 isolates were protease-positive. Additionally, two isolates showing chitinase activity also produced protease. Another major mechanism of disease suppression by PGPB is the production of antibiotic compounds. Despite the strong antagonisms of the 23 isolates against *P. oryzae* in the dual culture test, the crude extracts of all isolates obtained in this study failed to suppress the fungal growth. This result suggested the influence of culture media on antifungal compound production. The dual culture test was carried out on PDA while bacterial culture used for the extraction of antibiotic compounds was grown in NB. The influence of culture

media and growth conditions on antibiotic production was previously demonstrated in other studies. For example, optimization of culture media and growth conditions of *Streptomyces rimosus* MY02 increased the production rate of an antifungal compound against *Fusarium oxysporum* [57].

4. Conclusions

Epiphytic bacteria were isolated from roots, stems and leaves of rice plants. Characterization of these isolates based on the 16S rRNA gene sequences showed that they belonged to phyla *Firmicutes*, *Proteobacteria* and *Bacteroidetes*. The bacterial community on root surfaces was the most diverse group. Bacterial diversity from each location also followed the same trend. Ninety-one isolates displayed at least one of the tested direct plant growth promoting activities. The percentages of positive isolates from the four isolation sources were different. Isolates from Saraburi province showed the highest percentage (91.43%) followed by those from Bangkok (77.78%), Cholburi province (75.68%) and Supanburi province (75.00%). Twenty-three isolates showed the antagonistic activity against *P. oryzae*. The percentage of *P. oryzae* growth inhibition ranged from 73.10% to 100%. Protease and chitinase activities were detected in some of the antagonistic isolates. In contrast, crude extracts of all isolates were tested negative for the inhibition of *P. oryzae* growth. Several epiphytic bacteria isolated in the present study were potential candidates as PGPB for further *in planta* analyses.

5. Acknowledgements

Pyricularia oryzae culture was provided by Asst. Prof. Nonglak Parinthawong, Faculty of Agricultural Technology, King Mongkut's Institute of Technology Ladkrabang. We would also like to express our sincere gratitude towards all owners of the rice farms who donated rice samples for our experiment. This work was financially supported by the traveling grant of Faculty of Science, King Mongkut's Institute of Technology Ladkrabang.

References

[1] Glick, B.R., 2012. Plant growth-promoting bacteria: Mechanisms and applications. *Scientifca*, 963401. doi: 10.6064/2012/963401.

[2] Santi, C., Bogusz, D. and Franche, C., 2013., Biological nitrogen fixation in non-legume plants. *Annals of Botany*, 111, 743-767.

[3] Ahemad, M. and Kibret, M., 2014. Mechanisms and applications of plant growth promoting rhizobacteria: Current perspective. *Journal of King Saud Univeristy-Science*, 26(1), 1-20.

[4] Bhattacharyya, P.N. and Jha, D.K., 2011. Plant growth-promoting rhizobacteria (PGPR): emergence in agriculture. *World Journal of Microbiology and Biotechnology*, 28(4), 1327-1350.

[5] Olanrewaju, O.S., Glick, B.R. and Babalola, O.O., 2017. Mechanisms of action of plant growth promoting bacteria. *World Journal of Microbiology and Biotechnology*, 33(11), 197.

[6] Saha, M., Sarkar, S., Sarkar, B., Sharma, B.K., Bhattacharjee, S. and Tribedi, P., 2016. Microbial siderophores and their potential applications: a review. *Environmental Science and Pollution Research*, 23(5), 3984-3999.

[7] Enders, T.A. and Strader, L.C., 2015. Auxin activity: past, present, and future. *American Journal of Botany*, 102, 180-196.

[8] Spaepen, S. and Vanderleyden, J., 2011. Auxin and plant-microbe interactions. *Cold Spring Harbor Perspectives in Biology*, 3(4), pii: a001438. doi: 10.1101/cshperspect.a001438.
[9] Wang, K.L.C., Li, H. and Ecker, J.R., 2002. Ethylene biosynthesis and signaling networks. *The Plant Cell*. 14(Suppl), s131-s151. doi: 10.3389/fmicb.2015.00937.
[10] Singh, R.P., Shelke, G.M., Kumar, A. and Jha, P.N., 2015. Biochemistry and genetics of ACC deaminase: a weapon to "stress ethylene" produced in plants. *Frontiers in Microbiology*, 6, 937. doi: 10.3389/fmicb.2015.00937.
[11] Grichko, V.P. and Glick, B.R., 2001. Amelioration of flooding stress by ACC deaminase-containing plant growth-promoting bacteria. *Plant Physiology and Biochemistry*, 39, 11-17.
[12] Wilkinson, S. and Davies, W., 2010. Drought, ozone, ABA and ethylene: new insights from cell to plant to community. *Plant, Cell and Environment*, 33, 510-525.
[13] Ali, S. and Kim, W.C., 2018. Plant growth promotion under water: Decrease of waterlogging-induced ACC and ethylene levels by ACC deaiminase-producing bacteria. *Frontiers in Microbiology*, 9, 1096. doi: 10.3389/fmicb.2018.01096.
[14] Goswami, D., Thakker, J.N. and Dhandhukia, P.C., 2016. Portraying mechanics of plant growth promoting rhizobacteria (PGPR): A review. *Cogent Food and Agriculture*, 2, 1127500. doi: 10.1080/23311932.2015.1127500.
[15] Mao, D., Zhou, Q., Chen, C. and Quan, Z., 2012. Coverage evaluation of universal bacterial primers using the metagenomic datasets. *BMC Microbiology*, 12, 66. doi: 10.1186/1471-2180-12-66.
[16] Hongoh, Y., Yuzawa, H., Ohkuma, M. and Kudo, T., 2003. Evaluation of primers and PCR conditions for the analysis of 16S rRNA genes from a natural environment. *FEMS Microbiology Letters*, 221, 299-304.
[17] Yoon, S.H., Ha, S.M., Kwon, S., Lim, J., Kim, Y., Seo, H. and Chun, J., 2017. Introducing EzBioCloud: a taxonomically united database of 16S rRNA gene sequences and whole-genome assemblies. *International Journal of Systematic and Evolutionary Microbiology,* 67(5), 1613-1617.
[18] Ranganayaki, S., Mohan, C. and Ally, Z., 1981. Effect of sodium molybdate on microbial fixation of nitrogen. *Microbiology*, 21(8), 607-610.
[19] Nautiyal, C.S., 1999. An efficient microbiological growth medium for screening phosphate solubilizing microorganisms. *FEMS Microbiology Letters,* 170(1), 265-270.
[20] Schwyn, B. and Neilands, J.B., 1987. Universal chemical assay for the detection and determination of siderophores. *Analytical Biochemistry*, 160, 47-56.
[21] Ehmann, A., 1977. The Van Urk-Salkowski reagent-a sensitive and specific chromogenic reagent for silica gel thin-layer chromatographic detection and identification of indole derivatives. *Journal of Chromatography*, 132, 267-276.
[22] Dworkin, M. and Foster, J., 1958. Experiments with some microorganisms which utilize ethane and hydrogen. *Journal of Bacteriology*, 75, 592-601.
[23] Chaiharn, M. and Lumyong, S., 2009. Phosphate solubilization potential and stress tolerance of rhizobacteria from rice soil in Northern Thailand. *World Journal of Microbiology and Biotechnology*, 25(2), 305-314.
[24] Martins, G., Lauga, B., Miot-Sertier, C., Mercier, A., Lonvaud, A., Soulas, G. and Masneuf-Pomarède, I., 2013. Characterization of epiphytic bacterial communities from grapes, leaves, bark and soil of grapevine plants grown, and their relations. *PLoS ONE*, 8(8): e73013. doi: 10.1371/journal.pone.0073013.
[25] Raweekul, W., Wuttitummaporn, S., Sodchuen, W. and Kittiwongwattana, C., 2016. Plant growth promotion by endophytic bacteria isolated from rice (*Oryza sativa*). *Thammasat International Journal of Science and Technology*, 21(1), 6-17.

[26] Wang, W., Zhai, Y., Cao, L., Tan, H. and Zhang, R., 2016. Endophytic bacterial and fungal microbiota in sprouts, roots and stems of rice (*Oryza sativa* L.). *Microbiology Research*, 188-189, 1-8.
[27] Orhan, F., 2016. Alleviation of salt stress by halotolerant and halophilic plant growth-promoting bacteria in wheat (*Triticum aestivum*). *Brazilian Journal of Microbiology*, 47(3), 621-627.
[28] Sorkhoh, N.A., Ali, N., Dashti, N., AL-Mailemm D.M., Al-Awadhi, H., Eliyas, M. and Radwan, S.S., 2010. Soil bacteria with the combined potential for oil utilization, nitrogen fixation, and mercury resistance. *Biodegradation*, 64(3), 226-231.
[29] Xie, G.H., Cui, Z., Yu, J., Yan, J., Hai, W. and Steinberger, Y., 2006. Identification of *nif* genes in N2-fixing bacterial strains isolated from rice fields along the Yangtze River Plain. *Journal of Basic Microbiology*, 46(1), 56-63.
[30] Kumar, V. and Gera, R., 2014. Isolation of a multi-trait plant growth promoting *Brevundimonas* sp. and its effect on the growth of Bt-cotton. *3 Biotech*, 4(1): 97-101.
[31] Kuan, K.B., Othman, R., Rahim, K.A. and Shamsuddin, Z.H., 2016. Plant growth-promoting rhizobacteria inoculation to enhance vegetative growth, nitrogen fixation and nitrogen remobilization of maize under greenhouse conditions. *PLoS One*, 11(3): e0152478. doi: 10.1371/journal.pone.0152478.
[32] Dhole, A., Shelat, H., Vyas, R., Jhala, Y. and Bhange, M., 2016. Endophytic occupation of legume root nodules by *nifH*-positive non-rhizobial bacteria, and their efficacy in the groundnut (*Arachis hypogaea*). *Annals of Microbiology*, 66(4), 1397-1407.
[33] Ghosh, R., Barman, S., Mukherjee, R. and Mandal, N.C., 2016. Role of phosphate solubilizing *Burkholderia* spp. for successful colonization and growth promotion of *Lycopodium cernuum* L. (Lycopodiaceae) in lateritic belt of Birbhum district of West Bengal, India. *Microbiology Research*, 183, 80-91.
[34] Rajendran, G., Patel, M.H. and Joshi, S., 2012. Isolation and characterization of nodule-associated *Exiguobacterium* sp. from the root nodules of Fenugreek (*Trigonella foenum-graecum*) and their possible role in plant growth promotion. *International Journal of Microbiology*, 2012, 693982. doi: 10.1155/2012/693982.
[35] Hammer, N.D. and Skaar, E.P., 2011. Molecular mechanisms of *Staphylococcus aureus* iron acquisition. *Annual Reviews in Microbiology*, 65, 129-147.
[36] Balado. M., Souto, A., Vences, A., Careaga, V.P., Valderrama, K., Segade, Y., Rodríguez, J., Osorio, C.R., Jiménez, C. and Lemos, M.L., 2015. Two catechol siderophores, Acinetobactin and Amonabactin, are simultaneously produced by *Aeromonas salmonicida* subsp. *salmonicida* sharing part of the biosynthetic pathway. *ACS Chemical Biology*, 10(12), 2850-2860.
[37] de Souza, R., Ambrosini, A. and Passaglia, L.M.P., 2015. Plant growth-promoting bacteria as inoculants in agricultural soils. *Genetic and Molecular Biology*, 38(4), 401-419.
[38] Anandham, R., Indira Gandhi, P., Madhaiyan, M. and Sa, T., 2008. Potential plant growth promoting traits and bioacidulation of rock phosphate by thiosulfate oxidizing bacteria isolated from crop plants. *Journal of Basic Microbiology*, 48(6), 439-447.
[39] Selvakumar, G., Mohan, M., Kundu, S., Gupta, A.D., Joshi, P., Nazim, S. and Gupta S.H., 2008. Cold tolerance and plant growth promotion potential of *Serratia marcescens* strain SRM (MTCC 8708) isolated from flowers of summer squash (*Cucurbita pepo*). *Letters in Applied Microbiology*, 46, 171-175.
[40] Radzki, W., Gutierrez Mañero, F.J., Algar, E., Lucas García, J.A., García-Villaraco, A. and Ramos Solano, B., 2013. Bacterial siderophores efficiently provide iron to iron-starved tomato plants in hydroponics culture. *Antonie Van Leeuwenhoek*, 104(3), 321-330.
[41] Tian, F., Ding, Y., Zhu, H., Yao, L. and Du, B., 2009. Genetic diversity of siderophore-producing bacteria of tobacco rhizosphere. *Brazilian Journal of Microbiology*, 40(2), 276-284.

[42] Lin, H.R., Shu, H.Y. and Lin, G.H., 2018. Biological roles of indole-3-acetic acid in *Acinetobacter baumannii*. *Microbiology Research*, 216, 30-39.
[43] Jensen, J.B., Egsgaard, H., Onckelen, H.V. and Jochimsen, B.U., 1995. Catabolism of indole-3-acetic acid and 4- and 5-chloroindole-3-acetic acid in *Bradyrhizobium japonicum*. *Journal of Bacteriology*, 177, 5762-5766.
[44] Leveau, J.H.J. and Lindow, S.E., 2005. Utilization of the plant hormone indole-3-acetic acid for growth by *Pseudomonas putida* strain 1290. *Applied and Environmental Microbiology*, 71, 2365-2371.
[45] Liu, Y., Shi, Z., Yao, L., Yue, H., Li, H. and Li, C., 2013. Effect of IAA produced by *Klebsiella oxytoca* Rs-5 on cotton growth under salt stress. *Journal of General and Applied Microbiology*, 59(1), 59-65.
[46] Ali, B., Sabri, A.N., Ljung, K. and Hasnain, S., 2009. Auxin production by plant associated bacteria: impact on endogenous IAA content and growth of *Triticum aestivum* L. *Letters in Applied Microbiology*, 48(5), 542-547.
[47] Arshad, M., Shaharoona, B. and Mahmood, T., 2008. Inoculation with *Pseudomonas* spp. containing ACC-deaminase partially eliminates the effects of drought stress on growth, yield, and ripening of pea (*Pisum sativum* L.). *Pedosphere*,18, 611-620.
[48] Zhang, Y.F., He, L.Y., Chen, Z.J., Zhang, W., Wang, Q.Y., Qian, M. and Sheng, X.F., 2011. Characterization of lead-resistant and ACC deaminase-producing endophytic bacteria and their potential in promoting lead accumulation of rape. *Journal of Hazardous Materials*, 186, 1720-1725.
[49] Sun, Y., Cheng, Z. and Glick, B.R., 2009. The presence of a 1-aminocyclopropane-1-carboxylate (ACC) deaminase deletion mutation alters the physiology of the endophytic plant growth-promoting bacterium *Burkholderia phytofirmans* PsJN. *FEMS Microbiology Letters*, 1, 131-136.
[50] Grichko, V.P. and Glick, B.R., 2000. Identification of DNA sequences that regulate the expression of the *Enterobacter cloacae* UW4 1-aminocyclopropane-1-carboxylate deaminase gene. *Canadian Journal of Microbiology*, 46, 1159-1165.
[51] Zahir, A.A., Ghani, U., Naveed, M., Nadeem, S.M. and Asghar, H.N., 2009. Comparative effectiveness of *Pseudomonas* and *Serratia* sp. containing ACC-deaminase for improving growth and yield of wheat (*Triticum aestivum* L.) under salt-stressed conditions. *Archives of Microbiology*, 191(5), 415-424.
[52] Rais, A., Jabeen, Z., Shair, F., Hafeez, Y. and Hassan, M.N., 2017. *Bacillus* spp., a bio-control agent enhances the activity of antioxidant defense enzymes in rice against *Pyricularia oryzae*. *PLoS ONE*, 12(11): e0187412. doi: 10.1371/journal.pone.0187412.
[53] Spence, C., Alff, E., Johnson, C., Ramos, C., Donofrio, N., Sundaresan, V. and Bais, H., 2014. Natural rice rhizospheric microbes suppress rice blast infections. *BMC Plant Biology*, 14, 130. doi: 10.1186/1471-2229-14-130.
[54] Han, J.W., Kim, J.D., Lee, J.M., Ham, J.H., Lee, D. and Kim, B.S., 2014. Structural elucidation and antimicrobial activity of new phencomycin derivaives isolated from *Burkholderia glumae* strain 411gr-6. *Journal of Antibiotics*, 67, 721-723.
[55] Zhou-qi, C., Bo, Z., Guan-lin, X., Bin, L. and Shi-wen, H., 2016. Research status and prospect of *Burkholderia glumae*, the pathogen causing bacterial panicle blight. *Rice Science*, 23(3), 111-118.
[56] Turnbull, A.L., Liu, Y. and Lazarovits, G., 2012. Isolation of bacteria from the rhizosphere and rhizoplane of potato (*Solanum tuberosum*) grown in two distinct soils using semi selective media and characterization of their biological properties. *American Journal of Potato Research*, 89, 294-305.

[57] Yu, J., Liu, Q., Liu, Q., Liu, X., Sun, Q., Yan, J., Qi, X. and Fan, S., 2008. Effect of liquid culture requirements on antifungal antibiotic production by *Streptomyces rimosus* MY02. *Bioresource Technology*, 99(6), 2087-2091.

Electrical Modeling of Nickel-Metal Hydride Batteries for Personal Electric Vehicles

Prakasit Prabpal[1], Krischonme Bhumkittipich[1*] and Tetsunori Haraguchi[2]

[1]Department of Electrical Engineering, Faculty of Engineering
Rajamangala University of Technology Thanyaburi, Pathum Thani, Thailand
[2]Green Mobility Research Institute of Innovation for Future Society,
Nagoya University, Chikusa-Ku, Nagoya, Japan

Received: 30 May 2018, Revised: 27 February 2019, Accepted: 14 March 2019

Abstract

This article presents the electrical modeling of the nickel-metal hydride battery (NiMH), which is used in electric vehicles. According to the battery life cycle, the physical and electrical models of the proposed battery should be analyzed in detail for the condition to control the electric vehicle operation. This article focuses on the NiMH battery, which was used in personal electric vehicles. This type of personal electric vehicle is used to provide personal mobility for handicapped and elderly people. The proposed battery model is considered in both state-of-charge (SOC) and voltage-current characteristics to find the mathematical model of the NiMH battery. The proposed electrical model of the battery was studied under static and dynamic behaviors. The simulation results show that the proposed battery model can represent the behavior of a battery as the real behaviors. The MATLAB/Simulink environment is selected to analyze and simulate the battery model on both static and dynamic behaviors. Therefore, the proposed battery model can verify the study of the battery life cycle on the personal electric vehicle application for the future work.

Keywords: Battery, electric model, personal electric vehicle, electrochemical impedance spectroscopy, nickel-metal hydride batteries.
DOI 10.14456/cast.2019.8

1. Introduction

General electric vehicles can be classified into 5 types as follows: battery electric vehicle (BEV), plug-in hybrid electric vehicle (PHEV), hybrid electric vehicle (HEV), fuel cell electric vehicle (FCEV) and personal electric vehicle (PEV) [1-2]. The important elements of the general electric vehicle (EV) is the driving system, the car control and monitoring system, and the battery as the power source of the electric vehicle [3]. Different EV types from various manufacturers also use hybrid electric vehicle because of its high-power energy density. Figure 1 shows the diagram of a personal electric vehicle, which consists of a transmission system, an electric machine, a DC/AC

*Corresponding author: Tel.: +66-02-549-3571 Fax: +66-02-549-3422
E-mail: krischonme.b@en.rmutt.ac.th

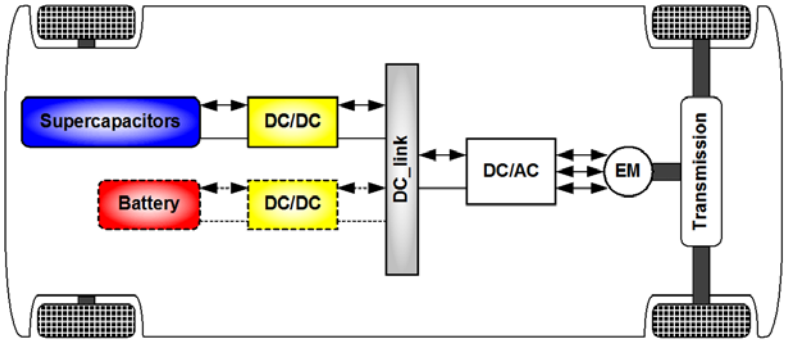

Figure 1. Basic diagram of a personal electric vehicle [4]

voltage of the battery is controlled by the DC/DC converter for the desired voltage value. Therefore, the state-of-charge of the battery was considered during the electric vehicle mobility.

The battery is a storage source of the electric vehicle that can be recharged by connecting with the charging cable at the charging station or household. The storage capacity of the NiMH battery is defined by parameters such as the voltage, current, and temperature. The state-of-charge condition of the battery is measured to analyze both dynamic and static behaviors. Therefore, the proposed study can classify the important features and electrical characteristics of the NiMH battery. The key factors to evaluate the NiMH battery are the SOC and state of health (SOH) of the battery. Meanwhile, the internal impedance modeling of the NiMH battery is considered under SOC and I - V characteristics [5]. The derivation of the internal impedance modeling was determined from the electrochemical impedance spectroscopy (EIS) technique. The voltage and current sinusoidal waveforms of the battery are shown in Figure 2.

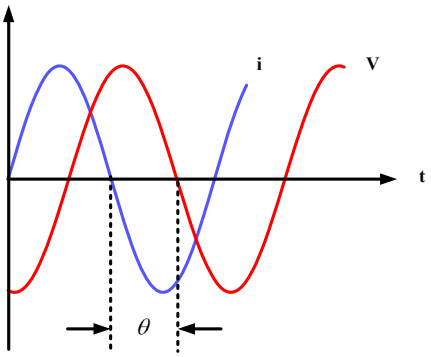

Figure 2. Signal voltage and electrical current at the terminal of the NiMH battery

The waveform of the voltage and current at the terminal of NiMH battery can be classified to find the difference in angle between current and voltage. The phase angle can be used to compute the battery impedance by using a Nyquist plot based on the sampling rate of the waveform. Therefore, we will propose the electrical modeling of the NiMH battery in a personal electric

vehicle, which provides personal mobility to support handicapped and elderly people. The proposed battery model is considered in both state-of-charge (SOC) and voltage-current characteristics to find the mathematical model of the NiMH battery.

2. Materials and Methods

2.1 NiMH Battery Testing

The NiMH battery was tested by using the test battery machine (TBM). The impedance equivalent models of the NiMH battery can be computed by measuring the value. The simulation of the EIS method was selected to define by varying the voltage range from 9.6 to 14.4 V and the ampere-hours rate is 6.5 Ah. Therefore, the voltage and ampere-hour rates are specified from the NiMH battery rate. Meanwhile, the charge and discharge time of the NiMH battery are defined from the ampere-hour rate and pulse charging condition. The voltage-current and phase shift angle of the battery can be presented as the portal angle, and the model diagram in Nyquist plot is shown in Figure 3 [6].

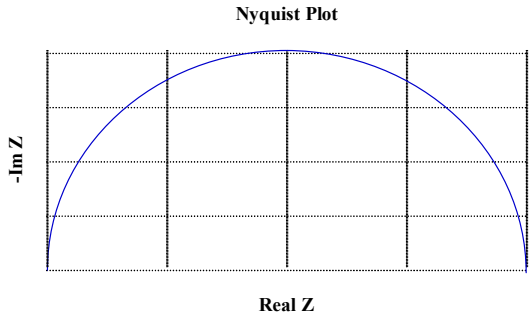

Figure 3. Nyquist plot of the battery model

Figure 3 shows a Nyquist plot of the NiMH battery as the impedance electric circuit. This cycle shows the real and imaginary values of the NiMH battery impedance, which are the resistance and capacitance values. The Nyquist plot also shows the size and phase of the impedance represented by the vector size of | Z | as shown in equation (1).

$$Z = \frac{V\angle 0^{\circ}}{I\angle\theta} = |Z_m|\angle -\theta \tag{1}$$

This NiMH battery model shows the parameters that are considered under the state-of-charge (SOC) and I -V characteristics. The nominal voltage parameter of the cells was varied from 9.6 to 14.4 V, and the ampere-hour magnitude is 4.5 Ah. A cell of the NiMH battery was tested to find the model as the electrical equivalent circuit model. The electrical characteristic of the NiMH battery was measured and analyzed using the electrical equivalent circuit [7]. The battery model can be formed in Thevenin equivalent circuit, which can calculate a voltage source as an open-circuit voltage. The resistance and capacitance (RC) are the dynamic electric models of the NiMH battery. The internal resistance (Ri) of the battery is normally the combination of the parameter, which has

been suggested by Chen and Rincon-Mora [8]. The dynamic behavior is modeled as polarization resistances R_1, R_2 and effective capacitances C_1, C_2. The model is used to characterize the transient response during the transfer of battery power. The electrical equivalent circuit of the battery can be determined by using equations (2) and (3), and the circuit model is presented in Figure 4.

$$V_{cell} = V_{oc} - \frac{V_1}{R_1 C_1} + \frac{I_1}{C_1} - \frac{V_2}{R_2 C_2} + \frac{I_2}{C_2} - R_i I_{batt} \tag{2}$$

$$V_{cell} = V_{oc} - V_1 - V_2 - R_i I_{batt} \tag{3}$$

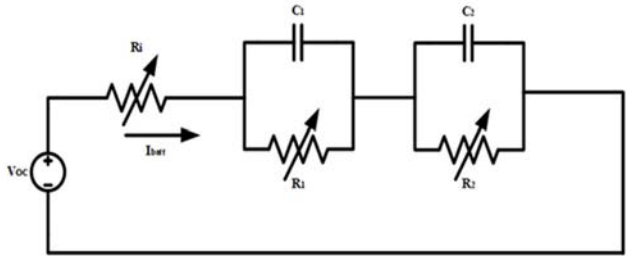

Figure 4. Equivalent circuit model of the NiMH battery

2.2 Electrical Parameter Calculation of the NiMH Battery

The internal resistance (R_i) of the NiMH battery appears when the charge stops with reference, which is an abrupt voltage decrease. The contiguous voltage decrease is associated with the internal resistance of the cell. The battery has a process of charge and discharge at various SOCs. The internal resistance can be calculated by equation (4).

$$R_i = \frac{V_1 - V_0}{I_{batt}} \tag{4}$$

The battery voltage was measured by using the open-circuit cell connection, where the cell voltage depends on the ambient temperature and the SOC [9-11]. The parameter behavior of an NiMH battery is nonlinear. The parameters are changed by the ambient temperature and SOC of the battery. The SOC model setting is used to set the temperature and difference number between charge and discharge. The parameters show the state-of-charge of the battery via the measurement of battery conditions. The initial capacity of the battery is determined in terms of the SOC and ampere-hours using equation (5).

$$V_{oc} = f(SOC)$$
$$SOC = SOC_0 - \int \frac{I_{batt}}{C_{init}} \tag{5}$$

The frequency response analysis determines the change in pulse charge in the operation frequency range of 40 Hz - 3 kHz with the 4.5-A, 14.4-V test circuit as shown in Figure 5.

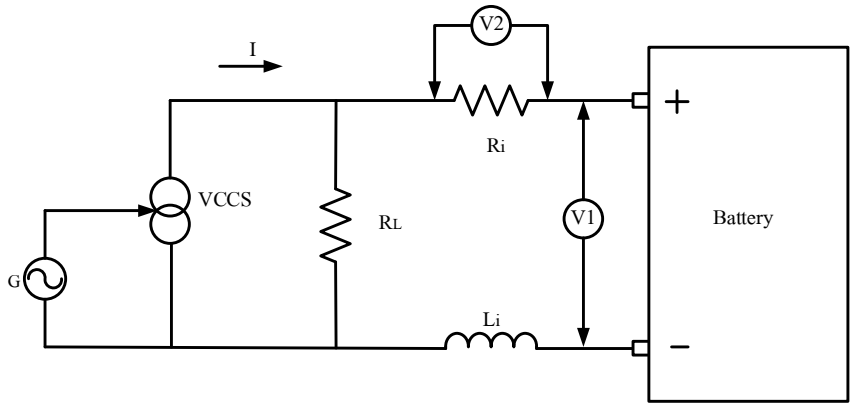

Figure 5. Electrical circuit for the frequency response testing of the batteries

Figure 5 shows that the frequency signal consists of a voltage-controlled current source (VCCS), a current detection resistor (R_i), a voltage divider resistor (R_L), and an external inductor (L_i). The variable inductance (L) in the tested battery can be computed by equation (6).

$$L = \frac{l}{\left(\frac{f_{r_1}}{f_{r_2}}\right)^2 - 1} \tag{6}$$

Where L is the inductance of the internal battery, l is the external inductor, f_{r1} is the test frequency that is not divided by the external inductor, and f_{r2} is the test frequency that is divided by the external inductor in a circuit. The spatial frequency response was analyzed by measuring the effects of each cycle of measurement. The phase difference was a measurement of the electrical current and the voltage of the load resistance. The resistance phase difference was varied from 100 mHz to 5 kHz, which was equal to 0 degree. The electrical circuit did not affect the phase difference in the frequency range. The operation frequency was used to find the equivalent circuit to prepare for the conditions before the battery testing. The battery must be controlled at ambient temperature before test setting. The two voltage waveforms were measured by an oscilloscope at the terminals of the battery (V_B) and voltage bracket resistance (V_{Ri}) as shown in Figure 6. Therefore, the impedance of the battery can be computed using equation (7).

$$Z = \frac{V_B \times R_i}{V_{R_i}} \times (\cos\theta + j\sin\theta) \tag{7}$$

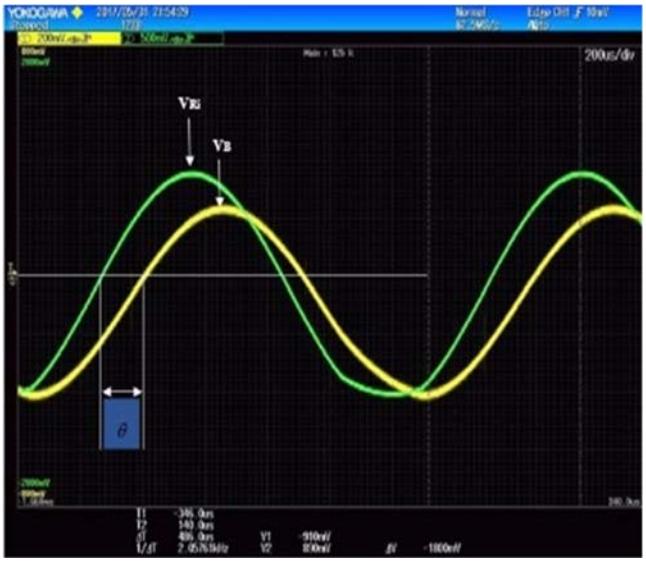

Figure 6. Two voltage waveforms of the proposed battery

Where Z is the impedance, V_B is the dropout voltage of the battery, V_{Ri} is the dropout voltage of resistance, and R_i is the internal resistance.

The model of the NiMH battery for the personal electric vehicle was found based on the electrical circuit model. The test voltage range of the NiMH battery was 9.6-14.4 V. The TBM was used to collect the experiment result to model the battery properties to the electrical circuit model. The experimental system was composed of an NiMH battery with a nominal voltage of 14.4 V and the ampere-hour of 4.5 Ah. The TBM used a data acquisition (DAQ) device and recorded the battery testing results. The experiment temperature was controlled at 25 °C to avoid the temperature effect. The TBM can charge and discharge a battery at a maximum current rate of 20 A. The TBM was arranged to measure 9 parameters as follows: the constant-current, final voltage, voltage/time, last voltage, constant power, constant ampere pulse, last voltage, pulse last voltage and final ampere-hour. It comprised the voltage, current, SOC measurements and a computer interface with summarized specifications of the TBM using the condition of pulse last voltage.

The testing of the NiMH battery obtained the SOC of the battery. The battery ampere-hour was 4.5 Ah for the testing condition. The pulse last voltage was presumed to compass the battery SOC value if the OCV value remained for a sufficient amount of time. The NiMH cell cannot operate in the steady-state mode during 600 s. However, the cell voltage increased after discharging and decreased after 600 s at the same SOC and OCV values.

3. Results and Discussion

The two waveforms can be calculated from the parameters in the electrical model of the proposed battery. The initial tests to measure the battery cell voltage were applied at regular intervals of 100 s to V_0, which was equal to 10.1 V. The proposed battery was charged from 4.5 V to 11.5 V until the highest voltage reached 10.9 V. The voltage was constant, but the electricity supply was

reduced to the final value. When the battery charging was full at 200 s, the battery discharging began at 4.5 A. The final voltage was equal to 9.6 V; then, the battery reached the equilibrium point. Figure 7 can be analyzed using the relationship between voltage and time to compute the battery parameters, which are shown in Figure 8.

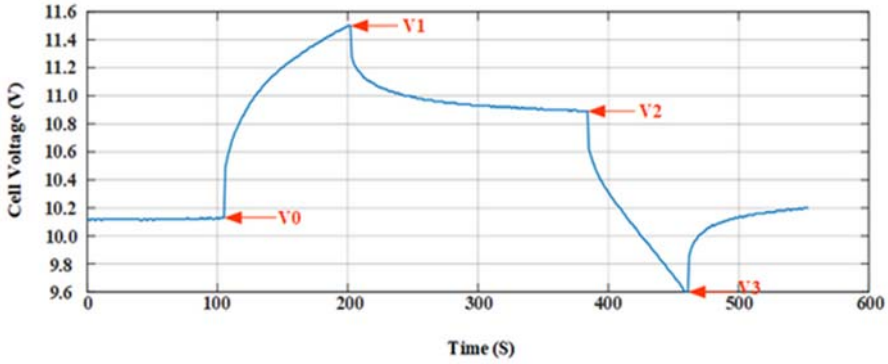

Figure 7. SOC voltage curve

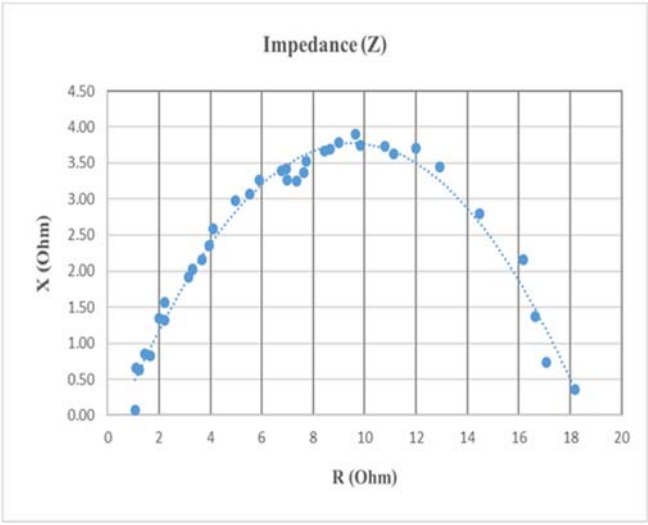

Figure 8. Nyquist plot of the frequency range from 100 mHz to 5 kHz

The equivalent circuit model of the proposed battery can be found by measuring the phase difference of the electrical current and voltage of the load resistance. The phase difference was varied from 100 mHz to 5 kHz. Using the Nyquist plot, we could calculate the inductance and R_2 and C_2 with the input voltage phase. It is more understandable that the capacitor discharge and discharge rates are not equal under the same cycle. The charging rate in the electrical model can be considered constant. The discharge testing had a longer time period than the charge time period. For the frequency response, the impedance of the battery can be calculated from the change rate of the phase difference. All variable parameters can be drawn in the equivalent circuit model as shown in Figure 9.

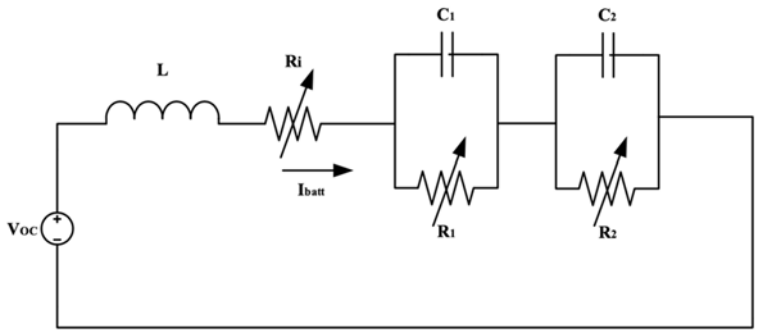

Figure 9. Electrical model of the NiMH battery

4. Conclusions

This article presents the electrical modeling of batteries with a focus on NiMH batteries in personal electric vehicles. The proposed battery model was considered in both SOC and voltage-current characteristics to find the mathematical model and electrical circuit model of the NiMH battery. The simulation results show that the proposed battery model can express the behavior of an NiMH battery. The MATLAB/Simulink environment was selected to analyze and simulate the battery electric model on both static and dynamic behaviors. The equivalent circuit model of the proposed battery can be found by measuring the phase difference of the electrical current and voltage of the load resistance. With the Nyquist plot, we can calculate the inductance and R_2 and C_2 using the input voltage phase. The charging rate in the electrical model can be considered constant. The discharge testing had a longer time period than the charge time period. For the frequency response, the impedance of the battery can be calculated from the change rate of the phase difference. Therefore, the proposed battery model can verify the study of the battery life cycle in personal electric vehicle applications in future work.

References

[1] Jaguemont, J., Boulon, L., Venet, P., Dube, Y. and Sari, A., 2016. Lithium-ion battery aging experiments at subzero temperatures and model development for capacity fade estimation. *IEEE Transaction on Vehicular Technology*, 65(6), 4328-4343.

[2] Kongjeen, Y. and Bhumkittipich, K., 2016. Modeling of electric vehicle loads for power flow analysis based on PSAT. *Proceedings of 13th International Conference on Electrical Engineering/Electronics, Computer, Telecommunications and Information Technology (ECTI-CON)*, June 28- July 1, 2016, 1-6.

[3] Kongjeen, Y., Junlakan, W., Bhumkittipich, K.and Mithulananthan, N., 2018. Estimation of the quick charging station for electric vehicles based on location and population density data. *International Journal of Intelligent Engineering&Systems*, 11 (3), 233-241.

[4] Kongjeen, Y. and Bhumkittipich, K., 2018. Impact of plug-in electric vehicles integrated into power distribution system based on voltage-dependent power flow analysis. *Energies*, 11(6), 1-16.

[5] Shin, D.-H., Jeong, J.-B, Kim, T.-H. and Kim, H.-J., 2013. Modeling of lithium battery cells for plug-in hybrid vehicles. *Journal of Power Electronics*, 13(3), 429-436.

[6] Jaguemont, J., Boulon, L. and Dube, Y., 2016. Characterzation and modeling of a hybrid-electric-vehicle lithium-ion battery pack at low temperatures. *IEEE Transaction on Vehicular Technology*, 65(1), 1-14.
[7] Gao, L., Liu, S., Dougal, R.A., 2008. Dynamic lithium-ion battery model for system simulation. *IEEE Transaction on Components and Packaing Technologies*, 25(3), 495- 505.
[8] Chen, M. and Rincon-Mora, G.A., 2006. Accurate electrical battery model capable of predicting runtime and I-V performance. *IEEE Transactions on Energy Conversion*, 21(2), 504-511.
[9] He, H., Xiong, R., Zhang, X., Sun, F. and Fan, J., 2011. State-of-charge estimation of the lithium-ion battery using an adaptive extended Kalman filter based on an improved Thevenin model. *IEEE Transaction on Vehicular Technology*, 60(4), 1461-1469.
[10] Abu-Sharkh, S. and Doerffel, D., 2004. Rapid test and non-linear model characterization of solid-state lithium-ion batteries. *Journal of Power Sources*,130, 226-274.
[11] Buller, S., Thele, M., Karden, E., Doncker, R.W., 2003. Impedance-based non-linear dynamic battery modeling for automotive application. *Journal of Power Sources*, 113, 422-430.

High Absorbable Cassava Starch/Poly (vinyl alcohol) Sponge for Medical Applications

Pusita Kuchaiyaphum[1*], Suphitsara Euaklang[1], Anucha Raksanti[2] and Chatrachatchaya Chotichayapong[1]

[1]Applied Chemistry Department, Faculty of Sciences and Liberal Arts, Rajamangala University of Technology Isan, Nakhon Ratchasima, Thailand

[2]Science and Technology Research Institute, Chiang Mai University, Chiang Mai, Thailand

Received: 25 October 2018, Revised: 28 February 2019, Accepted: 13 March 2019

Abstract

Absorbable cassava starch-based sponges are prepared by freeze-drying method. The mixing solutions of cassava starch, poly (vinyl alcohol) and glycerol with various weight ratios are put in the freeze-dryer machine at -40 ºC for 24 h to change to sponge form with interconnecting porosity. The obtained sponge at 50/35-15 weight ratio of CS/PVA-glycerol is soft yet tough, foldable and tolerable to the hands, easy to manipulate and cut into the desired form. The results of porosity and water absorption test reveal high water absorption of the sponge with 67% of total porosity and 522% of water absorption. Iodine test and UV-Vis absorption show no starch dispersion into the medium after sponge immersion in PBS for 7 days. The blood absorbability of the sponge is higher than gauze and cotton pad in the same size. The results demonstrate that the prepared sponge could effectively be used as absorbable for medical applications.

Keywords: Cassava starch, Poly (vinyl alcohol), absorbable sponge, medical application
DOI 10.14456/cast.2019.9

1. Introduction

Medical materials with porous structures and absorbable property have widely been used for many years and apply for medical applications including an absorbable surgical hemostatic agent [1-4]. As observed, a significant cause of death in trauma patients is unrestrained bleeding [5]. Thus, the priority in emergency medical treatment is to decrease unexpected blood loss. In the past years, numbers of hemostatic materials have been developed aiming to increase the survival rate and reduce bleeding problems in wounded patients [6-10].

*Corresponding author: Tel.: +66638877722
E-mail: pusita.ku@gmail.com

The hemostatic agent is an alternative to usual modalities of hemorrhage control. The required properties of the ideal hemostatic agents are non-toxic, good biocompatibility, ready and easy to use, light, stable, and can rapidly control huge bleeding with low-cost [11, 12]. The numerous natural polymers such as chitosan, cellulose, gelatin, collagen and starch have been examined for hemostatic biomaterial agent development due to their biocompatibility and inherent biological properties has increasingly been utilized in various fields, mostly due to its low cost, readily available, renewable, biocompatible and biodegradable [13, 14]. In the case of medical application, starch has been used as tissue engineering scaffolds, drug delivery devices, absorbing liquid sponges and absorbable hemostatic agents [16-25].

Apart from any other starch, cassava starch (CS) is one of the commonly used as models of eco-friendly biomaterials. CS is easy to process in several forms of medical materials such as film, gel, fibers and sponge. However, the mechanical properties of CS-sponges are usually poor. This can be relieved by blending with other synthetic polymers before a three-dimensional porous structure preparation.

Poly (vinyl alcohol) (PVA) is a non-toxic synthetic polymer produced from poly (vinyl acetate) through hydrolysis. It is an attractive material due to its outstanding characteristics and excellent properties such as biodegradability, biocompatibility, swelling, safety and strength [26-28]. Thus, PVA has found uses in different applications such as adhesives, paper, textile, food, pharmaceutical, biomedical, and commonly used in medical devices [29, 30]. PVA is frequently blended with many types of natural polymers to improve its mechanical properties and stability. CS contains free hydroxyl groups that can interact with PVA. However, the CS and PVA sponges have never been prepared for use as a hemostatic material.

The main purpose of this study is to prepare the CS/PVA sponges by a simple method without using chemical cross-linker to avoid the toxic residue. The CS/PVA solution was homogenized by glycerol addition. Then, the mixing solution was used to form the porous structure sponge using the freeze-drying method to produce a high absorbable anti-bleeding sponge. The effects of PVA and glycerol content on the physical and thermal properties, swelling, stability, porosity, and absorbability of the obtained CS/PVA sponges were also investigated. The potential for a hemostatic agent, blood absorbability of CS/PVA sponges was also studied.

2. Materials and Methods

2.1 Materials

Cassava starch (CS) was obtained from commercial Thailand cultivation. Poly (vinyl alcohol) (PVA) with the average molecular weight of 85,000-124,000 and 99 % hydrolyzed was purchased from Aldrich Chemical Co., Inc., USA. Glycerol with 86-89 % assay was purchased from Fluka Bio-Chemika, Germany. All chemicals used were analytical grade.

2.2 Fabrication of CS-based sponge

An aqueous solution of 3 % w/v CS was prepared by dissolving CS powder in distilled water at 65°C until the starch gelatinized. The 3 % w/v PVA was prepared by dissolving PVA powder in distilled water at 100°C for 60 min. The prepared CS and PVA solutions were mixed with glycerol at 50°C for 60 min to prepare CS/PVA-glycerol solutions with various weight ratios (50/25-25, 50/30-20, 50/35-15, 50/40-10, 50/45-05). Afterwards, the mixed solutions of CS/PVA-glycerol were poured into molds (1.5 cm radius and 1 cm height) and kept in a domestic freezer at -22°C for 24 h. The pre-freeze mixed solutions were lyophilized in a freeze-dryer (CoolSafe 110, Svan Vac

Newzeland) under vacuum at -40°C for 24 h to produce the porous structure sponge. In order to obtain an appropriate CS/PVA-glycerol composition for preparation of CS-based sponge, all obtained CS-based sponges with various weight ratios were composition optimized.

2.3 Characterization of CS-based sponges

2.3.1 Functional group analysis

The functional groups of samples were analyzed by Attenuated Total Reflectance-Fourier Transform Infrared Spectroscopy (ATR-FTIR). The ATR spectra of sponge samples were recorded with a Spectrum100 (Perkin Elmer Inc.) in the range between 4000 to 600 cm^{-1}.

2.3.2 Thermal stability

Thermal stability of the sponge samples was characterized using differential scanning calorimetry (DSC) and thermogravimetric analysis (TGA). The Perkin-Elmer DSC was used for DSC analysis with a heating rate of 10 °C/min over the temperature range of 40 to 200 °C under a purged nitrogen atmosphere. The TGA instrument used was STA 6000, Perkin-Elmer in non-isothermal mode, heating rate is 10 °C/min under an inert nitrogen atmosphere over the temperature range 50-600 °C.

2.3.3 CS-based sponge stability

The essential stabilities of the CS-based sponge were estimated by studying the *in-vitro* release of the carbohydrate from the prepared sponge [31]. The CS-based sponge sheets ($1.5\times1.5\times0.5$ cm^3) were immersed in 20 ml of phosphate buffer saline (PBS), pH 7.4 for 7 days. Then, the released carbohydrate in PBS was studied by pH measurement, iodine test using a UV-Vis spectrophotometer, UV-2401PC (SHIMAZU Corporation). Iodine solution was dropped into the PBS medium after 7 days of sponge sheet immersion and the PBS medium was measured at 580-600 nm by the UV-Vis spectrophotometer [32, 33].

2.3.4 CS-based sponge porosity

Percent porosity of the sponges was evaluated by the liquid displacement method [31]. The porosity is defined as total volume of the pores ($V_i - V_f$) divided by total volume of the porous sample ($V_m - V_f$). Sponge samples were immersed in hexane in measuring cylinder and the changed hexane volume was then observed, and the porosity of the sponges (ε) was calculated from equation (1).

$$\varepsilon = \frac{V_i - V_f}{V_m - V_f} \times 100 \quad (1)$$

Where V_i is an initial hexane volume in a measuring cylinder,
V_m is the hexane volume after the sponge immersion for 10 min,
V_f is the remaining hexane volume after the removal of the hexane absorbed sample.

2.3.5 Water absorption and water equilibrium

All dry sponge samples were weighed and immersed in water at 25 °C. After immersion at different time intervals, the sponges were removed from the medium and instantly weighed after absorbing excess water from the surface. The % water absorption (A) was calculated using equation (2). The

water equilibrium (*Weq*) in the swollen samples was calculated [34] using equation (3).

$$A = \frac{W_r - W_d}{W_d} \times 100\,\% \tag{2}$$

$$W_{eq} = \frac{W_s - W_d}{W_d} \times 100\,\% \tag{3}$$

Where W_d is the weight of the dried sponge,
W_r is the weight of the water-removed sponge,
W_s is the weight of the saturated swollen sponge.

2.3.6 Blood absorption capability

To compare the blood absorption capacity of the CS-based sponges with gauze and cotton pad, their absorption capacity was studied to estimate surgical blood loss as mentioned by Kristen *et al*. [35] with some modifications [36]. Each of the sponge, gauze and cotton pad samples in the same size ($3\times5\times0.5$ cm^3) was placed in Petri-dishes, the Petri-dishes were consecutively filled with 0.5 ml of collective amounts of fresh pig blood ranging from 0.5-5 ml. The saturation was defined as the point at which no dry sample was evident or felt.

3. Results and Discussion

3.1 Fabrication of CS-based sponge

As cassava starch (CS) is a renewable biopolymer, the obtained sponges are expected to contain higher CS content and can still be prepared to sponge form with good properties. Therefore, the CS/PVA-glycerol sponges with various weight ratios at 50/25-25, 50/30-20, 50/35-15, 50/40-10 and 50/45-05 were prepared. However, only the polymer blended solution with PVA content equivalent to or higher than 35 weight ratio and glycerol content equivalent to or lower than 15 weight ratio can be fabricated to the sponge form. This is because the polymer blended solution with PVA content lower than 35 makes the sponge break and brittle while a polymer blended solution with glycerol content higher than 15 makes the sponge unstable. This suggested that the addition of PVA and glycerol can help to form the CS-based sponges. The obtained sponges with various weight ratios of CS/PVA-glycerol were shown in Figure 1. The fabrication process intrinsically generated the porous structure of CS-based sponges. The moisture formed in the blended solution during the homogenization, after solvent evaporation by freeze-drying methods, promoted the formation of pores structure. The sponges at 50/35-15, 50/40-10 and 50/45-05 weight ratio of CS/PVA-glycerol were smooth, soft, tough, foldable and can simply be made into the desired shape. Therefore, the CS-base sponge with these three compositions was selected for more characterization.

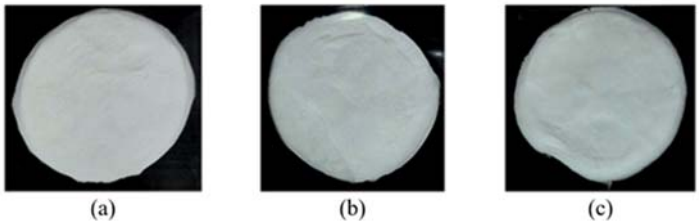

Figure 1. CS-based sponge with various weight ratios of CS/PVA-glycerol, (a) 50/35-15, (b) 50/40-10 and (c) 50/45-5

3.2 Functional group analysis

The CS-based sponge was prepared from CS, PVA and glycerol. The functional groups of the starting materials (Figure 2a) and the prepared samples with different proportions (Figure 2b) were confirmed by FTIR spectroscopy. All peaks emerged in CS, PVA and glycerol had also appeared in the CS-based sponge with a slight chemical shift value. In Figure 2b, there were the absorption peaks at 3277 cm^{-1}, 3279 cm^{-1} and 3278 cm^{-1}, which were corresponded to O-H stretching vibration of 50/35-15, 50/40-10 and 50/45-5 weight ratio of CS/PVA-glycerol, respectively. The absorption peaks at 1033 cm^{-1}, 1035 cm^{-1} and 1031 cm^{-1} corresponded to C-O stretching of the CS/PVA-glycerol sponges with the weight ratio of 50/35-15, 50/40-10 and 50/45-5, respectively. Comparing with CS, the O-H stretching and C-O stretching showed the absorption peaks at 3279 cm^{-1} and 997 cm^{-1}, respectively. In the CS/PVA-glycerol sponges, the peaks of O-H stretching showed stronger absorption peak, while C-O stretching shifted to higher wave number and became more intense, which indicated that the H-bonding increased. The FTIR results indicated that CS and PVA were blended by intermolecular force (H-bond), and the H-bonding density depended on the sponge composition. Moreover, the glycerol addition can improve the compatibility of CS and PVA due to the increase of H-bonding by more polymer chains motion.

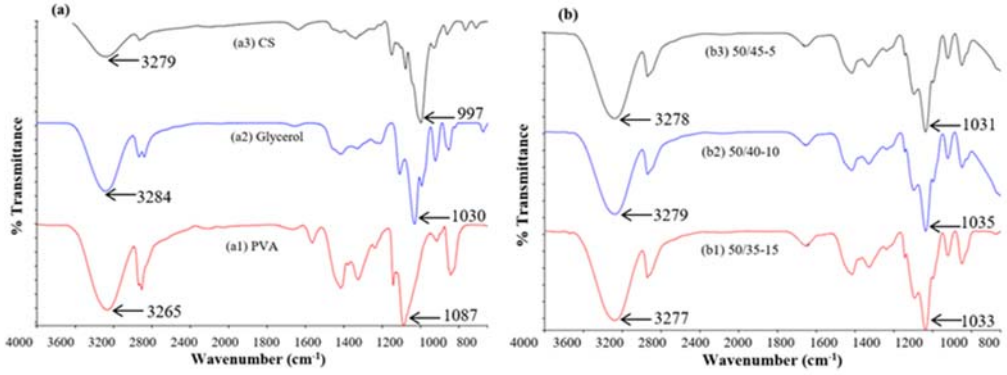

Figure 2. FTIR spectra of (a) starting materials (a1: PVA, a2: glycerol, a3: CS) and (b) CS-based sponge with various weight ratios of CS/PVA-glycerol (b1: 50/35-15, b2: 50/40-10, b3: 50/45-5)

3.3 Differential scanning calorimetry

Normally, the first heating run of starch DSC thermograms shows a broad endothermic peak at about 100 °C. The crystalline melting temperature in native starch was previously studied and reported. For example, in the case of the amylopectin part in sago starch, the melting temperature peak is between 50 and 150 °C [37] while some study revealed that the starch chains interacted with the remaining water by H-bonding which showed the endothermic peak at 126.9 °C due to the crystalline melting [38]. Moreover, there is a report presuming that it may be because of water adsorption occurring above room temperature during the heating scan [39]. At this moment, there is no conclusion for these descriptions but all native starch shows this peak [40]. As the discussion, in Figure 3, there is the broad peak at 93 °C, 94 °C and 96 °C on DSC thermogram of CS-based sponges at 50/35-15, 50/40-10 and 50/45-5 weight ratio of CS/PVA-glycerol, respectively. The CS-based sponge with higher glycerol content showed the lower temperature of the broad peak because glycerol functioned as the plasticizer which can increase the mobility of polymer chains and decrease the crystallinity of the sponge.

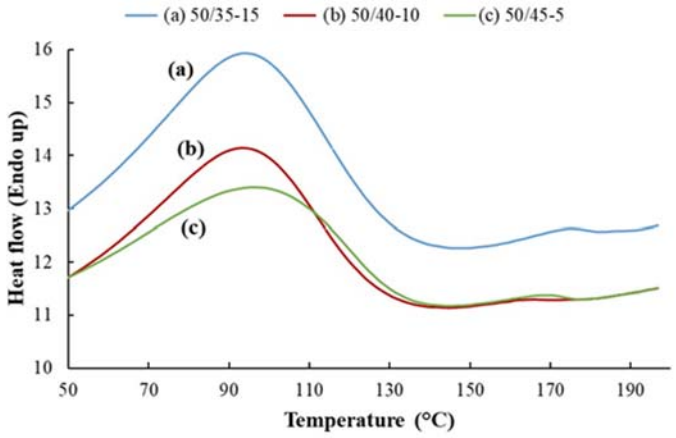

Figure 3. DSC thermogram of CS-based sponge with various weight ratios of CS/PVA-glycerol, (a) 50/35-15, (b) 50/40-10 and (c) 50/45-5

3.4 Thermogravimetric analysis

Figure 4 shows the weight remains against temperature as measured by TGA for various CS-based sponges. The TGA thermograms of CS-based sponges with various weight ratios of CS/PVA-glycerol showed three similar main stages of degradation process as discussed previously [41, 42]. The sponges presented an initial drop between 50 to 200 °C which corresponds to a mass loss of absorbed moisture and possibly, glycerol (boiling point of glycerol is about 198 °C). It should be noted that all sponges were dried at 50 °C before the TGA analysis, thus, most of the moisture was already removed, resulting in smaller mass loss of glycerol that relates with the amount of added glycerol into each composition of approximately 15%, 10% and 5% of 50/35-15, 50/40-10 and 50/45-5 weight ratio of CS/PVA-glycerol, respectively. The second stage (200-500 °C) is the main stage of decomposition and it can be attributed to CS and PVA depolymerization [43]. And the final

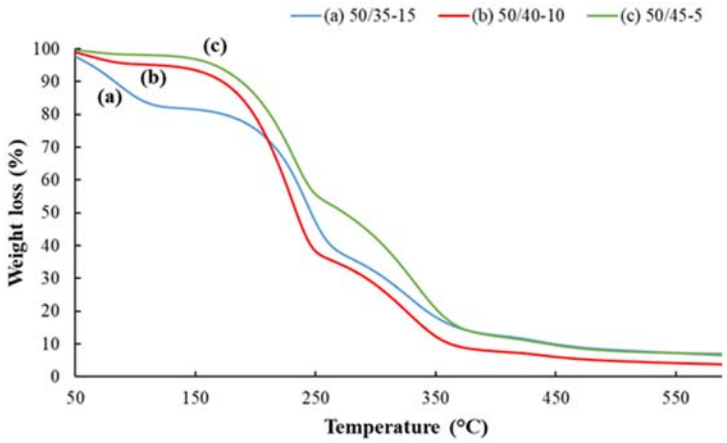

Figure 4. TGA thermogram of CS-based sponge with various weight ratios of CS/PVA-glycerol, (a) 50/35-15, (b) 50/40-10 and (c) 50/45-5

stage of weight loss above 500 °C is generally carbonization stage with slow degradation rate. Furthermore, CS-based sponges showed very little ash (less than 5%) after thermal degradation. The results concluded that the thermal stability of the prepared CS-based sponge was appropriate to meet the necessities for fabrication, storage, sterilization, and use as absorbable material.

3.5 CS-based sponge stability

This study was carried out to estimate the stability of the sponges. If the samples are to be operated successfully and stable, the main components as CS should not leach out from the sample. Accordingly, *in-vitro* carbohydrate releases from CS-based sponges were evaluated by pH measurement, iodine test, and UV-Vis absorption at 580-600 nm.

The leaching of carbohydrate from all CS-base sponges was observed after 7 days of sponge immersion, after that, there was not much change in pH value. Moreover, the iodine test, which was investigated by UV-Vis absorption at 580-600 nm (Figure 5), indicated that the CS-based sponge was almost unchanged and the leached-out fraction is negligible after 7 days. This behavior can conclude that the sponge can be used in the PBS medium up to 7 days.

From Figure 6, the percent porosity of the CS-based sponges drastically decreases with the decrease of glycerol content up to 10 % weight ratio, then it increases afterward due to the glycerol and PVA contents. This is because glycerol performed as a plasticizer which usually inserts between the CS and PVA chains to expand the free volume of the polymer chain. Moreover, increasing of PVA content leads to the sponges with lower porosities. However, the porosity of CS/PVA-glycerol sponge at 50/45-5 weight ratio increases possibly because this composition with a small amount of glycerol which is not enough for function as a plasticizer can help the CS and PVA chains more compatible.

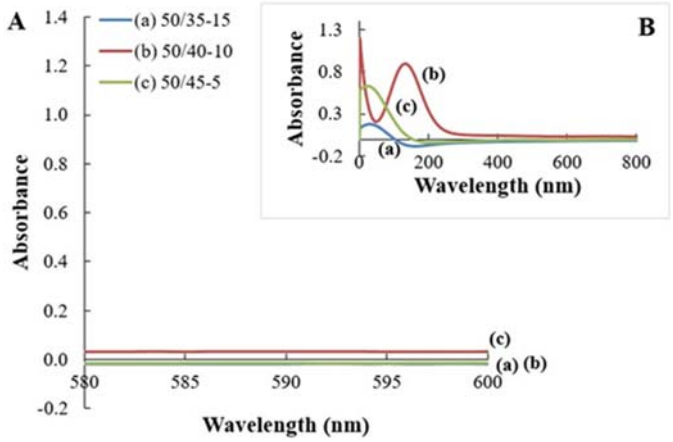

Figure 5. UV-Vis absorption of PBS medium after 7 days of CS-based sponge immersion (A) at 580-600 nm and (B) at 0-800 nm

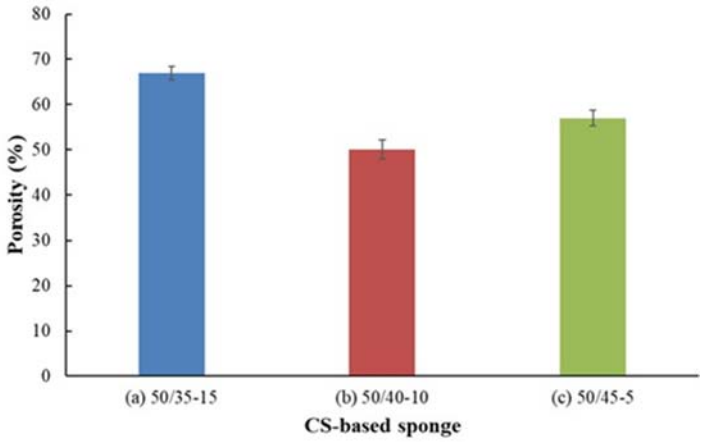

Figure 6. Percent porosity of CS-based sponge with various weight ratios of CS/PVA-glycerol, (a) 50/35-15, (b) 50/40-10 and (c) 50/45-5

3.6 Water absorption and water equilibrium

One of the important functions of the medical absorbable sponge is good liquid absorbing capability [44, 45]. The water absorption of CS-based sponges was presented in Figure 7. Three different ratios of CS-based sponges could absorb 3-5 times of their own dry weight in 80 s. Since the water absorption of the sponges is related to its porosity, thus water can be more easily absorbed in the sponges due to both porous structure and the absorbing of CS and PVA. This water uptake is higher than the reported value for porous materials [46-50] which demonstrated a usual water absorption of 10 - 200%. Moreover, the absorption rate increased continuously with time until its equilibrium at about 80 s.

From Figure 8, the water equilibrium of 50/35-15, 50/40-10 and 50/45-5 exhibited as 522%, 296% and 392%, respectively, that related to their porosity, thus water can be more easily absorbed in the porous sponge due to the openness of the sponge structure. In the case of the 50/35-15 weight ratio of CS/PVA-glycerol with 522 % water absorption at equilibrium, which was probably attributed to high absorbability sponge that could be used for medical absorbable materials.

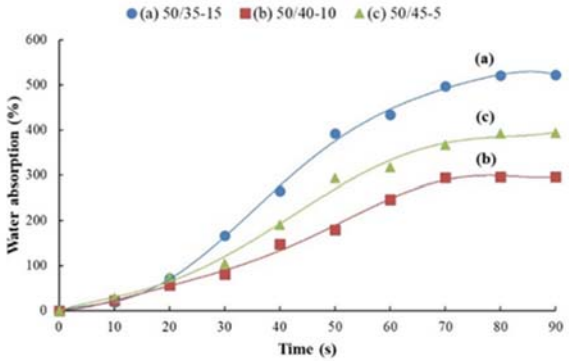

Figure 7. Water absorption of CS-based sponge with various weight ratios of CS/PVA-glycerol, (a) 50/35-15, (b) 50/40-10 and (c) 50/45-5 at various time intervals

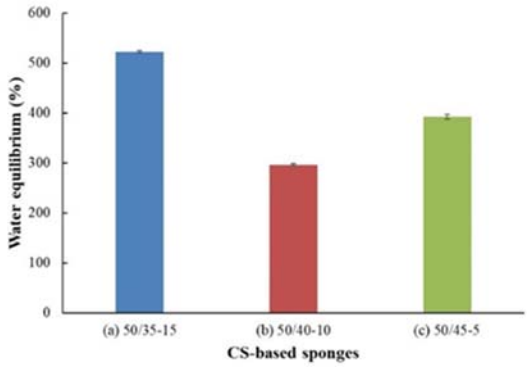

Figure 8. Water equilibrium of CS-based sponge with various weight ratios of CS/PVA-glycerol, (a) 50/35-15, (b) 50/40-10 and (c) 50/45-5

3.7 Blood capability

The comparison of viscosity, surface tension and relative density between fresh human blood and fresh and aged pig blood showed a notable similarity between the human and pig bloods, even when the pig blood is up to two weeks old, provided it has been incubated at 4°C for that period. This means that it is valid to use pig blood instead of human blood for educational purposes [51]. This blood capacity test of the CS-based sponge, the pig blood was used as a model blood. To study the blood capacity of the CS-based sponge, the 50/35-15 weight ratio of CS/PVA-glycerol was selected to study due to its highest water absorption. As shown in Figure 9, it revealed that the 50/35-15 of

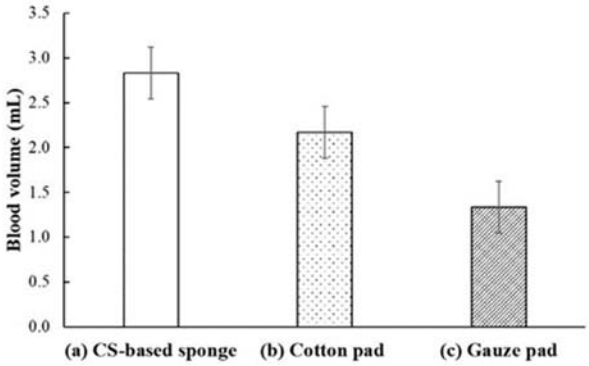

Figure 9. Blood absorption capacity of (a) CS/PVA-glycerol sponge at 50/35-15 weight ratio, (b) Cotton pad and (c) Gauze pad samples in the same size

CS/PVS-glycerol sponge completely absorbed a maximum of about 3 ml of the pig blood. The blood absorption capacity of the sponge is higher than gauze and cotton pad in the same size. Moreover, the CS-based sponge showed no sticking problem with skin due to its smooth surface and stability. These again suggested that the porous CS-based sponge could be used as an absorbable sponge for medical applications.

4. Conclusions

The absorbable CS-based sponge composite was successfully fabricated by using the freeze-drying method. The FTIR results indicated that the polymer compositions were blended by hydrogen bonding. The CS, PVA and glycerol contents affect the sponge properties and the water absorption of the sponge is also related to its porosity. The sponge at the 50/35-15 weight ratio of CS/PVA-glycerol was soft and easy to blend into the desired shape. Moreover, its absorption increased continuously with time and reached 522 % water absorption at 80 s. Iodine test and UV-Vis absorption showed that the CS-based sponge was almost unchanged and the leached-out fraction was negligible after sponge immersion in PBS for 7 days. Moreover, TGA result revealed that the thermal stability of the CS-based sponge was appropriate to meet the necessities for sterilization and its ash less than 5% after thermal degradation at 600 °C. Furthermore, blood absorption capacity of the 3×5 cm^2 sponge was about 3 ml, and the capacity can increase with the larger sponge size. As conclusion, the results demonstrated that the prepared sponge could be acceptable for use as absorbable material in biomedical applications.

5. Acknowledgements

The authors gratefully acknowledge the Rajamangala University of Technology Isan, Nakhon Ratchasima for all supports and liberality. Thanks to our colleagues who provided vision and knowledge that greatly assisted the research.

References

[1] Bunzen, D.L., Lins, N., Leal, M.D., Lira, M.M.D. and Neto, S.D.C., 2014. Middle ear packing materials: comparison between absorbable hemostatic gelatine sponge and sugarcane biopolymer sponge in rats. *Brazilian Journal of Otorhinolaryngology*, 80, 237-244.

[2] Chen, Y., Zhang, Y., Wang, F., Meng, W., Yang, X., Li, P., Jiang, J., Tan, H. and Zheng, Y., 2016. Preparation of porous carboxymethyl chitosan grafted poly (acrylic acid) superabsorbent by solvent precipitation and its application as a hemostatic wound dressing. *Materials Science and Engineering C*, 63, 18-29.

[3] Chang, Y.I., Yang, Y.Y., Cheng, W.Y. and Jang, L., 2017. Making PVF porous sponge with and without using the pore- forming agent. *Journal of the Taiwan Institute of Chemical Engineers*, 74, 246-254.

[4] Xie, Y., Yi, Z.X., Wang, J.X., Hou, T.G. and Jiang, Q., 2018. Carboxymethyl konjac glucomannan - crosslinked chitosan sponges for wound dressing. *International Journal of Biological Macromolecules*, 112, 1225-1233.

[5] Champion, H.R., Bellamy, R.F., Roberts, C.P. and Leppaniem, A., 2003. A profile of combat injury. *The Journal of Trauma Injury Infection and Critical Care*, 54, 13-19.

[6] Kozen, B.G., Kircher, S.J., Henao, J., Godinez, F.S. and Johnson, A.S., 2008. An alternative hemostatic dressing: comparison of CELOX, HemCon, and QuikClot. *Academic Emergency Medicine*, 15, 74-81.

[7] Ward, K.R., Tiba, M.H., Holbert, W.H., Blocher, C.R., Draucker, G.T., Proffitt, E.K., Bowlin, G.L., Ivatury, R.R. and Diegelmann, R.F., 2007. Comparison of a new hemostatic agent to current combat hemostatic agents in a swine model of lethal extremity arterial hemorrhage. *The Journal of Trauma Injury Infection and Critical Care*, 63, 276-284.

[8] Kheirabadi, B. S., Acheson, E. M., Deguzman, R., Crissey, J. M., Delgado, A. V., Estep, S.J. and Holcomb, J.B., 2007. The potential utility of fibrin sealant dressing in repair of vascular injury in swine. *The Journal of Trauma Injury Infection and Critical Care*, 62, 94-103.

[9] Kauvar, D.S., Lefering, R. and Wade, C.E., 2006. Impact of hemorrhage on trauma outcome: an overview of epidemiology, clinical presentations, and therapeutic considerations. *The Journal of Trauma Injury Infection and Critical Care*, 60, 3-11.

[10] Heckbert, S.R., Vedder, N.B., Hoffman, W., Winn, R.K., Hudson, L.D., Jurkovich, G.J. and Maler, R.V., 1998. Outcome after hemorrhagic shock in trauma patients. *The Journal of Trauma Injury Infection and Critical Care*, 45, 545-549.

[11] Johnson, D., Bates, S., Nukalo, S., Staub, A., Hines, A., Leishman, T., Michel, J., Sikes, D., Gegel, B. and Burgert, J., 2014. The effects of quikclot combat gauze on hemorrhage control in the presence of hemodilution and hypothermia. *Annals of Medicine and Surgery*, 3, 21-25.

[12] Khoshmohabat, H., Paydar, S., Kazemi, H.M. and Dalfardi, B., 2016. Overview of agents used for emergency hemostasis. *Trauma Monthly*, 21(1), e26023.

[13] Achneck, H.E., Sileshi, B., Jamiolkowski, R.M., Albala, D.M., Shapiro, M.L. and Lawson, J. H., 2012. A comprehensive review of topical hemostatic agents: efficacy and recommendations for use. *Annals of Surgery*, 251, 217-228.

[14] Doppalapudi, S., Katiyar, S., Domb, A.J. and Khan, W., 2015. Biodegradable natural polymers. In: F. Puoci, ed. *Advanced Polymers in Medicine*. Switzerland: Springer International Publishing, pp. 33-66.

[15] Nair, L.S. and Laurencin, C.T., 2006. Polymers as biomaterials for tissue engineering and controlled drug delivery. *Advances in Biochemical Engineering/Biotechnology*, 102, 47-90.

[16] Salgado, A.J., Gomes, M.E., Chou, A., Coutinho, O.P., Reis, R.L. and Hutmacher, D.W., 2002. Preliminary study on the adhesion and proliferation of human osteoblasts on starch-based scaffolds. *Materials Science and Engineering*: C, 20, 27-33.

[17] Salgado, A.J., Coutinho, O.P. and Reis, R.L., 2004. Novel starch-based scaffolds for bone tissue engineering: cytotoxicity, cell culture, and protein expression. *Tissue Engineering*,10, 465-474.
[18] Salgado, A.J., Figueiredo, J.E., Coutonho, O.P. and Reis, R.L., 2005. Biological response to pre-mineralized starch based scaffolds for bone tissue engineering. *Journal of Materials Science: Materials in Medicine*, 16, 267-275.
[19] Torgbo, S. and Sukyai, P., 2018. Bacterial cellulose-based scaffold materials for bone tissue engineering. *Applied Materials Today*, 11, 34-49.
[20] Shibata, N., Nishumura, A., Naruhashi, K., Nakao, Y. and Miura, R., 2010. Preparation and pharmaceutical evaluation of new sustained-release capsule including starch-sponge matrix (SSM). *Biomedicine & Pharmacotherapy*, 64, 352-358.
[21] Malafaya, P.B., Stappers, F. and Reis, R.L., 2006. Starch-based microspheres produced by emulsion crosslinking with a potential media dependent responsive behavior to be used as drug delivery carriers. *Journal of Materials Science: Materials in Medicine*, 17, 371-377.
[22] Bice, C.W., MacMasters, M.M. and Hilbert, G.E., 1944. Proposed use of starch sponges as internal surgical dressings absorbable by the body. *Science*, 100, 227-228.
[23] Vasconcelos, D.C.L., Brandão, F.G., Nunes, E.H.M., Caldeira, L., Houmard, M., Musse, A.P., Hatimondi, S.A., Nascimento, J.F. and Vasconcelos, W.L., 2012. Synthesis and structural characterization of potato starch sponges. *Journal of Non-Crystalline Solids*, 358, 2663-2666.
[24] Korchin, L., 1956. An investigation to determine the effects of starch sponge implanted in bone. *Journal of Dental Research*, 35, 446-457.
[25] Niu, W., Wang, Y., Liu, Y., Zhang, B., Liu, M., Luo, Y., Zhao, P., Zhang, Y., Wu, H., Ma, L. and Li, Z., 2017. Starch-derived absorbable polysaccharide hemostat enhances bone healing via BMP-2 protein. *Acta Histochemica*, 119, 257-263.
[26] Hassan, C.M. and Peppas, N.A., 2000. Structure and applications of poly (vinyl alcohol) hydrogels produced by conventional crosslinking or by freezing/thawing methods. *Advances in Polymer Science*, 153, 37-65.
[27] Baker, M.I., Walsh, S.P., Schwartz, Z. and Boyan, B.D., 2012. A review of polyvinyl alcohol and its uses in cartilage and orthopaedic applications. *Journal of Biomedical Materials Research Part B: Applied Biomaterials*, 100, 1451-1457.
[28] Zhang, Y., Ye, L., Cui, M., Yang, B., Li, J., Sun, H. and Yao, F., 2015. Physically crosslinked poly(vinyl alcohol) - carrageenan composite hydrogels: pore structure stability and cell adhesive ability. *RSC Advances*, 5, 78180-78191.
[29] Baker, M.I., Walsh, S.P., Schwartz, Z. and Boyan, B.D., 2012. Polyvinyl alcohol in medicine and pharmacy: a perspective. *Journal of Biomedical Materials Research Part B: Applied Biomaterials*, 100, 1451-1457.
[30] Gaaz, T.S., Sulong, A.B., Akhtar, M.N., Kadhum, A.A.H., Mohamad, A.B. and Al-Amiery, A.A., 2015. Properties and applications of polyvinyl alcohol, halloysite nanotubes and their nanocomposites. *Molecules*, 20, 22833-22847.
[31] Bhardwaj, N. and Kundu, S.C., 2011. Silk fibroin protein and chitosan polyelectrolyte complex porous scaffolds for tissue engineering applications. *Carbohydrate Polymers*, 85, 325-333.
[32] Gontard, N., Guilbert, S. and Cuq, L., 1992. Edible wheat gluten films: influence of the main process variables on film properties using response surface methodology. *Journal of Food Science*, 58, 190-195.
[33] Nwokocha, L.M. and Ogunmola, G.B., 2014. Colour of starch-iodine complex as index of retrogradability of starch pastes. *African Journal of Pure and Applied Chemistry*, 8, 89-93.
[34] Huang, X., Sun, Y., Nie, J., Lu, W., Yang, L., Zhang, Z., Yin, H., Wang, Z. and Hu, Q., 2015. Using absorbable chitosan hemostatic sponges as a promising surgical dressing. *International Journal of Biological Macromolecules*, 75, 322-329.

[35] Kristen, H., Connie, C.Y., Joseph, S. and Abel, T., 2007. A clinically practical way to estimate surgical blood loss. *Dermatology Online Journal*, 13, 17.
[36] Algadiem, E.A., Aleisa, A.A., Alsubaie, H.I., Buhlaiqah, N.R., Algadeeb, J.B. and Alsneini H.A., 2016. Blood loss estimation using gauze visual analogue. *Trauma Monthly*, 21, 34131.
[37] Hamdan, S., Hashim, D.M.A., Ahmad, M. and Embong, S., 2000. Compatibility studies of polypropylene (PP)-sago starch (SS) blends using DMTA. *Journal of Polymer Research*, 7, 237-244.
[38] Ge, X.C., Xu, Y., Meng, Y.Z. and Li, R.K.Y., 2005. Thermal and mechanical properties of biodegradable composites of poly (propylene carbonate) and starch-poly (methyl acrylate) graft copolymer. *Composites Science and Technology*, 65, 2219-2225.
[39] Mano, J.F., Koniarova, D. and Reis, R.L., 2003. Thermal properties of thermoplastic starch/synthetic polymer blends with potential biomedical applicability. *Journal of Materials Science: Materials in Medicine*, 14, 127-135.
[40] Kaewtatip, K. and Tanrattanakul, V., 2008. Preparation of cassava starch grafted with polystyrene by suspension polymerization. *Carbohydrate Polymers*, 73, 647-655.
[41] Galdeano, M.C., Grossmann, M.V.E., Mali, S., Bello-Perez, L.A., Garcia, M.A. and Zamudio-Flores, P.B., 2009. Effects of production process and plasticizers on stability of films and sheets of oat starch. *Materials Science and Engineering: C*, 29, 492-498.
[42] Saiah, R., Sreekumar, P.A., Leblanc, N. and Saiter, J.M., 2009. Structure and thermal stability of thermoplastic films based on wheat flour modified by monoglyceride. *Industrial Crops and Products*, 29, 241-247.
[43] Lomelí-Ramírez, M.G., Kestur, S.G., Manríquez-González, R., Iwakiri, S., Muniz, G.B. and Flores-Sahagun, T.S., 2014. Bio-composites of cassava starch-green coconut fiber: part II-structure and properties. *Carbohydrate Polymers*, 102, 576-583.
[44] Muzzarelli, R.A.A., 2009. Chitins and chitosans for the repair of wounded skin, nerve, cartilage and bone. *Carbohydrate Polymers*, 76, 167-182.
[45] Wang, C.C., Su, C.H. and Chen, C.C., 2008. Water absorbing and antibacterial properties of N-isopropyl acrylamide grafted and collagen/chitosan immobilized polypropylene nonwoven fabric and its application on wound healing enhancement. *Journal of Biomedical Materials Research Part A*, 84, 1006-1017.
[46] Anisha, B.S., Sankar, D., Mohandas, A., Chennazhi, K.P., Nair, S.V. and Jayakumar, R., 2013. Chitosan-hyaluronan/nano chondroitin sulfate ternary composite sponges for medical use. *Carbohydrate Polymers*, 92, 1470-1476.
[47] Costa, E.D., Pereira, M.M. and Mansur, H.S., 2009. Properties and biocompatibility of chitosan films modified by blending with PVA and chemically crosslinked. *Journal of Materials Science: Materials in Medicine*, 20, 553-561.
[48] Parida, U.K., Nayak, A.K., Binhani, B.K. and Nayak, P.L., 2011. Synthesis and characterization of chitosan-polyvinyl alcohol blended with cloisite 30B for controlled release of the anticancer drug curcumin. *Journal of Biomaterials and Nanobiotechnology*, 2, 414-425.
[49] Vimala, K., Mohan, Y.M., Sivudu, K.S., Varaprasad, K., Ravindra, S., Reddy, N.N., Padma, Y., Sreedhar, B. and MohanaRaju, K., 2010. Fabrication of porous chitosan films impregnated with silver nanoparticles: a facile approach for superior antibacterial application. *Colloids and Surfaces B: Biointerfaces*, 76, 248-258.
[50] Hou, Y., Xia, Y., Pan, Y., Tang, S., Sun, X., Xie, Y., Guo, H. and Wei, J., 2017. Influences of mesoporous zinc-calcium silicate on water absorption, degradability, antibacterial efficacy, hemostatic performances and cell viability to microporous starch based hemostat. *Materials Science and Engineering C: Materials for Biological Applications*, 76, 340-349.
[51] Raymond, M.A., Smith, E.R. and Liesegang, J., 1996. The physical properties of blood-forensic considerations. *Science and Justice*, 36, 153-160.

The Response of the Mediterranean Fruit Fly, *Ceratitis capitata* (Wied.) (Diptera:Tephritidae) Males to Trimedlure Diluted with Some Fixed Oils

Sherihan M. Al-amin[1,2*], Moustafa M. El-metwally[1], Nashat A. Ali[1] and Abdel-all A. Abdel-all[2]

[1]Plant Protection Rsearch Institute, Agricultural Research Center, Cairo, Egypt
[2]Faculty of Science, Assuit University, Assuit, Egypt

Received: 28 September 2018, Revised: 11 February 2019, Accepted: 20 March 2019

Abstract

The Mediterranean fruit fly, *Ceratitis capitata* (Wiedemann) has a high economic importance because of its rapid development and wide host range in the world. The chemical production of synthesized sex pheromone, trimedlure (TML) is more expensive so there are new trends to reduce the cost of TML. In this study, some of the fixed oils (sunflower oil, corn oil, and paraffin oil) were used to dilute TML in two concentrations, 75% and 50% and tested in the field by Jackson trap for one month in two areas (Saheil-saliem and Elbadary) in Assuit Governorate. In the first district (Saheil-saliem), no significant differences were found along the exposure of all treatments under normal field conditions except at TML-C 50% which was the lowest response (relative attractiveness of 11.92%). In the second district (Elbadary), TML-PF 75%, TML-SF 75% and TML-SF 50% showed highly significant differences when compared with other treatments but no significant differences among these three treatments were appeared. Infrared analysis (IR) and GC analysis were achieved on TML before and after dilution. According to IR analysis, it was found that there were no new function groups appeared after dilution with any fixed oils. Besides, no changes in retention time of TML after dilution were detectedin GC analysis.

Keywords: Medfly, MFF, trimedlure, TML, fixed oil, effectiveness, Jackson trap
DOI 10.14456/cast.2019.10

1. Introduction

The Mediterranean fruit fly, *Ceratitis capitata* (Wiedemann) is the dangerous fruit pest because the diversity of its hosts and its ability to tolerate cooler climates are better than most other species of tropical fruit flies. Its life cycle is short and has heavy populations. Early detection of incipient infestations of *C. capitata* is essential because it allows both the delimitation of the outbreak and the implantation of control and eradication measures while the pest population is still small.A rapid response not only limits crop damage but also reduces the programmatic costs incurred in the eradication effort [1, 2]. Alternatives were investigated to reduce production costs and volatility of trimedlure (TML) and capilure (CPL) containing TML plus extenders and enriched ginger root oil (EGRO) containing the male attractant α-copaene, have been compared with TML[3].

*Corresponding author. E-mail: tamersherihan@gmail.com

TML was used as sex pheromone to attract males of *C. capitata*. Regarding the latter, TML is now the standard male medfly attractant in USA detection programs and is deployed in solid dispensers (polymeric plugs) containing 2 g of the lure (and no toxicant) that are placed in Jackson traps, which in turn are suspended within the canopy of host trees [4].

TML provides a successful monitoring program by timing pesticide sprays more accurately. As TML is itself fairly expensive to be produced and also has high volatility, thus the objective of this work is to reduce the high price of this synthetic pheromones by diluting pure crude material by 50% with fixed oils. Three fixed oils were used in this experiment; corn oil, sunflower oil, and paraffin oil. TML was diluted with these oils into two concentrations, 75% and 50%. Comparison among different concentrations of TML was investigated under field conditions and detection response of adult's males to these treatments was also recorded.

2. Materials and Methods

2.1 Study area and orchards

The experiment was carried out in Assuit Governorate, Egypt in two locations (with high infestation by *Ceratitis capitata,* Mediterranean fruit fly or medfly or MFF): Saheil-saliem and Elbadary in about two feddans in mandarin orchards.

2.2 Experimentation

Three fixed oils, i.e. sunflower oil, corn oil and paraffin oil, were mixed with crude TML in two concentrations: 75% and 50%. A 2 cm-long wick was saturated with 2 ml of the treatments and hanged in Jackson trap. Jackson traps were prepared to hang on the tree at the height of 1.5-2 m. Three replicates were achieved for each treatment. The replicates were distributed randomly in the field and the distance between two adjacent was about 35 m to avoid interactions among treatment. A survey was done weekly for 5 weeks. A captured fly per trap per day (CTD) was weekly calculated.

2.3 Data analysis

Statistical analysis was done by one-way ANOVA. Two types of chemical analysis were achieved on TML and its dilutions. By using FTIR and GC analyses, a change of basic structure of TML is recorded. The infrared absorption spectrum of TML (before dilution), TML with corn oil (1:1), TML with sunflower oil (1:1) and TML with paraffin oil (1:1) was carried out.

3. Results and Discussion

3.1 The efficacy of TML and its response in the field before and after its dilution

3.1.1 The first district

Data presented in Tables 1 and 2 showed the response of MFF males to different TML concentrations. In Table 1, the result was recorded throughout the period of exposure in the field, by using L. S. D. test at probability 5% significant differences among all treatments in all concentrations. The efficiency of MFF males attracted to traps was observed during each weeks of exposure. When comparing TML as crude substance (98%) with TML diluted with paraffin oil (TML-PF 50% and TML-PF 75%), TML diluted with sunflower oil (TML-SF 50% and TML-SF 75%), and TML diluted with corn oil (TML-C 50% and TML-C 75%) on the first week, there were significance differences among TML 98% and other diluted TML with TML-SF 50% showed the

lowest result (2.35). There were no significant differences among the exposure period on the 2nd week. The response in the 5th week was generally higher than other weeks. On an average, no significant differences were recorded among the exposure of all treatments under normal field conditions, except at TML-C 50% which was significantly lower than other exposures (3.62).

Among all concentrations used throughout the first three weeks of study, no significant differences on the efficiency of MFF males attracted to traps were observed except for 98% concentration in the 1st week, which was significantly higher (7.74) than other tested concentrations. In the 4th week of study, no significant differences on the efficiency of MFF males attracted to traps were observed among all concentrations, except at TML-C 50%, which was significantly lower (2.39) than other tested concentrations. In the fifth week of study, TML-C 75% was superior (8.92).

In Table 2, it shows the efficiency of TML-baited Jackson traps and its different concentrations for five weeks. For TML aged one week, the attractiveness to MFF males was 31.63% but the efficiency gradually decreased to 14.12% after five weeks of exposure under normal field conditions. For TML-PF 75%, it showed more or less the same percentage of efficiency along the experiment procedure. However, the relative attractiveness of TML-PF 50% was higher when compared to week one and reached the highest efficiency in the 4th week at 19.55%. The high efficiency of TML-SF 75% was in the 2nd week at 21.85% while the efficiency of TML-SF 50% was 17.01% when the age of lure was in the 3rd week.

General means of males' number of CTD over the tested period of study (5 weeks) were 5.51 for 98%, 4.04 for 75% and 4.77 for 50% (diluted by paraffin oil), 4.79 for 75% and 4.11 for 50% (diluted by sun flower oil), 5.67 for 75% and 3.62 for 50% (diluted by corn oil) (Table 1). Values of average percentages of attracted males through 5 weeks were 18.06%, 13.05%, 14.61%, 15.88, 12.81, 14.83 and 10.93% for concentrations at 98%, TMC-PF 75%, TMC-PF 50%, TML-SF 75%, TML-SF 50%, TML-C 75% and TML-C 50%, respectively (Table2). These results indicated that there was semi-equal of the efficacy of each treatment towards adult males of MFF along the experiment and TML-C 50% was the lowest.

Table 1. Responses of MFF males to different concentrations of TML under field conditions in mandarin orchards in Saheil-saliem district.

Concentration of TML	Oil	Weeks of inspection*					General mean*
		1st	2nd	3rd	4th	5th	
98%	-	7.74[a]	2.93[a]	5.70[a]	4.50[a]	6.57[a]	**5.51[a]**
75%	TML-PF	3.46[b]	3.07[a]	3.82[a]	4.54[a]	5.28[b]	**4.04[a]**
50%		2.21[b]	2.75[a]	6.00[a]	6.39[a]	6.50[a]	**4.77[a]**
75%	TML-SF	4.57[b]	4.64[a]	4.03[a]	3.92[a]	6.78[a]	**4.79[a]**
50%		1.75[b]	3.21[a]	5.71[a]	4.61[a]	5.25[b]	**4.11[a]**
75%	TML-C	2.39[b]	2.03[a]	5.42[a]	6.32[a]	8.92[a]	**5.67[a]**
50%		2.35[b]	2.61[a]	2.89[a]	2.39[b]	7.85[a]	**3.62[b]**
L.S.D 5%		**3.13**	**2.82**	**2.51**	**2.63**	**2.98**	**1.55**

Note: TML=Trimedlure PF=paraffin oil SF= sunflower C= Corn oil p value < 0.05
*Different superscript letters in the same column means significant different.

Table 2. The relative attractiveness of MFF males captured into traps loaded with different TML concentrations in Saheil-saliem district.

Concentration of TML	Oil	Weeks of inspection					General mean
		1st	2nd	3rd	4th	5th	
98%	-	31.63%	13.79%	16.98%	13.77%	14.12%	**18.06%**
75%	TML-PF	14.14%	14.45%	11.41%	13.89%	11.35%	**13.05%**
50%		9.43%	12.95%	17.87%	19.55%	13.27%	**14.61%**
75%	TML-SF	18.78%	21.85%	12.00%	11.99%	14.76%	**15.88%**
50%		6.42%	15.11%	17.01%	14.11%	11.41%	**12.81%**
75%	TML-C	9.96%	9.56%	16.15%	19.34%	19.16%	**14.83%**
50%		9.61%	12.37%	8.61%	7.32%	16.76%	**10.92%**
Total		100.0%	100.0%	100.0%	100.0%	100.0%	**100.0%**

3.1.2 The second district

The results for the second district was presented in Table 3. In the first week, there were no significant differences among all different concentrations in captured *C. capitata* with L.S.D 5% of 2.90 except at TML-PF 50% with the lowest response of 1.17 whereas at TML-SF 50% gave the highest response of 9.46 in comparation with other treatments (Table 3). For lures aged 2 weeks, TML-SF 75% baits resulted in significantly higher trap captures (9.85) than others. In the 3rd week, TML-PF 75% had highly significant trap captures (5.21) whereas TML-C 50% had the lowest significant in the number of male medflies (2.28). In the 4th week, there were no significant differences among TML-SF 50%, TML-C 75% and TML-C 50%. Also, there were no significant differences among these three concentrations in the 5th week. In general, along with the exposure of all treatments under normal field condition, TML-PF 75%, TML-SF 75% and TML-SF 50% had highly significant differences in comparison with other treatments followed by crude substance at 98%.

Table 4 showed the percentage of the attractiveness of each treatment. Within the experiment, the percentage of attracting of adult males of MFF varied from week to week. For the lure aged 1 week, TML-SF 75% and TML-SF 50% gave higher efficiency than other lures with the efficiency of 20.61% and 32.13%, respectively. In the 2nd week, TML-SF 75% still showed higher efficiency than other lures (19.63%). For lures aged 3 weeks, TML-PF 75% and TML-SF 75% had higher efficiency at 21.37% and 19.77% in capture males of *C. capitata*. In the 4th week, TML (98%) and TML-PF 75% were superior than other treatments with the efficiency of 32.63% and 26.30%, respectively. In the 5th week, TML-PF 75% and TML-PF 50% had the higher efficiency at 28.17% and 20.26%, respectively. A high percentage of attracting the pest was TML 98% in the 4th week with 32.63% whereas TML-C 75% and TML-C 50% showed the lowest attractive along the exposure. Generally, TML-PF 75%, and TML-SF 75% were higher attractiveness to MFF adult males with 20.95% and 17.69%, respectively and TML-C 75% and TML-C 50% had the lowest attraction of 7.10% and 8.51%, respectively.

Table 3. Responses of MFF males to different concentrations of TML under field conditions in mandarin orchards in Elbadary district.

Concentration of TML	Oil	Week of inspection*					General mean*
		1st	2nd	3rd	4th	5th	
98%	-	2.82^{bc}	7.82^{abc}	3.18^{abc}	3.76^{a}	0.46^{b}	**3.59^{ab}**
75%	TML-PF	3.78^{bc}	7.92^{ab}	5.21^{a}	3.03^{ab}	1.53^{a}	**4.30^{a}**
50%		1.17^{c}	5.32^{b}	3.50^{abc}	1.42^{bc}	1.10^{ab}	**2.51^{b}**
75%	TML-SF	6.07^{b}	9.85^{a}	4.82^{ab}	1.75^{bc}	0.75^{ab}	**4.56^{a}**
50%		9.46^{a}	8.00^{ab}	2.67^{bc}	0.86^{c}	0.53^{b}	**4.31^{a}**
75%	TML-C	3.32^{bc}	5.82^{ab}	2.71^{bc}	0.35^{c}	0.53^{b}	**2.35^{b}**
50%		2.82^{bc}	5.43^{b}	2.28^{c}	0.35^{c}	0.53^{b}	**2.39^{b}**
L.S.D 5%		**2.90**	**2.89**	**1.98**	**1.80**	**0.76**	**1.20**

Note: TML=trimedlure PF=paraffin oil SF=sunflower oil C=corn oil p value< 0.05
***** Different superscript letters in the same column means significant different.

Table 4. The relative attractiveness of MFF males captured into traps loaded with different concentrations of TML in Elbadary district.

Concentration of TML	Oil	Weeks of inspection					General mean
		1st	2nd	3rd	4th	5th	
98%		9.66%	15.59%	13.04%	32.63%	8.47%	**15.88%**
75%		13.14%	15.78%	21.37%	26.30%	28.17%	**20.95%**
50%	TML-PF	3.97%	10.61%	14.36%	12.32%	20.26%	**12.30%**
75%		20.61%	19.63%	19.77%	15.19%	13.28%	**17.69%**
50%	TML-SF	32.13%	15.95%	10.95%	7.46%	9.76%	**15.23%**
75%		11.27%	11.61%	11.12%	3.03%	9.76%	**7.10%**
50%	TML-C	9.57%	10.82%	9.36%	3.03%	9.76%	**8.51%**
Total		100%	100%	100%	100%	100%	**100%**

3.2 The chemical structure of TML before and after dilution with some fixed oils

From IR and GC analysis, it was found that the infrared absorption spectrum of each solution showed the same characteristic of maximum absorption bands as presented in Figures 1-4 and there were no new function groups appeared after dilution.

The characteristic band at 2,957.16 cm^{-1} was corresponding to aliphatic cyclohexane, ester group forming 1,780.73 cm^{-1} was corresponding to carbonyl group band and C-O group at 1,280.21 cm^{-1}, methyl group band at 1,457.20 cm^{-1} and chlorine group occurred at 845.70 cm^{-1}. All these functional groups occurred after dilution with any oil used in this study.

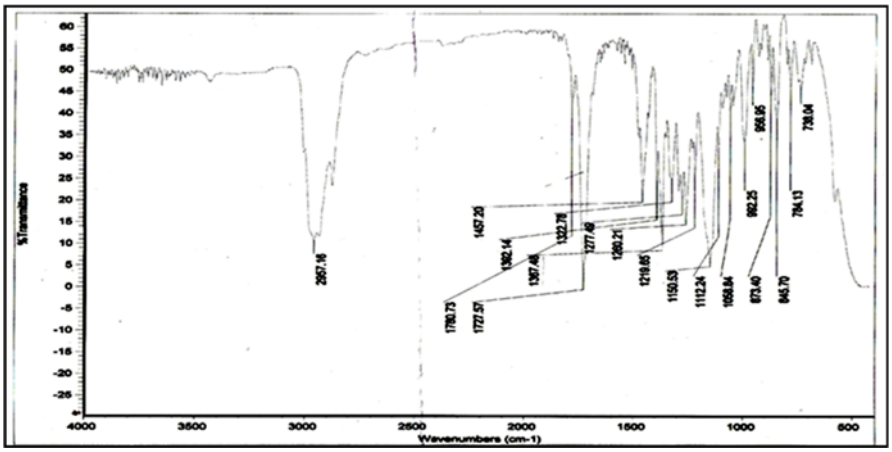

Figure 1. IR spectrum of TML before dilution

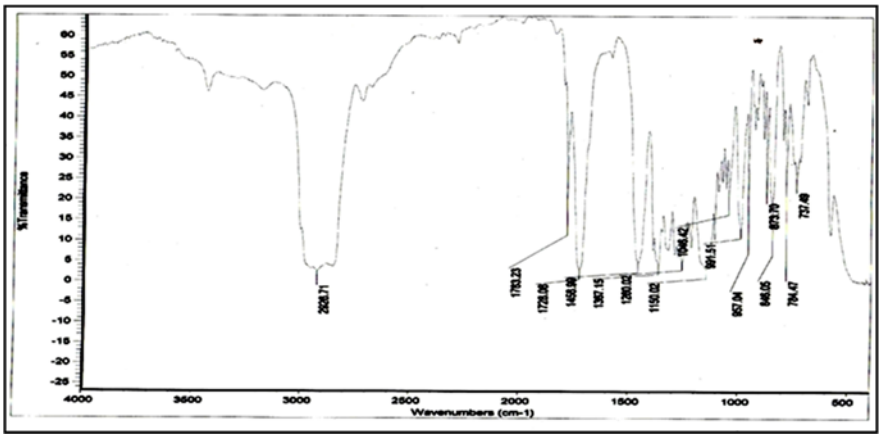

Figure 2. IR spectrum of TML after dilution with paraffin (1:1) showing no new function group

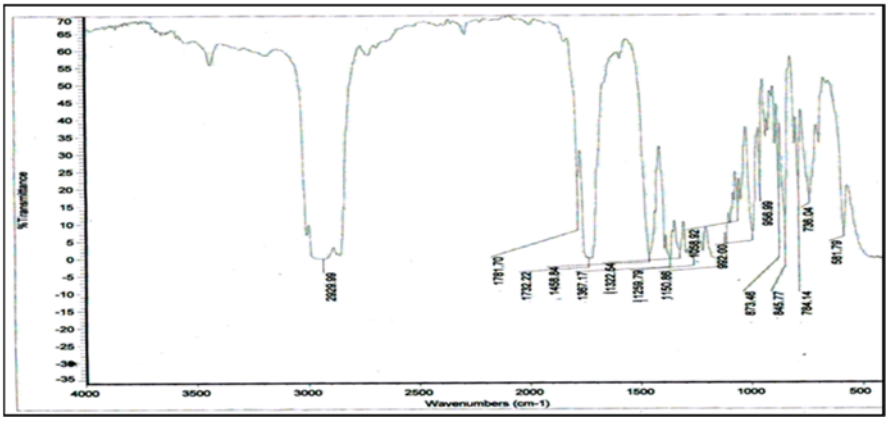

Figure 3. IR spectrum of TML after dilution with corn oil (1:1) showing no function group appeared compared to reference

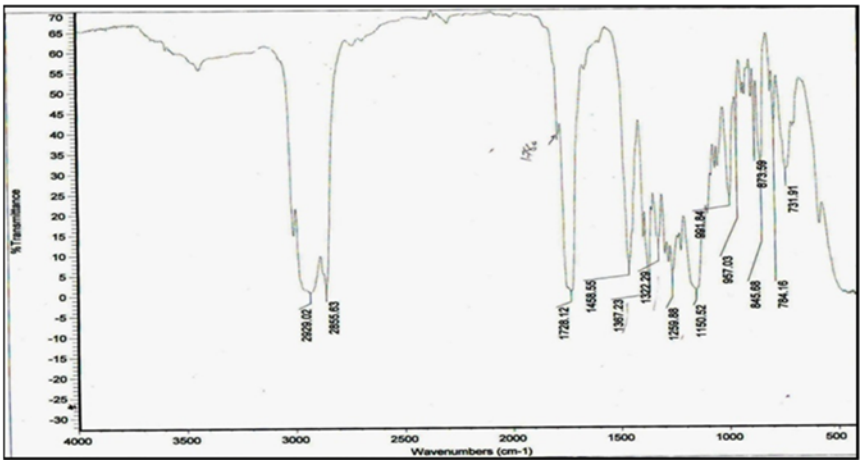

Figure 4. IR spectrum of TML after dilution with sunflower oil (1:1) showing no function groups appeared compared to reference

Another chemical analysis was achieved through GC analysis of each solution; TML before and after dilution, and analysis of each oil. For TML after dilution with each oil, it was found that there was no change in retention time approximately to any diluted solution that appeared at 0.395, 1.415, 1.400, 1.400, 1.395, 1.400 and 1.395 min of TML, sunflower oil, corn oil, paraffin oil, TML-PF 50%, TML-SF 50%, and TML-C 50%.

TML has retention time at 0.395 min. Disappearance of TML retention time after dilution may be due to the composition of new unstable hydrogen bonds between the oil and TML that make them miscible together. However, no change in the main chemical structure of TML or TML was broken at the beginning of injection at boiling point temperature (104-134˚C) lower than that used in diluted solution (200-250˚C).

The reasons of dilution of TML with these oils can be summarized as follows:

1) Paraffin oil, corn oil and sunflower oil were fixed oils and used as carrier oil. Unlike essential oils, they do not contain concentrated aroma, have mild distinctive smell and do not evaporate. The use of carrier oils should be as natural and clear as possible. Carrier oils can be easily blended to combine their properties of viscosity, acceptability, lubrication, absorption, and aroma and so forth [5].

2) TML has ester group and the tested oils also have ester group, that means high miscibility without any change in basic structure of TML, as shown in Figures 1-4.

3) Each oil used in this study is cheap and available in markets.

3.3 Discussion

The pheromone is a complex medley having three to five major components that attract females [6, 7] plus at least 50 minor components whose function has not been elucidated [8]. Gas chromatograph and IR spectrum analyses indicated that there are changes in the main chemical structure of TML. Because of its high cost and its high volatility, recent researches focused attention on several alternatives that were effective male lures towards the medfly. Ceralure, an iodinated analogue of TML, was shown to be 4-9 times as attractive to male medflies as TML [9, 10]. Capilure, that replaces a portion of TML with proprietary extenders that evaporate [11, 12], was used for *C. capitata* detection [3, 4, 13-15]. In addition to these TML-based alternatives,

enriched ginger root oil (*Zingeber officinale* L.), which contained α-copaene, was used as attractant to male medflies [3, 16-19] that may be more superior than TML.

The results of our experiments confirm the finding of El - Abbassi and El - Metwally [20] who tested the efficiency of different concentrations of sex attractant trimedlure (TML) diluted with paraffin oil on attractant males of the Mediterranean fruit fly, *C. capitata* (Wiedemann). They found that 75% concentration of TML was superior to 98% concentration throughout 8 weeks and especially in guava orchards. Data obtained from these trials are in agreement with results reported by Jang *et al.* [10] who found that doses of (-) ceralure B1 of 87.5% and 75% were as effective as 98% concentration in attracting med fly. Jang *et al*. [9] also found that in outdoor olfactometer cage and in field tests, there were no significant differences in medfly male capture into traps loaded with 10.0 µg and 1.0 µg of TML. Moreover, in the second week captures at traps baited with 10 mg TML decreased drastically and they were not significantly greater than control. Our results were also in alignment with data obtained by Khrimian *et al*. [21] and Khrimian [22] who developed an easier synthesis of the racemic ceralure B1, and subsequent studies showed that >75% optically pure (-)-ceralure B1 could be as effective as the 98% (-)-ceralure B1, and the racemic ceralure B1 was also attractive. The results of our experiments confirm the finding of Nabih [23] who mentioned that no significant differences between ginger oil of purity 100% and ginger oil 75% in attracting MFF males.

Early detection of incipient infestations of *C. capitata* is essential because it allows both the delimitation of the outbreak and the implantation of control and eradication measures while the pest population is still small. A rapid response of *C. capitata* to TML not only limits crop damage but also reduces the programmatic costs incurred in the eradication effort [1, 2].

The chemical structures of trimedlure or TML before and after dilution do not change. There are no change in chemical structures of main compound (TML) in comparison to TML before dilution and no new function groups appear in any treatment comparative to target material (TML). Thus, the efficacy of TML after dilutions was not affected. This work is the first time of applying diluted TML which indicates the economic importance for the application in the field because it can give similar result as crude TML (98%).

4. Conclusions

In conclusion, dilution of trimedlure or TML with some of the fixed oils as carriers to avoid the interaction between TML and the diluted substances can also be used for attracting adult males of MFF besides the use of pure TML. This procedure will reduce the cost of TML by diluting 1l of TML to 2l with fixed oils like paraffin oil, sunflower oil and corn oil. These oils are cheap, available and not volatile for a longer period that enable TML to keep its effectiveness in the field for a long time without renewal preparations.

References

[1] Lace, D.R. and Gates, D.B., 1994. Sensitivity of detection trapping systems for Mediterranean fruit flies (Diptera:Tephritidae) in southern California. *Journal of Economic Entomology*, 87, 1377-1383.

[2] Papadopoulos, N. T., Katsoyannos, B. I., Kouloussis, N. A., Hendarichs, J., Carey, J. R. and Heath, R. R., 2001. Early detection and population monitoring of *Ceratitis capitata* (Diptera: Tephritidae) in a mixed fruit orchard in northen Greece. *Journal of Economic Entomology*, 94(4), 971-978.

[3] Shelly, T.E., 2013. Detection of male Mediterranean fruit flies (Diptera: Tephritidae) : performance of trimedlure relative to capilure and enriched ginger root oil. *Proceedings of the Hawaiian Entomological Society*,45, 1-7.

[4] International Atomic Energy Agency, 2003. *Trapping Guidelines for Area-wide Fruit Fly Programmes*., Vienna: IAEA.

[5] Thomas, D. B., Holler, T.C., Heath, R. R., Salinas, E. J. and Moses, A. L., 2001. Trap-lure combinations for surveillance of *Anastrepha* fruit flies (Diptera: Tephritidae) . *Florida Entomologist* 84(3), 344-351.

[6] Heath, R. R., Landolt, P. J., Tumlison, J. H., Chambers, D. L. Murphy, R. E., Doolihle, R. E., Dueben, B.D., Sivinski, J. and Calkins, C.O., 1991. Analysis, synthesis, formulation, and field testing of three major components of male Mediterranean fruit fly pheromone. *Journal of Chemical Ecology*,17(9), 1925-1940.

[7] Jang, E. B., Light, D. M., Binder, R. G., Flath, R. A. and Carvalho, L. A., 1994. Attraction of female Mediterranean fruit flies to the 5 major components of males produced pheromone in a laboratory flight tunnel. *Journal of Chemical Ecology*, 20, 9-20.

[8] Jang, E.B., Light, D.M., Dickens, J.C., McGovern, T.P. and Nagata, J.T., 1989. Electroantennogram responses of Mediterranean fruit fly, *Ceratitis capitata* (Diptera: Tephritidae) to trimedlure and its trans- isomers. *Journal of Chemical Ecology*, 15, 2219-2231.

[9] Jang, E. B., Holler, T., Cristofaro, M., Lux, S., Raw, A. S., Moses, A. L. and Carvalho, L. A., 2003. Improved attractants for Mediterranean fruit fly, *Ceratitiscapitate* (Wiedemann) : responses of sterile and wild flies to (-) enantimer of ceralure B1. *Journal of Economic Entomology*, 96, 1719-1723.

[10] Jang, E.B., Kharimian, A., Holler, T.C., Cassana-Giner, V., Lux, S. and Carvalho, L.A., 2005. Field response of Mediterranean fruit fly (Diptera: Tephritidae) to ceralureB1: evaluations of enantiomeric B1 ratios on fly captures. *Journal of Economic Entomology*, 98, 1139-1143.

[11] Leonhardt, B. A., Rice, R. E., Harte, E. M. and Cunningham, R. T., 1984. Evaluation of dispensers containing trimedlure, the attractant for the Mediterranean fruit fly (Diptera:Tephritidae). *Journal of Economic Entomology*, 77, 744-749.

[12] King, J. R and Landot, P. J., 1984. Rates of loss of trimedlure from cotton wicks under South-Florida field conditions. *Journal of Economic Entomology*, 77, 221-224.

[13] Baker, P. S., Hendrichs, J. and Liedo, P., 1988. Improvement of attractant dispensing systems for the Mediterranean fruit fly (Diptera: Tephritidae) sterile release program in Chiapas,Mexico. *Journal of Economic Entomology*, 81, 1068-1072.

[14] Nackagwa, S., Harris, E. J. and Keiser, I., 1981. Performance of capilure in capturing Mediterranean fruit flies in Steiner plastic or cardboard sticky traps. *Journal of Economic Entomology*, 74, 244-245.

[15] Rice, R. E., Cunningham, R. T. and Leonhardat, B. A., 1984. Weathering and efficiency of trimedlure dispensers for attraction of Mediterranean fruit flies (Diptera: Tephritidae). *Journal of Economic Entomology*, 77, 750-756.

[16] Flath, R. A., Cunningham, R. T., Mon, T. R. and John, J. O., 1994. Additional male Mediterranean fruit fly (*Ceratitis capitata* Wied.) attractants from Angelica seed oil (*Angelica archangelica* L.). *Journal of Chemical Ecology,* 20, 1969-1984.

[17] Flath, R.A., Cunningham, R.T., Mon, T.R. and John, J.O., 1994. Male lures for Mediterranean fruit fly (*Ceratitis capitata* Wied.): structural analogs of α-copaene. *Journal of Chemical Ecology,* 20, 259-2609.

[18] Mwatawala, M., Virigilio, M., Quilici, S., Dominic, M. and De Meyer, M., 2012. Field evaluation of the relative attractiveness of enriched ginger root oil (EGO) lure and trimedlure for African *Ceratitis* species (Diptera: Tephritidae). *Journal of Applied Entomology*, 137 (5), 321-400.
[19] Shelly, T. E. and Pahio, E., 2002. Relative attractiveness of enriched ginger root oil and trimedlure to male Mediterranean fruit flies (Diptera: Tephritidae). *Florida Entomologist,* 85 (4),545-551.
[20] El- Abbassi, T. S. and El- Metwally, M. M., 2013. Response of the Mediterranean fruit fly, (*Ceratitis capitata* Wied.) males to different concentrations of trimedlure under field conditions in Egypt. *Bullitin of the Entomological Society of Egypt* (unpublished data).
[21] Khrimian, A., Margaryoan, A. K. and Schmidt, W. F., 2003. An improved synthesis of ethyl cis-5-iodo-trans-2-methyl cyclohexanecaroboxylate, a potent attractant for the Mediterranean fruit fly. *Tetrahydron*, 59,5475-5480.
[22] Khrimian, A., 2004. *Method of the Synthesis of Ceralure B1*. U.S. Patent6, 777,573.
[23] Nabih, S. A., 2013. *Extraction and Analysis of Some Fruit Flies Attractants*. MSc. Mansoura University.

The Lyapunov Analyses of MERS-Cov Transmission in Thailand

Jiraporn Lamwong[1], Puntani Pongsumpun[2*], I-Ming Tang[3] and Napasool Wongvanich[4]

[1]Department of Fundamental Applied Sciences, Thatphanom College, Nakhon Phanom University, Nakhon Phanom, Thailand
[2]Department of Mathematics, Faculty of Science, King Mongkut's Institute of Technology Ladkrabang, Bangkok, Thailand
[3] Computational and Applied Science for Smart Innovation Cluster (CLASSIC), Faculty of Science, King Mongkut's University of Technology Thonburi, Bangkok, Thailand
[4]Department of Instrumentation and Control Engineering, Faculty of Engineering, King Mongkut's Institute of Technology Ladkrabang, Bangkok, Thailand

Received: 4 March 2019, Revised: 4 April 2019, Accepted: 4 April 2019

Abstract

This work investigates the transmission model of MERS-Cov using SEIR model which divides the total human population into four subclasses: susceptible, exposed, infected and recovered. Two equilibrium points were exhibited: the disease-free equilibrium E_1^* and the endemic equilibrium E_2^*. The basic reproduction number was computed via the next generation method. Two types of global stability of these equilibrium points were investigated through the theory of Lyapunov. Specifically, the exponential stability was investigated using a square type Lyapunov candidate function; while the asymptotic stability was investigated through a Logarithm type Lyapunov candidate function. It is theoretically shown that, when the reproductive number is less than unity. The disease-free equilibrium state is globally asymptotically stable, and the endemic equilibrium state is globally asymptotically stable if the reproductive number is greater than unity. Numerical results with parameters obtained from the previous work also illustrates the global asymptotical stability of the MERS-Cov system. These results can further be used for the design of a controller that drives the MERS-Cov system and the effective control reproductive number is less than 1 so that the stability of the controlled system would be similar to that of the uncontrolled disease-free system.

Keywords: Global dynamical modeling method, Lyapunov function method, MERS, transmission model, basic reproductive number, next generation method, disease-free equilibrium state, endemic equilibrium state
DOI 10.14456/cast.2019.11

*Corresponding author: Tel.:662-329-8000 Ext. 6196 Fax: 662-329-8412
E-mail: kppuntan@kmitl.ac.th

1. Introduction

MERS-Cov is the short name for Middle East Respiratory Syndrome. Cov has been added since the disease was caused by a corona virus. It was first detected in 2012 in Saudi Arabia as a case of severe viral pneumonia which developed to a case of acute respiratory distress syndrome and death [1]. In Thailand, the first case was a 75 years old male from Oman, who was reported with the symptoms on 18 June 2015. On 23 January 2016, a second case from an Arab person was reported.The third case was reported in a person from Kuwait on 30 July 2016.MERS-Cov transmission has been found in many countries around the world; Asia, Europe, the United States and North Africa. World Health Organization (WHO) reported 2,123 laboratory-confirmed infection cases with corona virus world wide, including at least 740 deaths in 27 countries during September 2012 to January 2018 [2].

On 23 August 2017, the one additional Middle East Respiratory Syndrome (MERS-Cov) case was reported by the national IHR focal point of the United Arab Emirates (UAE) [3].The risk assessment by WHO indicates that MERS-Cov causes severe human infections resulting in high mortality and has demonstrated the ability to transmit between humans. So far, the observed human-to-human transmissions have occurred mainly in health care settings. Figure 1 shows the confirmed cases of infections and deaths in 2016, with peaks around March, July and October. It is implied that MERS-Cov infection cases occur worldwide.

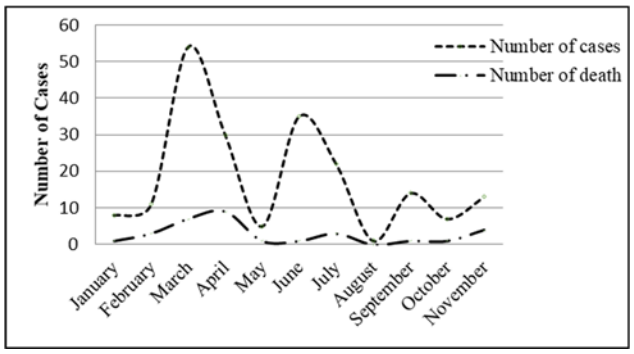

Figure 1. Confirmed global cases and death of MERS from 1 January 2016 to15 November 2016 [4].

In 2013, Aburizaiza *et al.*[5] investigated the Anti–Middle East Respiratory Syndrome Antibodies in Blood Donors and Slaughterhouse workers in Jeddah and Makkah. Their investigation looked for the antibodies using immune fluorescence assay (IFA) , a differential recombinant IFA, and a plaque-reduction serum neutralization assay. Altogether, 130 blood donors were sampled during 2012 in Jeddah and 226 slaughter house workers were sampled in October 2012 in Jeddah and Makkah, Saudi Arabia. In 2014, Chowell *et al.* [6] formulated a mathematical model to study the outbreak of MERS-Cov during April-October 2013 in Arabian Peninsula. Kim *et al.* [7] studied MERS-Cov transmission dynamics in South Korea, resulting in the formulation of SEIAHR model (susceptible-exposed- infectious- infection but asymptomatic-hospitalized-recovery). They found the basic reproductive number in two periods. First period was very large due to the superspreader. The second period was reduced significantly after intensive interventions to reduce the basic reproduction number. The literature reviews arouses our interests in the development of the mathematical model and Lyapunov stability analyses. This work considers the global dynamical transmission model, where three types of stability, namely, local, exponential and asymptotic stabilities were investigated through the use of the Lyapunov function

candidates. Specifically, the square-type Lyapunov functions were used to show the exponential stability of the equilibrium points, while the logarithmic-type Lyapunov candidates was chosen to illustrate the global asymptotical stability of the equilibrium points. The next generation method was also applied to compute the basic reproductive number.

2. Formulation of the Model and Stability Analyses

In this model, we study Susceptible-Exposed-Infected-Recovered (or SEIR) model to describe the dynamical transmission of MERS in Thailand.We assume that the transmission of corona virus is possible only through the pathway of person-to-person contacts, not through the camel-to-person contacts, which would be possible if we were considering the situation in Saudi Arabia. The human population is classified into four sub-classes: susceptible individuals (S^h), exposed individuals (E^h), infected individuals (I^h) and recovered individuals (R^h). The total population of the human at time t is denoted $N^h(t)$ where $N^h(t) = S^h(t) + E^h(t) + I^h(t) + R^h(t)$. Human recruitment rate is denoted as B and δdenotes the rate at human-to-human MERS-Cov contract occurs. The rate of expose for susceptible human is given by $\frac{\delta S^h I^h}{N^h}$. The rate at which the exposed human become infected is denoted as φ. Recovery rate of human with MERS-Cov is γ. where μ and α are the natural death rate and the additional disease death rate due to the MERS-Cov infection, respectively. The number of members in the susceptible class is increased by the human recruitment rate B and reduced by infection and the natural death. The exposed population is increased by the infection of a susceptible, but is reduced through natural death. The infected population increases when an exposed person becomes infectious but is diminished by recovery from the disease, natural death and additional disease death. The recovered population is increased by the recovery of infected person and decreased by a natural death. The transmission schematic is shown in Figure 2.

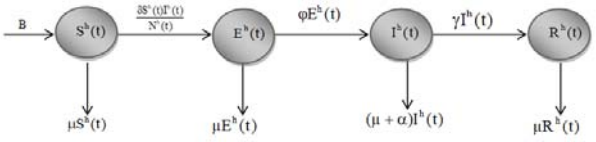

Figure 2. Flow chart of transmission model of human population

The transmission flow chart admits the following system of differential equations defined:

$$\frac{dS^h}{dt} = B - \left(\mu + \frac{\delta I^h}{N^h}\right) S^h \tag{1}$$

$$\frac{dE^h}{dt} = \frac{\delta S^h I^h}{N^h} - (\mu + \varphi) E^h \tag{2}$$

$$\frac{dI^h}{dt} = \varphi E^h - (\mu + \alpha + \gamma) I^h \tag{3}$$

$$\frac{dR^h}{dt} = \gamma I^h - \mu R^h \tag{4}$$

The non-negativeness of the solutions

Proposition 1 Let $(S^h(t), E^h(t), I^h(t), R^h(t))$ be the solutions of equations (1)-(4).

Denoting also the invariant set $\phi = \left\{(S^h, E^h, I^h, R^h) \in R_+^4 : N^h \le \frac{B}{\mu}\right\}$. Then the closed set ϕ is positive invariant.

Proof We begin by setting $N^h(t) = (S^h + E^h + I^h + R^h)$ and assume that $N^h = \frac{B}{\mu}$. Note that the total population N^h is non-negative definite on R_+^4 Then we have:

$$\frac{dN^h}{dt} = \frac{dS^h}{dt} + \frac{dE^h}{dt} + \frac{dI^h}{dt} + \frac{dR^h}{dt}$$

$$\frac{dN^h}{dt} = B - \left(\mu + \frac{\delta I^h}{N^h}\right) S^h + \frac{\delta S^h I^h}{N^h} - (\mu + \varphi) E^h + \varphi E^h - (\mu + \alpha + \gamma) I^h + \gamma I^h - \mu R^h$$

$$\frac{dN^h}{dt} = B - \mu N^h - \alpha I^h \le B - \mu N^h$$

Then it follows that $\frac{dN^h}{dt} \le 0$ on $0 \le N^h(t) \le N^h(0) e^{-\mu t} + \frac{B}{\mu}(1 - e^{-\mu t})$. As $t \to \infty, e^{-\mu t} \to \infty$ and we have $\lim_{t \to \infty} N^h(t) \le \frac{B}{\mu}$, $N^h(t)$ approaches $\frac{B}{\mu}$. Since the region of all solutions of ϕ is in R_+^4.

2.1 Equilibrium Points

Proposition 2 Equations (1)-(4) have two equilibrium points: for $R_0 \le 1$ the equilibrium points is the disease free steady state $E_1^*(S^{h*}, E^{h*}, I^{h*}, R^{h*}) = \left(\frac{B}{\mu}, 0, 0, 0\right) \in \phi$. For $R_0 > 1$, the equilibrium point is the endemic steady state $E_2^*(S^{h*}, E^{h*}, I^{h*}, R^{h*}) \in \phi$ and satisfies $S^{h*}, E^{h*}, I^{h*}, R^{h*} > 0$, where

$$S^{h*} = \frac{BN^h}{\mu N^h + \delta I^{h*}} \tag{5}$$

$$E^{h*} = \frac{B\delta I^{h*}}{(\mu + \psi)(\delta I^{h*} + \mu N^h)} \tag{6}$$

$$I^{h*} = \frac{B\delta\psi - \mu N^h(\alpha + \gamma + \mu)(\mu + \psi)}{\delta(\alpha + \gamma + \mu)(\mu + \psi)} \tag{7}$$

and

$$R^{h*} = \frac{\gamma I^{h*}}{\mu} \tag{8}$$

Proof Steady states $(S^{h*}, E^{h*}, I^{h*}, R^{h*})$ of our equations are found by setting equations (1)-(4) to zero.

$$B - \left(\mu + \frac{\delta I^h}{N^h}\right) S^h = 0 \tag{9}$$

$$\frac{\delta S^h I^h}{N^h} - (\mu + \varphi)E^h = 0 \tag{10}$$

$$\varphi E^h - (\mu + \alpha + \gamma)I^h = 0 \tag{11}$$

$$\gamma I^h - \mu R^h = 0 \tag{12}$$

From equation (9) we have $S^{h^*} = \frac{BN^h}{\mu N^h + \delta I^{h^*}}$

Equation (10) implies:

$$E^{h^*} = \frac{\delta S^{h^*} I^{h^*}}{N^h(\mu + \varphi)}$$

$$E^{h^*} = \frac{\delta\left(\frac{BN^h}{\mu N^h + \delta I^{h^*}}\right) I^{h^*}}{N^h(\mu + \varphi)}$$

$$E^{h^*} = \frac{B\delta I^{h^*}}{(\mu + \varphi)(\delta I^{h^*} + \mu N^h)}$$

Equation (11) implies:

$$I^{h^*} = \frac{\varphi E^{h^*}}{\alpha + \gamma + \mu}$$

$$I^{h^*} = \frac{\varphi\left(\frac{B\delta I^{h^*}}{(\mu + \varphi)(\delta I^{h^*} + \mu N^h)}\right)}{\alpha + \gamma + \mu}$$

$$I^{h^*} = \frac{B\delta\varphi - \mu N^h(\alpha + \gamma + \mu)(\mu + \varphi)}{\delta(\alpha + \gamma + \mu)(\mu + \varphi)}$$

Equation (12) implies:

$$R^{h^*} = \frac{\gamma I^{h^*}}{\mu}$$

Remark 1 The local stability of E_1^* is obtained by next generation matrix [8-9]. We identify classes E and I as being relevant. The disease-free steady state $E_1^*(S^{h^*}, E^{h^*}, I^{h^*}, R^{h^*}) = \left(\frac{B}{\mu}, 0, 0, 0\right)$

Gains and losses:

$$\begin{vmatrix} Gains\,to\,E: & (\delta S^h I^h)/N^h \\ Gains\,to\,I: & 0 \\ Losses\ from\,E: & (\mu + \varphi)E^h \\ Losses\ from\,I: & -\varphi E^h + (\mu + \alpha + \varphi)I^h \end{vmatrix}$$

The F (gains) and V (losses) matrices

$$F = \begin{bmatrix} \frac{\partial}{\partial E^h}\left(\frac{\delta S^h I^h}{N^h}\right) & \frac{\partial}{\partial E^h}(0) \\ \frac{\partial}{\partial I^h}\left(\frac{\delta S^h I^h}{N^h}\right) & \frac{\partial}{\partial I^h}(0) \end{bmatrix}$$

$$V=\begin{bmatrix} \frac{\partial}{\partial E^h}\left((\mu+\varphi)E^h\right) & \frac{\partial}{\partial E^h}(-\varphi E^h+(\mu+\alpha+\varphi)I^h) \\ \frac{\partial}{\partial I^h}\left((\mu+\varphi)E^h\right) & \frac{\partial}{\partial I^h}(-\varphi E^h+(\mu+\alpha+\varphi)I^h) \end{bmatrix}$$

Then we have

$$F=\begin{bmatrix} 0 & 0 \\ \frac{\delta S^h}{N^h} & 0 \end{bmatrix} \Rightarrow F=\begin{bmatrix} 0 & 0 \\ \frac{B\delta}{\mu N^h} & 0 \end{bmatrix}$$

$$V=\begin{bmatrix} \mu+\varphi & -\varphi \\ 0 & \mu+\alpha+\varphi \end{bmatrix}$$

$$V^{-1}=\frac{1}{(\mu+\varphi)(\mu+\alpha+\varphi)}\begin{bmatrix} \mu+\alpha+\varphi & \varphi \\ 0 & \mu+\varphi \end{bmatrix}$$

$$V^{-1}=\begin{bmatrix} \frac{1}{\mu+\varphi} & \frac{\varphi}{(\mu+\varphi)(\mu+\alpha+\varphi)} \\ 0 & \frac{1}{\mu+\alpha+\varphi} \end{bmatrix}$$

$$G=FV^{-1}$$

$$G=\begin{bmatrix} 0 & 0 \\ \frac{B\delta}{\mu N^h} & 0 \end{bmatrix}\begin{bmatrix} \frac{1}{\mu+\varphi} & \frac{\varphi}{(\mu+\varphi)(\mu+\alpha+\varphi)} \\ 0 & \frac{1}{\mu+\alpha+\varphi} \end{bmatrix}$$

$$G=\begin{bmatrix} 0 & 0 \\ \frac{B\delta}{\mu N^h(\mu+\varphi)} & \frac{\varphi B\delta}{\mu N^h(\mu+\varphi)(\mu+\alpha+\varphi)} \end{bmatrix}$$

R_0 is the dominant eigenvalue of the matrix $G=FV^{-1}$. Then we have

$$R_0=\frac{\varphi B\delta}{\mu N^h(\mu+\varphi)(\mu+\alpha+\varphi)} \tag{13}$$

2.2 Exponential stabilities of the equilibrium states

Theorem 1 Let $E_1^*=(S^{h^*},E^{h^*},I^{h^*},R^{h^*})=\left(\frac{B}{\mu},0,0,0\right)$, and $\alpha_3=\max\left(\mu+\frac{\delta I}{N},\mu+\gamma\right)$. The disease free equilibrium E_1^* is exponentially stable in the $\frac{dF}{dt}=B-\mu N^h-\alpha I^h\le B-\mu N^h$ when $R_0<1$.

Proof Consider the following Lyapunov candidate:

$$V_1=\frac{1}{2}\left(S^h\right)^2+\frac{1}{2}\left(E^h\right)^2+\frac{1}{2}\left(I^h\right)^2+\frac{1}{2}\left(R^h\right)^2 \tag{14}$$

Let $\mathbf{x}\equiv\begin{bmatrix} S^h & E^h & I^h & R^h \end{bmatrix}^T$ be the vector of states. It is obvious from the Lyapunov candidate V_1 that the following in equality is satisfied:

$$\alpha_1\|\mathbf{x}\|^2\le V_1(\mathbf{x})\le\alpha_2\|\mathbf{x}\|^2 \tag{15}$$

where α_1 and α_2 are both unity. Consider differentiating the Lyapunov candidate in the trajectory of the system:

$$V_1'(\mathbf{x}) = -\beta S^h - \left(\mu - \frac{\delta I}{N}\right)\left(S^h\right)^2 - \frac{E^h \delta S^h I^h}{N} - \left(\mu+\gamma\right)\left(E^h\right)^2 + I^h E^h \varphi - \left(\mu+\alpha+\gamma\right)\left(I^h\right)^2 + \gamma IR - \mu\left(R^h\right)^2$$
$$\leq \alpha_2\left(\left\|S^h\right\|^2 + \left\|E^h\right\|^2 + \left\|I^h\right\|^2 + \left\|R^h\right\|^2\right)$$
$$\leq \alpha_3\left\|\mathbf{x}\right\|^2 \tag{16}$$

Hence it follows that the differential inequality:

$$V'(\mathbf{x}) \leq \frac{\alpha_3}{\alpha_2} V(\mathbf{x}) = \alpha_3 V(\mathbf{x}) \tag{17}$$

or $V(\mathbf{x}) \leq |V(\mathbf{x}_0)| e^{-\alpha_3 t}$ which hereby implies the exponential stability of the MERS-Cov system.

Theorem 2 Let $E_2^* = (S^{h*}, E^{h*}, I^{h*}, R^{h*})$, and that $\gamma = \frac{\delta S^{h*}}{N}$, $\mu = \frac{B}{S^{h*}}$. The endemic equilibrium E_2^* is exponentially stable in the $\frac{dF}{dt} = B - \mu N^h - \alpha I^h \leq B - \mu N^h$ when $R_0 > 1$ with $\beta_2 = \max\left(\left(\mu + \frac{\delta I}{N}\right), \frac{\varphi\beta\delta}{\mu N(\mu+\varphi)R_0}\right)$.

Proof Consider the following Lyapunov candidate:

$$V_2 = \frac{1}{2}(S - S^*)^2 + \frac{1}{2}E^2 + \frac{1}{2}I^2 \tag{18}$$

The derivative of $V_2(\mathbf{x})$ in the trajectory of the model is given by:

$$V_2' = BS^h - \left(\mu + \frac{\delta I^h}{N^h}\right)\left(S^h\right)^2 - S^*\left(B - \left(\mu + \frac{\delta I^h}{N^h}\right)S^h\right) - \frac{E^h \delta I^h}{N^h} - \left(\mu+\gamma\right)\left(E^h\right)^2 + \varphi I^h E^h - \left(\mu+\alpha+\gamma\right)\left(I^h\right)^2$$
$$\leq -\left(\mu + \frac{\delta I^h}{N^h}\right)\left(S^h\right)^2 - \left(\mu+\gamma\right)\left(E^h\right)^2 - \left(\mu+\alpha+\gamma\right)\left(I^h\right)^2 - \mu\left(R^h\right)^2$$
$$\leq \beta_2\left(\left(S^h\right)^2 + \left(E^h\right)^2 + \left(I^h\right)^2 + \left(R^h\right)^2\right) \tag{19}$$

where $\beta_2 = \max\left(\left(\mu + \frac{\delta I}{N}\right), \frac{\varphi\beta\delta}{\mu N(\mu+\varphi)R_0}\right)$. It then follows again that $V_2'(\mathbf{x}) \leq \frac{\beta_3}{\beta_2} V_2(\mathbf{x}) = \beta_3 V_2(\mathbf{x})$, or $V_2(\mathbf{x}) \leq |V_2(\mathbf{x}_0)| e^{-\beta_3 t}$ which thus implies exponential stability of the system.

2.3 Global stability of the equilibrium states

Theorem 3 Let $E_1^* = (S^{h*}, E^{h*}, I^{h*}, R^{h*}) = \left(\frac{B}{\mu}, 0, 0, 0\right)$, and $\alpha = \frac{B\delta}{\mu N^h}$. The disease free equilibrium E_1^* is globally asymptotically stable in the $\frac{dF}{dt} = B - \mu N^h - \alpha I^h \leq B - \mu N^h$ when $R_0 < 1$.

Proof We consider a Lyapunov function $P(S^h, E^h, I^h, R^h) = (S^h - S^{h*}\ln S^h) + E^h + I^h + R^h$, then we have $P(S^{h*}, E^{h*}, I^{h*}, R^{h*}) = P\left(\frac{B}{\mu}, 0, 0, 0\right) = 0$ and the derivative with respect to time in the trajectory of the system yields:

$$\frac{dP}{dt} = S^{h\prime}\left(1 - \frac{S^{h*}}{S^h}\right) + E^{h\prime} + I^{h\prime} + R^{h\prime}$$

$$\frac{dP}{dt}=\left(B-\mu S^h-\frac{\delta S^h I^h}{N^h}\right)\left(1-\frac{S^{h*}}{S^h}\right)+\frac{\delta S^h I^h}{N^h}-(\mu+\varphi)E^h+\varphi E^h-(\mu+\alpha+\gamma)I^h+\gamma I^h-\mu R^h$$

$$\frac{dP}{dt}=\left(B-\mu S^h-\frac{\delta S^h I^h}{N^h}\right)\left(1-\frac{S^{h*}}{S^h}\right)+\frac{\delta S^h I^h}{N^h}-\mu E^h-\varphi E^h+\varphi E^h-\mu I^h-\alpha I^h-\gamma I^h+\gamma I^h-\mu R^h$$

$$\frac{dP}{dt}=\left(B-\mu S^h-\frac{\delta S^h I^h}{N^h}\right)\left(1-\frac{S^{h*}}{S^h}\right)+\frac{\delta S^h I^h}{N^h}-\alpha I^h-\mu E^h-\mu I^h-\mu R^h$$

$$\frac{dP}{dt}=B\left(1-\frac{S^{h*}}{S^h}\right)-\mu S^h+\mu S^{h*}+\frac{\delta I^h S^{h*}}{N^h}-\alpha I^h-\mu E^h-\mu I^h-\mu R^h$$

Substituting $S^{h*}=\frac{B}{\mu}$ yields:

$$\frac{dP}{dt}=B\left(1-\frac{S^{h*}}{S^h}\right)-\mu S^h+\frac{\mu B}{\mu}+\frac{B\delta I^h}{\mu N^h}-\alpha I^h-\mu E^h-\mu I^h-\mu R^h$$

$$\frac{dP}{dt}=B\left(1-\frac{S^{h*}}{S^h}\right)-\mu S^h+B-\mu E^h-\mu I^h-\mu R^h$$

$$\frac{dP}{dt}=B\left(1-\frac{S^{h*}}{S^h}\right)-\frac{B\mu S^h}{B}+B-\mu E^h-\mu I^h-\mu R^h$$

$$\frac{dP}{dt}=B\left(1-\frac{S^{h*}}{S^h}\right)+B\left(1-\frac{\mu S^h}{B}\right)-\mu E^h-\mu I^h-\mu R^h$$

$$\frac{dP}{dt}=B\left(1-\frac{S^{h*}}{S^h}\right)+B\left(1-\frac{S^h}{S^{h*}}\right)-\mu E^h-\mu I^h-\mu R^h$$

$$\frac{dP}{dt}=B\left(2-\frac{S^{h*}}{S^h}-\frac{S^h}{S^{h*}}\right)-\mu E^h-\mu I^h-\mu R^h$$

$$\frac{dP}{dt}=B\left(\frac{2S^{h*}S^h-S^{h*2}-S^{h2}}{S^{h*}S^h}\right)-\mu E^h-\mu I^h-\mu R^h$$

$$\frac{dP}{dt}=-B\left(\frac{(S^{h*}-S^h)^2}{S^{h*}S^h}\right)-\mu E^h-\mu I^h-\mu R^h$$

$$\frac{dP}{dt}=-\left[B\left(\frac{(S^{h*}-S^h)^2}{S^{h*}S^h}\right)+\mu E^h+\mu I^h+\mu R^h\right]<0 \qquad (20)$$

Then we have $\frac{dP}{dt}\le 0$ and all terms in Equation (20) are non-positive with $\frac{dP}{dt}=0$ if and only if $S^{h*}=S^h, E^h=0, I^h=0$ and $R^h=0$ in the equations (1)-(4). Using LaSalle' s extension to Lyapunov's method [10], the solution does not exist for $E_1^*(S^{h*},E^{h*},I^{h*},R^{h*})\in\phi$. Therefore, the globally asymptotically stable of the disease-free equilibrium E_1^* is satisfied.

Theorem 4 Let $E_2^*=(S^{h*},E^{h*},I^{h*},R^{h*})$. If $R_0>1$, then the endemic equilibrium point E_2^* is globally stable in the $\frac{dF}{dt}=B-\mu N^h-\alpha I^h\le B-\mu N^h$

Assume that

$$\begin{cases} \gamma = \dfrac{\delta S^{h^*}}{N^h} \\ \mu = \dfrac{B}{S^{h^*}} \end{cases}$$

Proof Let a Lyapunov function candidate be $K(S^h, E^h, I^h, R^h) = (S^h - S^{h^*} \ln S^h) + E^h + I^h$.

Then we have

$$\frac{dK}{dt} = (S^{h\prime} - \frac{S^{h^*}}{S^h} S^{h\prime}) + E^{h\prime} + I^{h\prime}$$

$$\frac{dK}{dt} = \left(B - \mu S^h - \frac{\delta S^h I^h}{N^h} \right) \left(1 - \frac{S^{h^*}}{S^h} \right) + \frac{\delta S^h I^h}{N^h} - (\mu + \varphi) E^h + \varphi E^h - (\mu + \alpha + \gamma) I^h$$

$$\frac{dK}{dt} = B\left(1 - \frac{S^{h^*}}{S^h} \right) - \mu S^h + \mu S^{h^*} - \mu E^h - \mu I^h - \alpha I^h$$

$$\frac{dK}{dt} = B\left(1 - \frac{S^{h^*}}{S^h} \right) - \frac{BS^h}{S^{h^*}} + \frac{BS^{h^*}}{S^{h^*}} - \mu E^h - \mu I^h - \alpha I^h$$

$$\frac{dK}{dt} = B\left(1 - \frac{S^{h^*}}{S^h} \right) + B\left(1 - \frac{S^h}{S^{h^*}} \right) - \mu E^h - \mu I^h - \alpha I^h$$

$$\frac{dK}{dt} = -B\frac{(S^{h^*} - S^h)^2}{S^h S^{h^*}} - \mu E^h - \mu I^h - \alpha I^h$$

$$\frac{dK}{dt} = -\left[B\frac{(S^{h^*} - S^h)^2}{S^h S^{h^*}} + \mu E^h + \mu I^h + \alpha I^h \right] < 0, \forall (S^{h^*}, E^{h^*}, I^{h^*}, R^{h^*}) \in \phi \tag{21}$$

Hence, the derivative $\frac{dK}{dt} \le 0, \forall (S^{h^*}, E^{h^*}, I^{h^*}, R^{h^*}) \in \phi$ with $\frac{dK}{dt} = 0$ if and only if $S^{h^*} = S^h, E^h = 0$ and $I^h = 0$ in the equations (1)-(4). Hence by LaSalle's extension to Lyapunov's method [10], the endemic equilibrium state E_2^* is globally asymptotically point on ϕ.

3. Results and Discussion

In this section, we give some numerical results of the presented system. The parameters are taken from the work of Lamwong *et al.* [11] for the Thai population only.

Table 1. Parameters used in the numerical simulation [11]

Parameter name	Value
B	$1/(75 \times 365)$
N^h	2000
δ	0.05
μ	$1/(75 \times 365)$
φ	1/50
α	1/365
γ	1/50

The numerical solutions with the initial condition of $\left[N^h - 2, 0, 0, 0 \right]^T$ are plotted in the graphs as shown in Figure 3(a-d). Form Figure 3(a). the trajectory of the susceptibles starts at a value close to 2000, which then decays and steadies at around 400 around t=1000 days. The plots of the exposed and infected populations start at zeros, peaking at around t=600 days, before reaching the steady state at a value near zero at around t =1000 days. The plot of the recovered population response in Figure 3(d) shows the reverse case of the plot of Figure 3(a). Specifically, there is zero initial response in the recovered population compartment. This number then increases exponentially and is steady at approximately 1400 after 1000 days. The steady state being reached by each compartments of the system is a nonzero number, thereby depicting an endemic equilibrium which is asymptotically stable.

4. Conclusions

In this work, we analyzed the standard dynamical modeling method where both types of typical Lyapunov candidate functions used for investigating epidemiological models were chosen. An exponential stability was investigated with the use of the square-type Lyapunov candidate, while the logarithm type Lyapunov candidate was chosen to show the global asymptotic stability of the equilibrium points. The model exhibits two equilibrium point, namely the disease-free steady state E_1^* and the endemic steady state E_2^*. The basic reproductive number is calculated by using the next generation method. If basic reproductive number is less than one, the disease-free equilibrium state is globally asymptotically stable. The endemic equilibrium state is globally asymptotically stable if the reproductive numberis more than one. Four theorems were proposed as regards the stability of the MERS-Cov transmission using Lyapunov stability theories. Theorems 1 and 2 proved the exponential stability of the MERS-Cov system, while Theorems 3 and 4 proved the global asymptotical stability of the MERS-Cov system.

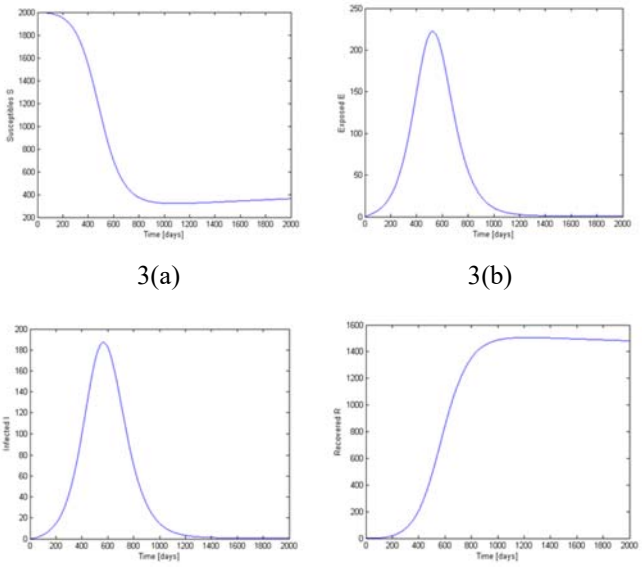

3(a) 3(b)

3(c) 3(d)

Figure 3. (a) The susceptible population (b) The exposed population (c) The infected population and (d) The recovered population.

5. Acknowledgements

This work is supported by Thatphanom College, Nakhon Phanom University, King Mongkut's Institute of Technology Ladkrabang and National Research Council of Thailand. The financial support provided by King Mongkut's University of Technology Thonburi through the KMUTT 55th Anniversary Commemorative Fund is also acknowledged.

References

[1] Hemida, M.G., Elmoslemany, A., Al-Hizab, F., Alnaeem, A., Almathen, F., Faye, B., Chu, D.K.W., Perera, R.A.P.M and Peiris, M., 2017. Dromedary camels and the transmission of Middle East respiratory syndrome coronavirus (MERS-CoV). *Transboundary and Emerging Diseases*, 64(2) 344-353.

[2] Ministry of Public Health, 2016. Middle East Respiratory Syndrome. [online] Available at: http://203.157.41.165/beid_2014/sites/default/files/situation_mers_30.9.60.pdf

[3] World Health Organization, 2017. Middle East respiratory syndrome coronavirus (MERS-CoV) -United Arab Emirates. [online] Available at: http://www.who.int/csr/don/21-september-2017-mers-uae/en/

[4] Ministry of Public Health, 2016. Middle East Respiratory Syndrome. [online] Available at: http://203.157.41.165/beid_2014/sites/default/files/situation_mers_151159.pdf

[5] Aburizaiza, A.S., Mattes, F.M., Azhar, E.I., Hassan, A.M., Memish, Z.A., Muth, D., Meyer, B., Lattwein, E., Müller, M.A. and Drosten, C., 2014. Investigation of anti-middle east respiratory syndrome antibodies in blood donors and slaughterhouse workers in Jeddah and Makkah, Saudi Arabia, Fall 2012. *The Journal of Infectious Diseases*, 209 (2), 243-246.

[6] Chowell, G., Blumberg, S., Simonsen, L., Miller, M.A. and Viboud, C., 2014. Synthesizing data and models for the spread of MERS-CoV, 2013: Key role of index cases and hospital transmission. *Epidemics*, 9, 40-51.

[7] Kim, Y., Lee, S., Chu, C., Choe, S., Hong, S. and Shin, Y., 2016. The characteristics of Middle Eastern respiratory syndrome coronavirus transmission dynamics in South Korea. Osong Public Health and Research perspectives, doi:10.1016/j.phrp.2016.01.001

[8] van den Driessche, P. and Watmough, J., 2002. Reproduction numbers and sub-threshold endemic equilibria for compartmental models of disease transmission. *Mathematical Biosciences,* 180, 29-48.

[9] Heffernan, J.M., Smith R.J. and Wahl, L.M., 2005. Perspectives on the basic reproduction ratio. *Journal of the Royal Society Interface,* 2, 281-293.

[10] LaSalle, J.P., 1976. *The Stability of Dynamical Systems*. Philadelphia: Society for Industrial and Applied Mathematics.

[11] Lamwong, J., Tang, I.M. and Pongsumpun, P., 2018. Mers model of Thai and South Korean population. *Current Applied. Science and Technology,* 18(1), 45-57.

Study of Several Exponential Smoothing Methods for Forecasting Crude Palm Oil Productions in Thailand

Kittiphoom Suppalakpanya[1], Ruamporn Nikhom[2], Thitima Booranawong[3] and Apidet Booranawong[4*]

[1]Faculty of Agro-Industry, Rajamangala University of Technology Srivijaya, Nakhon Si Thammarat, Thailand
[2]Faculty of Engineering, Thaksin University, Phatthalung Campus, Phatthalung, Thailand
[3]Faculty of Management Sciences, Nakhon Si Thammarat Rajabhat University, Nakhon Si Thammarat, Thailand
[4]Department of Electrical Engineering, Faculty of Engineering, Prince of Songkla University, Songkhla, Thailand

Received: 30 January 2019, Revised: 25 April 2019, Accepted: 25 April 2019

Abstract

In this paper, a study of several exponential smoothing methods for forecasting crude palm oil productions in Thailand during January 2018 to March 2018 is presented. The exponential smoothing methods include the Double Exponential Smoothing (DES) method, the Multiplicative Holts-Winters (MHW) method, the Additive Holt-Winters (AHW) method, the Improved Additive Holts-Winters (IAHW) method, and the Extended Additive Holts-Winters (EAHW) method. The input data from January 2006 to December 2017 are collected from the database of the Department of Internal Trade, Ministry of Commerce, Thailand. The major contributions of our paper are twofold. First, the well-known exponential smoothing methods (i.e. the DES, the MHW, and the AHW methods) and the recent methods proposed in the literature (i.e. the IAHW and the EAHW methods) are tested and evaluated. Here, the best forecast results by optimal solutions are determined. Second, different sets of input data including 3-year data (2015-2017), 6-year data (2012-2017), 9-year data (2009-2017), and 12-year data (2006-2017) are used as the inputs for all forecasting methods. Here, how the different sets of input data affect forecasting accuracy are revealed. Our study demonstrates that the traditional AHW and the recently proposed EAHW methods provide the smallest forecasting error measured by Mean Absolute Percentage Error (MAPE) in forecasting crude palm oil productions. The study also indicates that both the AHW and the EAHW methods significantly show accurate forecast results when 12-year input data are applied. Forecast results of January 2018 to March 2018 and the trends of the average monthly and yearly palm oil productions are also reported. We believe that the research methodology and results presented in this work can be useful for strategy setting of the Thai agriculturist and government.

Keywords: exponential smoothing methods, forecasting, crude palm oil productions, Thailand
DOI 10.14456/cast.2019.12

*Corresponding author: Tel.: 66 74 558831 Fax: 66 74 287276
E-mail: apidet.boo@gmail.com, apidet.b@psu.ac.th

1. Introduction

Oil palm (*Elaeis guineensis*) is the most popular oil crop in tropical rain forest regions. Thailand is the third largest palm oil producers in the world, following Indonesia and Malaysia [1]. Most of the palm oil produced in Thailand is used for domestic consumption in terms of food and an alternative fuel feedstock. During 2012-2016, the volume of crude palm oil consumed for food products and biodiesel was increased by 1.78% and 8.11% per year, respectively [2]. To arrange the food security and economic stability, the Thailand government, by the Department of Energy Business, allocates biodiesel productions with some flexibility blending ratios of B100 (pure biodiesel) and diesel, based on the volume of crude palm oil output situation. The biodiesel blending ratio which commonly used in Thailand is varied from B3 to B7 (or 3%v/v to 7%v/v biodiesel blended with diesel) [3]. As on the 1st quarter of 2017, the volume of crude palm oil obviously increased, thus the Department of Energy Business had an announcement to raise the biodiesel blending ratio from B5 to B7 on 8 May 2017. Hence, the excess volume of crude palm oil supplied from markets was absorbed to prevent the fall in oil price problem. For this reason, an accuracy of forecasting future volume of crude palm oil with appropriate forecasting methods is an implement for the government to make immediate decision and to devise a suitable strategic plan of palm oil management in Thailand.

To forecast time-series data, the well-known traditional exponential smoothing methods are widely used: the Holt's linear exponential smoothing method (or the DES method) and the Holt-Winters methods (the MHW and the AHW methods). They are suitably used for data that trend and seasonality behaviors are present. Although the mentioned methods are not new as presented in the research literature, they are popularly used in practice and various applications as reported by many researchers [4-11]. Here, many studies apply such methods due to their simplicity, robustness, low complexity, and algorithm efficiency [4-11].

According to the studies in the literature, the works related to forecasting using exponential smoothing methods were described here. We note that we concentrate on forecasting of palm oil productions/or prices which directly relates to this work. In Siregar *et al.* [12], a comparative study of exponential smoothing methods for forecasting palm oil productions in Indonesia was introduced. The input data from 2010 to 2014 (5-year data) were tested with the DES, the MHW, and the AHW methods. The authors concluded that the AHW method showed better performance than the DES and the MHW methods. In Wan Ahmad and Ahmad [13] exponential smoothing methods were applied to forecast crude palm oil prices in Malaysia in 2013. Forecasting accuracy of the exponential smoothing methods was reported, and the authors summarized that such methods could be efficiently applied for the considered application. Finally, forecasting oil prices using time-series methods was presented in Tularam and Saeed [14, 15]. The authors showed that the Holts-Winters methods with the input data from October 2011 to March 2016 collected from the United States Energy Information Administration, gave the better results in forecasting crude oil prices.

According to the efficacy of the exponential smoothing methods in practice as introduced above, in this paper we apply them to forecast crude palm oil productions in Thailand. Several exponential smoothing methods including the DES, the MHW, the AHW, the IAHW, and the EAHW methods are selected and tested. The input data from January 2006 to December 2017 are gathered from the database of the Department of Internal Trade, Ministry of Commerce, Thailand. The contributions of our study are twofold. First, three traditional forecasting methods (i.e. the DES, the MHW, and the AHW methods) and two recent methods proposed in the literature (i.e. the IAHW and the EAHW methods) are tested. Thus, forecast results determined by optimal methods are provided. Second, four sets of input data (i.e. 3-year data (2015-2017), 6-year data (2012-2017), 9-year data (2009-2017), and 12-year data (2006-2017)) are inserted as the input data. Thus, how the different sets of the input data affect forecasting accuracy of the selected methods is studied. Our

study shows that the AHW and the EAHW methods give the smallest forecasting error measured by the MAPE, in forecasting crude palm oil productions. In addition, the study reveals that, using more input data, like 12-year data, the AHW and the EAHW methods significantly provide more accurate results. Forecast results of January 2018 to March 2018 by the optimal methods and average monthly and yearly crude palm oil productions are also reported in this paper.

2. Materials and Methods

2.1 Input data

Monthly crude palm oil productions from January 2006 to December 2017 (12 years) as the input data are collected from the database of the Department of Internal Trade, Ministry of Commerce, Thailand [16]. They are illustrated in Table 1.

2.2 Forecasting methods

The DES, MHW, AHW, IAHW, and EAHW methods are described here**.** They are also summarized in Table 2. We note that, as mentioned in the introduction section, such forecasting methods as the different methods of the exponential smoothing family are selected for the test because they are widely used in practice and several applications as reported in [4-11], and many studies apply them due to their simplicity, robustness, low complexity, and algorithm efficiency [4-11]. In addition, we found that how well they perform in the case of the crude palm oil productions with the different sets of input data as proposed in this work was not yet investigated.

The DES method: The DES method is suitably used to forecast data which shows a trend [9, 10, 17]. It includes a trend factor to the equation**.** Three equations are incorporated in this method as shown in equations (1) to (3), where L_i is the estimate of the level of the data series at the sample number i, X_i is the input value (the crude palm oil production provided in Figure 1), b_i is the estimate of the trend of the data series, α and β are the weighting factors with values between 0 and 1, and Y_{i+m} is the forecast value (the forecast crude palm oil production) for the period $i+m$, where m is the number of forecast periods ahead.

$$L_i = \alpha\left(\frac{X_i}{S_{i-m}}\right) + (1-\alpha)(L_{i-1} + b_{i-1}) \tag{1}$$

$$b_i = \beta(L_i - L_{i-1}) + (1-\beta)b_{i-1} \tag{2}$$

$$Y_{i+m} = L_i + mb_i \tag{3}$$

Table 1. Monthly crude palm oil productions (metric ton) from January 2006 to December 2017

Monthly crude palm oil productions of the years 2006 to 2017												
Month	**2006**	**2007**	**2008**	**2009**	**2010**	**2011**	**2012**	**2013**	**2014**	**2015**	**2016**	**2017**
1	37,235.8	75,633.1	86,608.3	83,585.0	89,568.0	49,965.8	130,127.1	190,823.7	110,592.2	60,449.7	85,652.2	96,750.7
2	68,668.1	73,969.1	115,134.3	84,333.1	114,489.7	71,223.3	123,789.3	157,840.0	131,987.8	93,956.9	109,332.7	110,879.5
3	113,396.9	86,889.5	148,951.3	118,579.1	140,780.3	119,903.5	136,420.3	162,546.9	204,559.9	169,545.7	166,879.1	180,740.8
4	128,698.6	77,806.1	133,871.3	122,636.5	124,297.8	136,278.8	127,853.4	151,158.1	199,945.7	209,645.9	170,696.2	217,009.7
5	122,438.9	80,216.8	168,465.4	116,402.9	130,425.2	165,055.8	133,911.1	173,196.9	237,217.6	239,227.0	148,475.5	224,189.5
6	91,600.1	73,414.6	143,853.7	102,521.2	119,990.6	171,253.8	117,452.5	162,095.4	198,461.7	195,580.7	130,196.3	169,887.0
7	85,809.1	78,821.0	141,235.1	108,375.9	118,336.7	170,619.2	134,117.8	176,227.3	174,780.5	160,435.9	127,011.5	159,035.2
8	97,282.3	94,843.8	129,386.2	117,770.0	106,585.9	165,445.9	168,176.0	186,602.8	142,937.7	152,098.0	144,704.7	186,413.0
9	102,093.5	99,581.6	130,114.4	128,550.3	95,806.4	158,593.3	184,083.2	162,276.6	129,878.1	154,470.7	148,685.9	206,238.5
10	110,888.5	105,753.8	115,786.0	123,265.8	79,920.0	192,014.4	183,739.6	166,583.9	127,726.0	160,573.2	133,706.2	243,361.2
11	93,603.3	97,369.2	86,881.2	87,626.9	57,898.4	180,255.7	178,281.2	138,454.7	90,218.7	132,042.0	131,053.4	253,231.2
12	76,644.5	75,152.1	75,189.8	68,836.7	44,531.5	150,102.3	165,537.8	113,775.4	62,830.2	104,853.8	118,331.0	233,256.7

As recommended by researchers [9, 10, 17-19], the initial values for L_i and b_i are set using equations (4) and (5), where n is the number of months in a year. In addition, optimal values of α and β are also automatically determined. They are selected when the forecasting error (MAPE) is minimized [19]. In this work, the minimization problem is solved using the Solver function in Microsoft Excel. More details and examples can be found in Tratar and Srmcnik [19]. We note that a brief description of the implementation of the DES method and the Solver function in Microsoft Excel are illustrated as an example in an Appendix.

$$L_1 = X_1 \tag{4}$$

$$b_1 = \frac{X_n - X_1}{n-1} \tag{5}$$

Table 2. Summary of the DES, the MHW, the AHW, the IAHW and the EAHW methods

Methods	Level, trend, and seasonal components	Initial values	Forecast value
DES	$L_i = \alpha X_i + (1-\alpha)(L_{i-1} + b_{i-1})$ $b_i = \beta(L_i - L_{i-1}) + (1-\beta)b_{i-1}$	$L_1 = X_1$ $b_1 = \frac{X_n - X_1}{n-1}$	$Y_{i+m} = L_i + mb_i$
MHW	$L_i = \alpha\left(\frac{X_i}{S_{i-m}}\right) + (1-\alpha)(L_{i-1} + b_{i-1})$ $b_i = \beta(L_i - L_{i-1}) + (1-\beta)b_{i-1}$ $S_i = \gamma\left(\frac{X_i}{L_i}\right) + (1-\gamma)S_{i-n}$	$L_n = \frac{X_1 + X_2 + ... + X_n}{n}$ $b_1 = \frac{X_n - X_1}{n-1}$ $S_i = \frac{X_i}{L_n}$	$Y_{i+m} = (L_i + mb_i)S_{i-n+m}$
AHW	$L_i = \alpha(X_i - S_{i-m}) + (1-\alpha)(L_{i-1} + b_{i-1})$ $b_i = \beta(L_i - L_{i-1}) + (1-\beta)b_{i-1}$ $S_i = \gamma(X_i - L_i) + (1-\gamma)S_{i-n}$	$L_n = \frac{X_1 + X_2 + ... + X_n}{n}$ $b_1 = \frac{X_n - X_1}{n-1}$ $S_i = X_i - L_n$	$Y_{i+m} = L_i + mb_i + S_{i-n+m}$
IAHW	$L_i = \alpha X_i - S_{i-m} + (1-\alpha)(L_{i-1} + b_{i-1})$ $b_i = \beta(L_i - L_{i-1}) + (1-\beta)b_{i-1}$ $S_i = \gamma(X_i - L_i) + (1-\gamma)S_{i-n}$	$L_n = \frac{X_1 + X_2 + ... + X_n}{n}$ $b_1 = \frac{X_n - X_1}{n-1}$ $S_i = X_i - L_n$	$Y_{i+m} = L_i + mb_i + S_{i-n+m}$
EAHW	$L_i = \alpha X_i - \delta S_{i-m} + (1-\alpha)(L_{i-1} + b_{i-1})$ $b_i = \beta(L_i - L_{i-1}) + (1-\beta)b_{i-1}$ $S_i = \gamma(X_i - L_i) + (1-\gamma)S_{i-n}$	$L_n = \frac{X_1 + X_2 + ... + X_n}{n}$ $b_1 = \frac{X_n - X_1}{n-1}$ $S_i = X_i - L_n$	$Y_{i+m} = L_i + mb_i + S_{i-n+m}$

The Holt-Winters methods: The Holt-Winters methods are suitably used when both trend and seasonality patterns are present in the data series [9, 10, 17]. The Holt-Winters methods incorporate three equations: the first for the level, the second for the trend, and third for seasonality. Generally, there are two Holt-Winters methods: the MHW and the AHW methods, depending on whether the seasonality is modelled in multiplicative or additive forms.

The MHW method is shown in equations (6) to (9), where (7) is identical to (2), S_i is the multiplicative seasonal component, γ is the weighting factor ($0 \le \gamma \le 1$), and n is the seasonality length (the number of months in a year). As recommended by researchers [9, 10, 17-19], to initialize the level, trend and seasonal components, (10), (5) and (11) are used, respectively, where $i = 1, 2, 3, \ldots, 12$.

$$L_i = \alpha\left(\frac{X_i}{S_{i-m}}\right) + (1-\alpha)(L_{i-1} + b_{i-1}) \tag{6}$$

$$b_i = \beta(L_i - L_{i-1}) + (1-\beta)b_{i-1} \tag{7}$$

$$S_i = \gamma\left(\frac{X_i}{L_i}\right) + (1-\gamma)S_{i-n} \tag{8}$$

$$Y_{i+m} = (L_i + mb_i)S_{i-n+m} \tag{9}$$

$$L_n = \frac{X_1 + X_2 + \ldots + X_n}{n} \tag{10}$$

$$S_i = \frac{X_i}{L_n} \tag{11}$$

For the AHW method, it is shown in equations (12) to (15), where (2), (7), and (13) are the same. As recommended by researchers [9, 10, 17-19], the initial values for the level and trend are the same as those for the MHW method. In addition, to initialize the seasonal component, equation (16) is used instead.

$$L_i = \alpha(X_i - S_{i-m}) + (1-\alpha)(L_{i-1} + b_{i-1}) \tag{12}$$

$$b_i = \beta(L_i - L_{i-1}) + (1-\beta)b_{i-1} \tag{13}$$

$$S_i = \gamma(X_i - L_i) + (1-\gamma)S_{i-n} \tag{14}$$

$$Y_{i+m} = L_i + mb_i + S_{i-n+m} \tag{15}$$

$$S_i = X_i - L_n \tag{16}$$

In both MHW and AHW methods, optimal values of the weighting factors are also automatically determined during the test. They are determined by minimizing the MPAE, and the minimization problem is solved using the Solver function in Microsoft Excel.

The IAHW method: The IAHW method was recently introduced by Tratar in 2015 [20]. It is shown in equation (17), where the difference between the AHW and IAHW methods is only the equation for the level. The trend and seasonal components remain unchanged**.** In the IAHW method, α occurs only at the input X_i and not at the seasonal component S_{i-m}**.** Here, when $\alpha X_i > S_{i-m}$ (the smoothed value is higher than the average in its seasonality), the level increases in comparison with the level in the earlier period**.** The opposite adjustment occurs when $\alpha X_i < S_{i-m}$. For the initial values for level, trend, and seasonal components, they are the same as those for the AHW method. In addition, optimal values of the weighting factors are determined by minimizing the MPAE, where the minimization problem is solved using the Solver function in Microsoft Excel. Here, the solving method is the evolutionary algorithm, and the constraints are $0 \le \alpha, \beta, \gamma \le 1$.

$$L_i = \alpha X_i - S_{i-m} + (1-\alpha)(L_{i-1} + b_{i-1}) \tag{17}$$

The EAWH method: The EAHW method was also recently proposed by Tratar in 2016 [19, 21]. It is shown in equation (18). The difference between the AHW and EAHW methods is the equation for the level**.** The EAHW allows to smooth the seasonal component more or less than the AHW method, depending on the value of δ ($1 \le \delta \le 0$). If $\delta = \alpha$, the EAHW method reduces to the AHW method. If $\delta = 1$, the EAHW method becomes the IAHW method. The initial values for the level, trend and seasonal components are identical to those for the AHW method. Also, optimal values of the weighting factors are automatically determined using the Solver function in Microsoft Excel.

$$L_i = \alpha X_i - \delta S_{i-m} + (1-\alpha)(L_{i-1} + b_{i-1}) \tag{18}$$

2.3 Performance metrics

In this work, the forecasting error referred to the Mean Absolute Percentage Error or MAPE [19, 22-24] is selected as the performance metric. It is used because it provides the accurate and fair comparison of forecasting methods. The MAPE is not prone to change in the magnitude of time series to be forecasted as recommended by Gentry *et al*. [25] and Alon *et al*. [26]. Moreover, it is frequently used in practice as reported by Ravindran and Warsing [27] and Booranawong and Booranawong [28]. The MAPE is shown in equation (19), where *N* is the number of data samples, e_i is the forecasting error from $Y_i' - Y_i$, Y_i' and Y_i are the actual data and the forecast data, respectively. The 95% confidence interval (CI) is also provided for the average results.

$$MAPE = \frac{\sum_{i=1}^{N} \left| \frac{e_i}{Y_i'} \right|}{N} \times 100 \tag{19}$$

3. Results and Discussion

Figure 1 demonstrates the comparison of the MAPE results determined by the DES, the MHW, the AHW, the IAHW, and the EAHW methods with their optimal weighting factors, when 3-year data, 6-year data, 9-year data, and 12-year data are applied. Here, for fair comparison, the MAPE is calculated from the forecast results of January 2016 to December 2017 ($N = 24$). We note that for the MHW, the AHW, the IAHW, and the EAHW methods, the input data of the first years (12 months) are used for setting the initial values.

The results indicate that, to forecast crude palm oil productions, the AHW and the EAHW methods give the smallest MAPEs (i.e. 6.94 and 7.05, respectively) when 12-year data are applied. Here, by considering the 95% CI, the performance by both methods is not significantly different. In addition, the results also reveal that using more input data, the MAPE is significantly reduced in the cases of the MHW, the AHW, the IAHW and the EAHW methods. However, this is not for the case of the DES method; the MAPEs are not different.

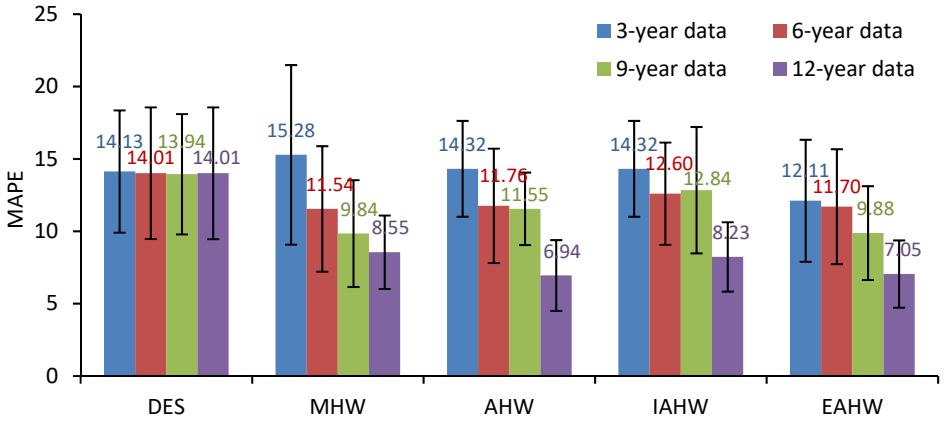

Figure 1. The comparison of the MAPE determined by each forecasting method, when 3-year data (2015-2017), 6-year data (2012-2017), 9-year data (2009-2017) and 12-year data (2006-2017) are applied.

Figure 2 illustrates the comparison of the raw data shown in Table 1 and the forecast data determined by the forecasting methods with their optimal weighting factors, when 12-year data are applied. The optimal weighting factors which give the minimum of the MAPE, and the forecast results of January 2018 to March 2018 are also provided in Table 3. As seen in Figure 2, the forecast data determined by the AHW and the EAHW methods are closer to the raw data than those methods. These results relate to the MAPE results as introduced in Figure 1; a good matching result represents the small MAPE. In Figure 3, we also demonstrate the comparison of the raw data and the forecast data determined by the EAHW method, when 3-year data and 12-year data are applied. Such an example shows that the forecast result using 12-year data is closer to the raw data than using 3-year data.

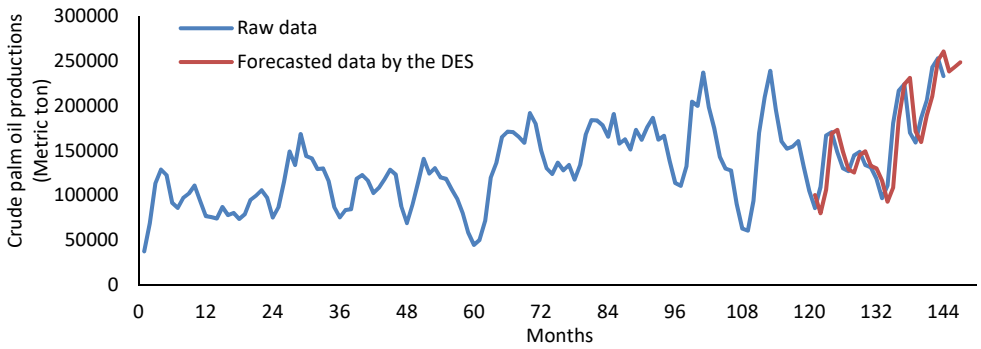

(a) Forecast data by the DES method; 12-year data

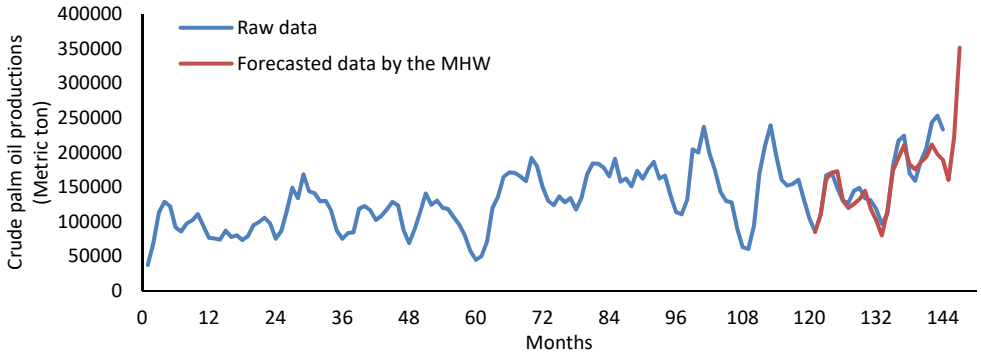

(b) Forecast data by the MHW method; 12-year data

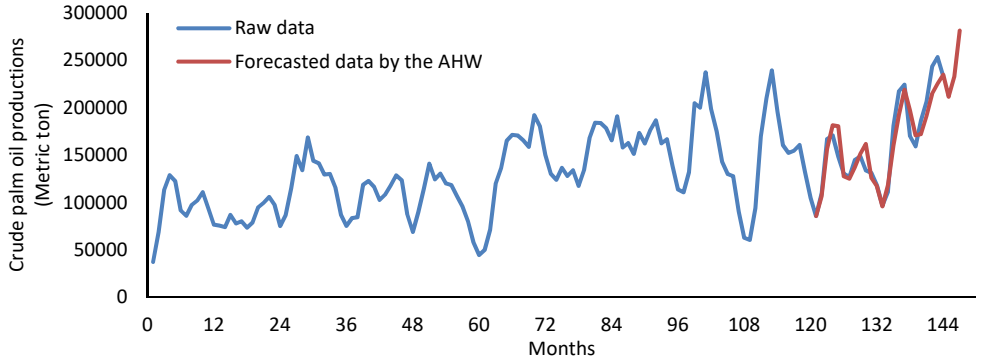

(c) Forecast data by the AHW method; 12-year data

Figure 2. The comparison of the crude palm oil productions between the raw data and the forecast data determined by each forecasting method, when 12-year data are applied.

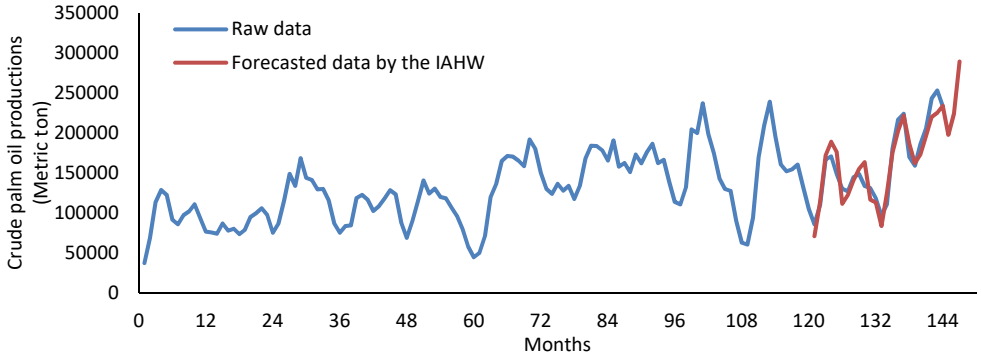

(d) Forecast data by the IAHW method; 12-year data

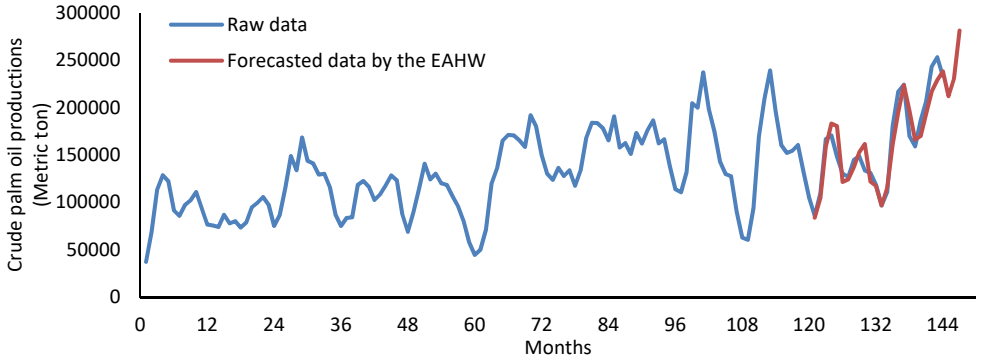

(e) Forecast data by the EAHW method; 12-year data

Figure 2. (cont.) The comparison of the crude palm oil productions between the raw data and the forecast data determined by each forecasting method, when 12-year data are applied.

Table 3. The optimal weighting factors and the forecast data of January 2018 to March 2018

Methods	Optimal weighting factors				Forecasted productions (2018)		
	α	β	γ	δ	Jan.	Feb.	March
DES	1	0.0905	-	-	238,388	243,520	248,652
MHW	0.3085	0.2655	0.0990	-	160,258	221,592	351,574
AHW	0.7975	≈0	0.1719	-	**211,328**	**232,285**	**281,082**
IAHW	0.9718	0	1	-	197,820	224,201	289,507
EAHW	0.9303	0	0.5615	0.9344	**211,991**	**230,492**	**281,301**

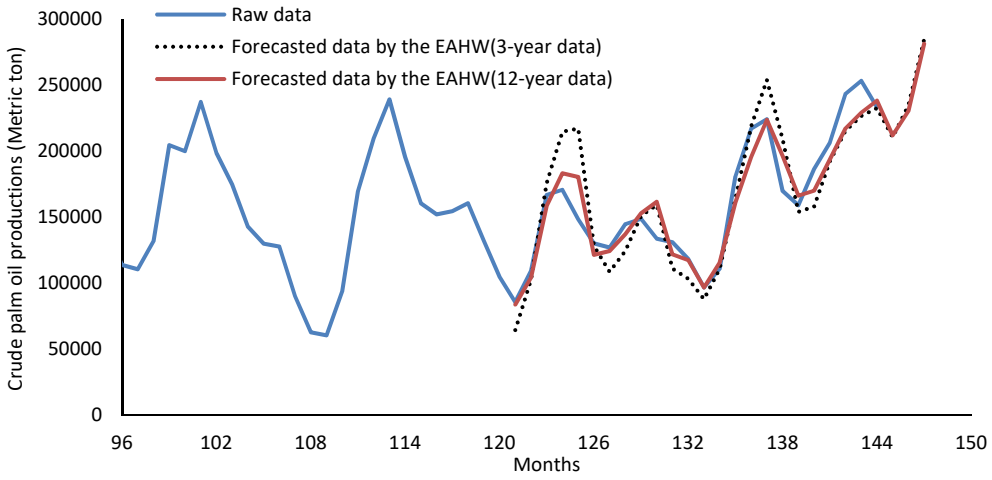

Figure 3. The comparison of the crude palm oil productions between the raw data and the forecast data determined by the EAHW method, when 3-year data and 12-year data are applied.

As shown in Table 3, the results reveal that the forecast data of January 2018 to March 2018 by all forecasting methods have the same trend**.** The crude palm oil production increases. Here, the results by the AHW and the EAHW methods are more reliable, since they provide the smallest MAPEs as presented before.

The average monthly productions of the crude palm oil using 3-year data and 12-year data are illustrated in Figure 4. The results demonstrate that the trends of the average monthly productions using 3-year data and 12-year data are likely the same. They follow the circle pattern. We can also observe that the forecast results of January 2018 to March 2018 as seen in Table 3 are consistent with the average monthly productions of January to March as seen in Figure 4.

The average yearly productions of the crude palm oil using 12-year data are also illustrated in Figure 5. A four-order polynomial trend line is fitted to the average results, and the R-squared value is also provided. The result indicates that the average yearly production of the crude palm oil during 2006 to 2017 have increased. There is more possibility that in 2018, the productions of the crude palm oil will increase.

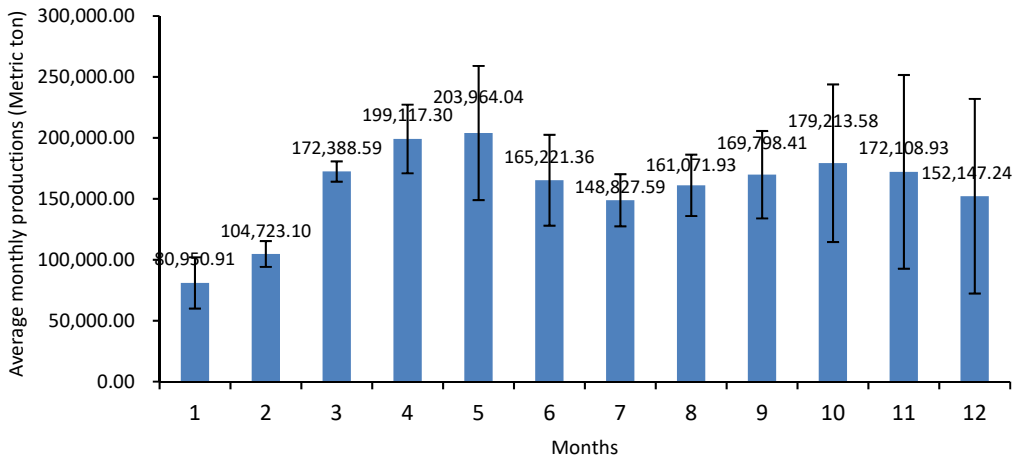

(a) 3-year data (2015-2017); there is more variation during October to December

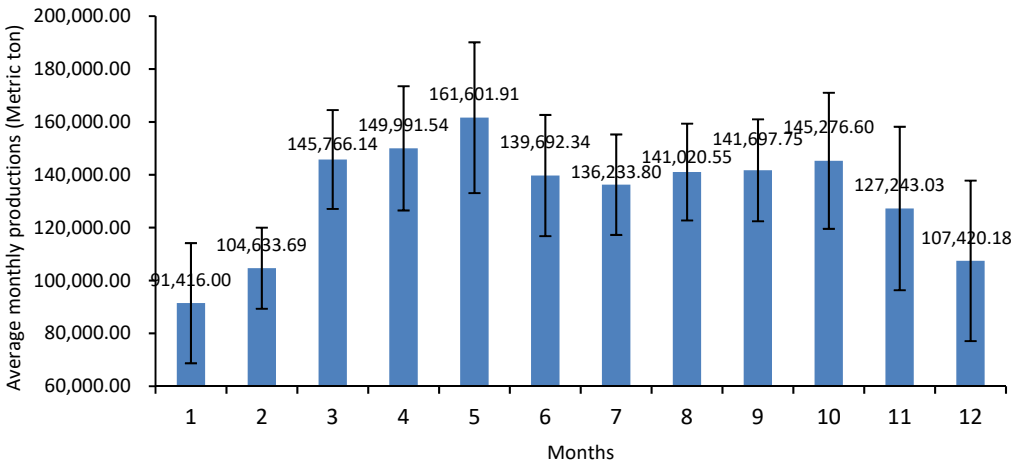

(b) 12-year data (2006-2017)

Figure 4. The average monthly productions of the crude palm oil.

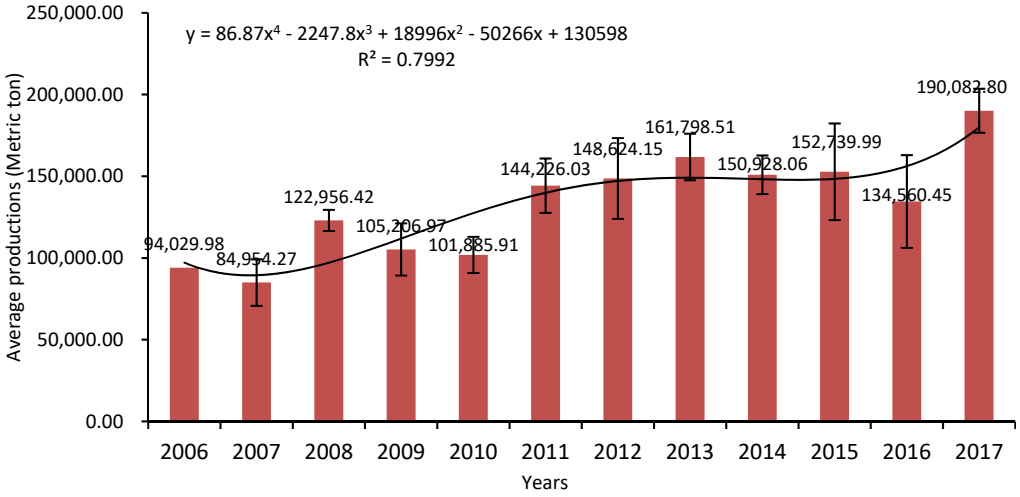

Figure 5. The average yearly productions of the crude palm oil; 12-year data (2006-2017)

The findings as presented in this work can be useful as an information for planning a suitable strategy of the Thai agriculturist and government. For example, if crude palm oil productions in Thailand markets can be accurately predicted, an appropriate plan for managing the use of biodiesel can be immediately set. As announced by the Thai governments during 2015 to 2017, the biodiesel blending ratio was changed from 3.5% to 6% by volume of diesel (or B3.5 to B6) during April 2015, 7% to 5% during July 2016, and 5% to 7% during May 2017 to present. Here, the change depends on the number of crude palm oil productions in Thailand markets. As shown by the forecast results in Table 3, we found that the crude palm oil productions of January 2018 to March 2018 will increase. Consequently, to handle such a situation, the biodiesel blending ratio should be kept at 7% or higher, and the exportation of crude palm oil productions should be more supported (to prevent the decrease of crude palm oil prices).

4. Conclusions

In this work, several exponential smoothing methods including the DES, the MHW, the AHW, the IAHW, and the EAHW methods are employed to forecast crude palm oil productions in Thailand during January 2018 to March 2018. The input data from January 2006 to December 2017 are collected from the Department of Internal Trade, Ministry of Commerce, Thailand. Our study demonstrates that the well-known AHW and the recently proposed EAHW methods provide the smallest forecasting error (i.e. MAPEs are 6.94 and 7.05 for the AHW and the EAHW methods, respectively). Our study also reveals that both forecasting methods show more accurate results when more input data are used; the forecast results using 12-year data are closer to the observed data than using 9-year data, 6-year data, and 3-year data. Additionally, the trends of average monthly and yearly crude palm oil productions are also reported in this paper.

In the future work, to enhance the forecasting accuracy, other input data related to the crude palm oil production will be selected and tested, and more efficient forecasting methods will also be proposed.

5. Acknowledgements

We express our thanks to the Faculty of Agro-Industry, Rajamangala University of Technology Srivijaya, the Faculty of Engineering, Thaksin University, Phatthalung Campus, the Faculty of Management Sciences, Nakhon Si Thammarat Rajabhat University, and the Faculty of Engineering, Prince of Songkla University, for supporting this research.

References

[1] Petchseechoung, W., 2017. *Thailand industry outlook 2017-19: oil palm industry*. [online] Available at: https://www.krungsri.com/bank/getmedia/ac87c171-db74-442b-ae29-5b69572896ca/IO_Oil_Palm_2017_EN.aspx

[2] Bureau of Agricultural Economic Research, 2017. *Agricultural commodity situation and trend (2017)*. [e-book] Office of Agricultural Economics. Available through: http://www.oae.go.th/assets/portals/1/files/ebook/agri_situation2560.pdf

[3] Bureau of Agricultural Economic Research, 2018. *Agricultural commodity situation and trend (2018)*. [e-book] Office of Agricultural Economics. Available through: http://www.oae.go.th/assets/portals/1/files/ebook/agri_situation2561.pdf

[4] Gelper, S., Fried, R., and Croux, C., 2010. Robust forecasting with exponential and Holt-Winters smoothing. *Journal of Forecasting*, 29, 285-300.

[5] Brown, R. G., 1956. Exponential smoothing for predicting demand. *Proceeding of the 10th National Meeting of the Operations Research Society of America*, San Francisco. USA, November 14-15, 1956, 1-15.

[6] Hunter, J.H., 1986. The exponentially weighted moving average. *Journal of Quality Technology*, 18(4), 203-210.

[7] Winters, P., 1960. Forecasting sales by exponentially weighted moving averages. *Management Science*, 6, 324-342.

[8] Gardner, E.S., 1985. Exponential smoothing: the state of the art. *Journal of Forecasting*, 4, 1-28.

[9] Montgomery, D.C., Jennings, C.L. and Kulahci, M., 2008. *Introduction to Time Series Analysis and Forecasting*. New Jersey: John Wiley and Sons.

[10] Kalekar, P. S., 2004. *Time Series Forecasting Using Holt-Winters Exponential Smoothing*. Kanwal Rekhi School of Information Technology.

[11] Ramos, P., Santos, N. and Rebelo, R., 2015. Performance of state space and ARIMA models for consumer retail sales forecasting. *Robotics and Computer-Integrated Manufacturing*, 34, 151-163.

[12] Siregar, B., Butar-Butar, I.A., Rahmat, R.F., Andayani, U. and Fahmi, F., 2017. Comparison of exponential smoothing methods in forecasting palm oil real production. *Journal of Physics Series*, 801,1-9.

[13] Wan Ahmad, W.K.A. and Ahmad, S., 2013. Arima model and exponential smoothing method: a comparison. *API Conference Proceedings*, 1522 (1), 1312-1321.

[14] Tularam, G.A. and Saeed, T., 2016. Oil-price forecasting based on various univariate time-series models. *American Journal of Operations Research*, 6, 226-235.

[15] Tularam, G.A. and Saeed, T., 2016. The use of exponential smoothing (ES), Holts and Winter (HW) and Arima models in oil price analysis. *International Journal of Mathematics, Game Theory and Algebra*, 25(1), 13-22.

[16] The Department of Internal Trade. Ministry of Commerce, 2018. *Prices and situation of agricultural commodities (oil palm)*. [online] Available at: http://www.dit.go.th/

[17] Holt, C.C., 2004. Forecasting seasonals and trends by exponentially weighted moving averages. *International Journal of Forecasting*, 20(1), 5-10.
[18] Dhakre, D.S., Sarkar, K.A. and Manna, S., 2016. Forecasting price of Brinjal by Holt Winters method in West Bengal using MS Excel. *International Journal of Bio-resource, Environment and Agricultural Sciences*, 2(1), 232-235.
[19] Tratar, L.F. and Srmcnik, E., 2016. The comparison of Holt-Winters method and multiple regression methods: a case study. *Energy*, 109, 266-276.
[20] Tratar, L.F., 2015. Forecasting method for noisy demand. *International Journal of Production Economics*,161, 64-73.
[21] Tratar, L.F., Mojskerc, B. and Toman, A., 2016. Demand forecasting with four-parameter exponential smoothing. *International Journal of Production Economics*, 181, 162-173.
[22] Booranawong, T. and Booranawong, A., 2017. Simple and double exponential smoothing methods with designed input data for forecasting a seasonal time series: in an application for lime prices in Thailand. *Suranaree Journal of Science & Technology*, 24(3), 301-310.
[23] Booranawong, T. and Booranawong, A., 2017., An exponentially weighted moving average method with designed input data assignments for forecasting lime prices in Thailand. *Journal Teknologi*, 79(6), 53-60.
[24] Chatfield, C., 2001. *Time-Series Forecasting*. New York: Chapman & Hall.
[25] Gentry, T.W., Wiliamowski, B.M. and Weatherford, L.R., 1995. A comparison of traditional forecasting techniques and neural networks. *Intelligent Engineering Systems through Artificial Neural Networks*, 5, 765-770.
[26] Alon, I., Qi, M. and Sadowski, R.J., 2001. Forecasting aggregate retail sales: a comparison of artificial neural networks and traditional methods. *Journal of Retailing and Consumer Services*, 8(3), 147-156.
[27] Ravindran, A. and Warsing, D.P., 2013. *Supply Chain Engineering: Models and Applications*. New York. NY: CRC Press.
[28] Booranawong, T. and Booranawong, A., 2018. Double exponential smoothing and Holt-Winters methods with optimal initial values and weighting factors for forecasting lime, Thai chili and lemongrass prices in Thailand. *Engineering and Applied Science Research*, 45(1), 32-38.

Appendix

An example of the implementation of the DES method in Excel program

The implementation of the DES method and the use of the Solver function in Excel program are illustrated as an example here. More details can be found in [19, 21]. A snapshot of Excel spreadsheet is shown in Figure 6, where L_i, b_i, L_1, b_1, and Y_{i+m} are calculated. Such calculations are corresponding to equations (1), (2), (4), (5), and (3), as presented in Section 2. In Figure 7, the Solver optimization tool with setting is shown. The MAPE is minimized by adjusting the values of the weighting factors, where they are in the range between 0 and 1 and their optimal values are automatically determined.

	A	B	C	D	E	F	G
1	**DES METHOD**					95%CI	4.554186
2			Alpha	0.999996		SD	11.383303
3			Beta	0.090526		MAPE	14.008253
4	**Month**	***Xi***	***Li***	***bi***	***Yi***	***ei* (Error)**	**Abs%Error**
5	1	37235.8	37235.8	3582.61			
6	2	68668.1	68667.98	6103.719			
7	3	113396.9	=$D$2*B7+(1-$D$2)*(C6+D6)				
8	4	128698.6	128698.6	10116.43			
9	5	122438.9	122439	8633.971			

(a) The calculation of L_i, where C7 = $D$2*B7 + (1-$D$2)*(C6+D6) refers to $L_3 = \alpha X_3 + (1-\alpha)(L_2 + b_2)$

	A	B	C	D	E	F	G
1	**DES METHOD**					95%CI	4.554186
2			Alpha	0.999996		SD	11.383303
3			Beta	0.090526		MAPE	14.008253
4	**Month**	***Xi***	***Li***	***bi***	***Yi***	***ei* (Error)**	**Abs%Error**
5	1	37235.8	37235.8	3582.61			
6	2	68668.1	68667.98	6103.719			
7	3	113396.9	113396.7	=$D$3*(C7-C6)+(1-$D$3)*D6			
8	4	128698.6	128698.6	10116.43			
9	5	122438.9	122439	8633.971			

(b) The calculation of b_i, where D7 = $D$3*(C7-C6) + (1-$D$3)*D6 refers to $b_3 = \beta(L_3 - L_2) + (1-\beta)b_2$

	A	B	C	D	E	F	G
1	**DES METHOD**					95%CI	4.554186
2			Alpha	0.999996		SD	11.383303
3			Beta	0.090526		MAPE	14.008253
4	**Month**	***Xi***	***Li***	***bi***	***Yi***	***ei* (Error)**	**Abs%Error**
5	1	37235.8	=B5	3582.61			
6	2	68668.1	68667.98	6103.719			
7	3	113396.9	113396.7	9600.288			
8	4	128698.6	128698.6	10116.43			
9	5	122438.9	122439	8633.971			

(c) The calculation of L_1, where C5 = B5 refers to $L_1 = X_1$

Figure 6. Implementation of the DES method in Excel program

	A	B	C	D	E	F	G
1	**DES METHOD**					95%CI	4.554186
2			Alpha	0.999996		SD	11.383303
3			Beta	0.090526		MAPE	14.008253
4	**Month**	***Xi***	***Li***	***bi***	***Yi***	***ei* (Error)**	**Abs%Error**
5	1	37235.8	37235.8	=(B16-B5)/11			
6	2	68668.1	68667.98	6103.719			
7	3	113396.9	113396.7	9600.288			
16	12	76644.51	76644.6	1276.109			
17	13	75633.14	75633.15	1069.026			

(d) The calculation of b_1, where D5 = (B16-B5)/11 refers to $b_1 = (X_{12}-X_1)/(12-1)$

	A	B	C	D	E	F	G
1	**DES METHOD**					95%CI	4.554186
2			Alpha	0.999996		SD	11.383303
3			Beta	0.090526		MAPE	14.008253
4	**Month**	***Xi***	***Li***	***bi***	***Yi***	***ei* (Error)**	**Abs%Error**
5	1	37235.8	37235.8	3582.61			
6	2	68668.1	68667.98	6103.719			
7	3	113396.9	113396.7	9600.288			
125	121	85652.25	85652.31	-5806.31	100381	-14728.8	17.196001
126	122	109332.8	109332.7	-3137	=C125+(1*D125)		26.969745
127	123	166879.1	166878.9	2356.408	106195.7	60683.48	36.363731

(e) The calculation of Y_{122}, where E126 = C125 + (1*D125) refers to $Y_{122}=L_{121} + (1*b_{121})$

Figure 6. (cont.) Implementation of the DES method in Excel program

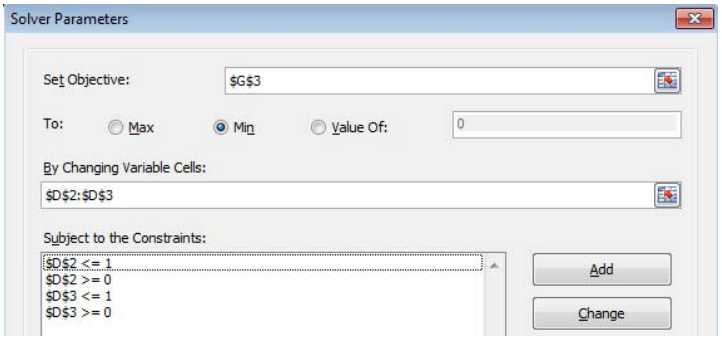

Figure 7. Excel solver setting.

Size Distributions of Particulate Matter and Particle-bound Polycyclic Aromatic Hydrocarbons and Their Risk Assessments during Cable Sheath Burning

Thidarat Keawhanu[1], Achariya Suriyawong[2] and Suwannee Junyapoon[1*]

[1]Department of Chemistry, Faculty of Science, King Mongkut's Institute of Technology Ladkrabang, Bangkok, Thailand
[2]Department of Environmental Engineering, Faculty of Engineering, Chulalongkorn University, Bangkok, Thailand

Received: 18 March 2019, Revised: 7 May 2019, Accepted: 8 May 2019

Abstract

Burning of electric cable sheath leads to the emission of small particles and toxic pollutants that cause severe air pollution and human health effects. In this study, size distributions of particulate matter and p-PAHs during open burning of cable insulation were examined. Lifetime cancer risk of PAHs was also assessed. The particulate samples were collected on quartz fiber filters using an eight-stage cascade impactor with flow rate of 28.3 L min^{-1}. The exposed filter was extracted with acetonitrile and then measured by GC-MS in the SIM mode for 16 PAHs identification. It was found that average concentrations of ultrafine, fine and coarse particles were 1,045.82 µg m^{-3} (11.45 % of the total mass), 3,557.50 µg m^{-3} (38.96 % of the total mass) and 4,529.03 µg m^{-3} (49.59 % of the total mass), respectively. The particle size distributions were bimodal with one major peak in the size range of 5.8-4.7 µm and another minor peak in the size range of 1.1-0.65 µm. The concentrations of 16 PAHs adsorbed on ultrafine, fine and coarse particle were 717.86 ng m^{-3} (11.47% of the total PAHs), 3,645.43 ng m^{-3} (58.23% of the total PAHs) and 1,897.19 ng m^{-3} (30.30% of the total PAHs), respectively. Distributions of BaA, BaP, DbA and BgP were unimodal with a peak in accumulation mode while those of Acy, Ace and Fla were bimodal with two peaks in accumulation mode. Distributions of Flu, Phe, Ant, Pyr, Chr, BbF and BkF were multimodal with peaks in accumulation and coarse modes whereas InP was not detected. The inhalable particles (PM_{10}) contained mainly 5-ring PAHs (55.67% of total PAHs) followed by 4-ring PAHs (27.58% of total PAHs), and 3-ring PAHs (14.98% of total PAHs). Only small amount of 2-ring PAHs (1.36% of total PAHs) and 6-ring PAHs (0.41% of total PAHs) was observed. The fraction of PAHs adsorbed on PM_{10} was ranked in the order Group 2B (53.45%) > Group 3 (33.86%) > Group 1 (10.71%) > Group 2A (1.98%). The average concentrations of 16 PAHs and $B[a]P_{eq}$ were 6,260.47 ng m^{-3} and 1,014.35 ng m^{-3}, respectively. The estimated lifetime lung cancer risk during wire burning was 8.83E-02.

Keywords: cable sheath, open burning, particulate matter, p-PAHs, risk assessment, size distribution
DOI 10.14456/cast.2019.13

*Corresponding author: E-mail: suwannee.ju@kmitl.ac.th

1. Introduction

Electric cable wire is an essential part of all electrical and electronic devices. Nowadays, large quantities of electronic waste (e-waste) such as discarded computers, televisions, refrigerators are produced worldwide due to high consumption and shorter life span of electronic products [1]. This leads subsequently to massive generation of used cable wire. As it is composed of copper wire, which is high economic value, recycling of used cable is increasingly interested. There are several techniques used to recover copper from cable wire such as stripping, crushing, burning, high pressure water jet, cryogenic process and chemical treatment [2]. However, open burning is a common technique for cable wire recycling in informal sector, where most of e-waste is managed unsafely. As cable sheath consists of polyvinyl chloride (PVC), polyethylene (PE), silicone rubber and flame retardant [3], burning of the plastic insulation releases a large amount of small particles and particle-bound toxic elements such as heavy metals, polychlorinated biphenyls and polycyclic aromatic hydrocarbons (PAHs) into the surroundings [4, 5].

Atmospheric particles comprise a wide range of particle sizes. They can be classified based on their origin into primary and secondary particles. The former is directly released from an emission source while the latter is formed from chemical or photochemical reactions of pollutants both in gas and particle phases [6, 7]. The compositions and sizes of individual particles are changed during distribution in the atmosphere, relying on formation and destruction processes. Small particles can remain suspended for long time and be dispersed for long distance in the air. Thus, size distribution of particles and their compositions are able to indicate their emission sources and fate of transport in the environment [6]. Particulate matters, especially less than 2.5 micrometers in diameter, are correlated with the increased respiratory and cardiovascular diseases because they can penetrate into the respiratory tract, and some may transfer to bloodstream [8]. Several studies also indicated that smaller particle sizes potentially caused more health risk [9].

Burning of cable sheath is one of the main sources of PAHs derived from informal recycling of e-waste [5, 10]. Generally, PAHs in the atmosphere are found in vapor phase (g-PAHs) and particle phase (p-PAHs) [11]. The partitioning of a given PAH compound between particle and vapor phases depends on its vapor pressure, particle size and composition as well as ambient temperature [12, 13]. Allen *et al*. [14] reported that size distribution of atmospheric particle-bound PAHs related to vaporization and condensation mechanisms. In the atmosphere, low-molecular weight PAHs (2-3 rings; MW $\leq$ 178) are mainly found in a vapor phase (g-PAHs) while high molecular weight species (MW $\geq$ 228) are largely adsorbed on particles (p-PAHs) [15, 16]. Harrison *et al*. [17] also proposed that most PAHs, especially those with more than four aromatic rings, easily adsorb onto combustion aerosols. Specific compounds of PAHs are potentially toxic or mutagenic to humans that are associated with the increased risk of developing lung cancer [18, 19]. Previous studies revealed that high molecular weight PAHs were potentially more carcinogenic than low molecular weight ones [20]. It was found that carcinogenic PAHs were likely attached on fine particles [21-23]. In addition, p-PAHs remain in the surroundings for long period because they cannot be easily removed from the atmosphere by photolysis and other degradation pathways [24]. Since inhalation deposition of airborne pollutants depends on particle sizes, fine particle-bound PAHs can travel deep into the human respiratory system and cause adverse health impact [25, 26]. However, the effects on human health of PAHs depend on their toxicity, concentration, exposure time and exposure routes. The available information on size distribution of particle bound-PAHs (p-PAHs) released from open burning of cable sheath is still limited. This study aimed to investigate size distributions of particles and p-PAHs in different particle size ranges emitted from open burning of electric cable sheath. Risk assessment of PAHs via inhalation exposure was also determined using lifetime cancer risk of PAHs.

2. Materials and Methods

2.1 Air sampling

Size distributions of particulate matter and p-PAHs adsorbed on inhalable particles emitted from burning of electric cable sheath were examined in a laboratory scale at Faculty of Science, King Mongkut's Institute of Technology Ladkrabang. One kg of cable sheath was burnt in open air. The air sample was collected on quartz fiber filters (Toyo Roshi Kaisha, Japan) using an eight-stage cascade impactor (Thermo Andersen, USA). The air sample was taken at a flow rate of 28.3 L min^{-1} for 30 min. The sampler was placed at 1.5 m above ground level in the downwind direction (1.5 meters). The particle sizes were separated into nine interval fractions: 10.0-9.0, 9.0-5.8, 5.8-4.7, 4.7-3.3, 3.3-2.1, 2.1-1.1, 1.1-0.65, 0.65-0.43, and <0.43 μm. The sampling procedure was conducted following US EPA method [27]. The gravimetric measurement was run in triplicate. Details of the analysis are explained in Phoothiwut and Junyapoon [28].

2.2 PAHs analysis

In this study, 16 PAHs consisting of naphthalene (Nap, 2-ring) acenaphthylene (Acy, 3-ring), acenaphthene (Ace, 3-ring), fluorene (Flu, 3-ring) phenanthrene (Phe, 3-ring), anthracene (Ant, 3-ring), fluoranthene (Fla, 4-ring), pyrene (Pyr, 4-ring), benzo[*a*]anthracene (BaA, 4-ring), chrysene (Chr, 4-ring), benzo[*b*]fluoranthene (BbF, 5-ring), benzo[*k*]fluoranthene (BkF, 5-ring), benzo[*a*]pyrene (BaP, 5-ring), dibenzo[*a,h*] anthracene (DbA, 5-ring), indeno[1,2,3-*cd*] pyrene (InP, 6-ring) and benzo[*ghi*] perylene (BgP, 6-ring) adsorbed on particles were extracted and analyzed using the Compendium Method TO-13A, modification from US EPA [29]. Each sample filter was cut into small pieces and then sonicated with 15 ml acetonitrile (99.9% HPLC grade, Sigma-Aldrich, USA) for 30 min. The extracts were analyzed by GC-MS in SIM mode (Agilent Technologies, USA) with an HP-5MS GC fused-silica capillary column, 30 m × 0.25 mm i.d. × 0.25 μm film thickness (J&W Scientific, USA). The carrier gas used was helium (99.999% purity, Praxair, Thailand) at a flow rate of 1.0 ml min^{-1}. Field blank sample was also measured using the same method as the sample. Recovery efficiencies were examined in triplicate using spike method. Details of the PAHs analysis are described in Phoothiwut and Junyapoon [28].

2.3 Calculation of lifetime lung cancer risk of PAHs

Lifetime lung cancer risk of PAHs was presented as excess cancer risk (ECR) from PAHs associated with particles through inhalation pathway. A mixture of PAHs concentrations was converted to benzo(a)pyrene toxic equivalent ($B[a]P_{eq}$). Total $B[a]P_{eq}$ can be calculated from equation 1.

$$\sum B[a]P_{eq} = \sum_{i=1}^{n}(C_i \times TEF_i) \quad (1)$$

Where C_i was the concentration of individual PAH congener attached on particles, TEF_i was the toxic equivalence factor of individual PAHs. TEF_i value of Nap, Acy, Ace used the factors provided by Nisbet and LaGoy [30] and the other PAHs used the values proposed by Larsen and Larsen [31]. ECR was calculated following the Office of Environmental Health Hazard Assessment (OEHHA) of the California Environmental Protection Agency (Cal EPA) [32, 33] as shown in equation 2.

$$ECR = \sum B[a]P_{eq} \times UR_{B[a]P} \quad (2)$$

Where $UR_{B[a]P}$ (unit risk) of 8.7×10^{-5} was the estimate number of people for lifetime cancer risks from inhalation at a B[a]P equivalent concentration of 1 ng m^{-3} within a lifetime of 70 years [34, 35].

3. Results and Discussion

3.1 Concentrations and size distributions of particulate matter

In this study, nine inhalable fractions of particles were divided into three size ranges according to their formation mechanisms: ultrafine (nuclei mode, $d_{ae}<0.4$ µm), fine (accumulation mode, $0.4<d_{ae}<2.1$ µm) and coarse particles ($d_{ae}>2.1$ µm). The concentrations of ultrafine, fine and coarse particles in ambient air during burning of cable sheath were in the range of 364.73-1,694.72 µg m^{-3} with an average of 1,045.82±665.58 µg m^{-3}, 1,953.33-4,431.41 µg m^{-3} with an average of 3,557.50±1,391.11 µg m^{-3} and 1,385.97-6,126.13 µg m^{-3} with an average of 4,529.03±2,722.09 µg m^{-3}, respectively as shown in Figure 1(a). The wide concentration ranges of particles were observed. This may be due to the variation

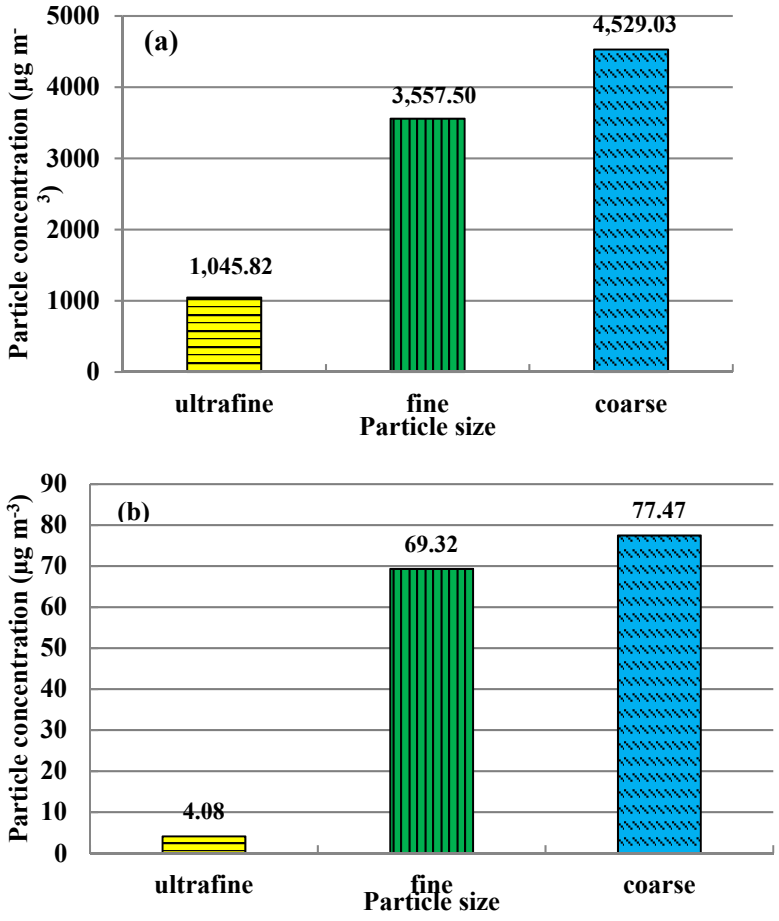

Figure 1. Concentrations of particle size range during open burning of cable sheath (a) and during no burning activity (b)

of burning and atmospheric conditions. The concentration range of each particle size during burning of cable sheath were significantly higher than those during no burning activity (Figure 1(b)).These results reveal that two main atmospheric components were coarse (49.59 % of the total mass) and fine particles (38.96 % of the total mass), and the minor component was ultrafine particles (11.45 % of the total mass). There was no mean difference between concentrations of coarse and fine particles (p-value>0.05). The size distribution plot of atmospheric particles during burning of cable sheath was bimodal with one major peak in the coarse particle size range (5.8-4.7 µm) and another minor peak in the fine particle size range (1.1-0.65 µm) as shown in Figure 2(a) while trimodal distribution was found during no burning activity (Figure 2(b)). Coarse particles are likely originated from incomplete combustion of plastic sheath whereas fine particles may be formed through different atmospheric formation mechanisms such as condensation of vapor species and accumulation of ultrafine particles [6].

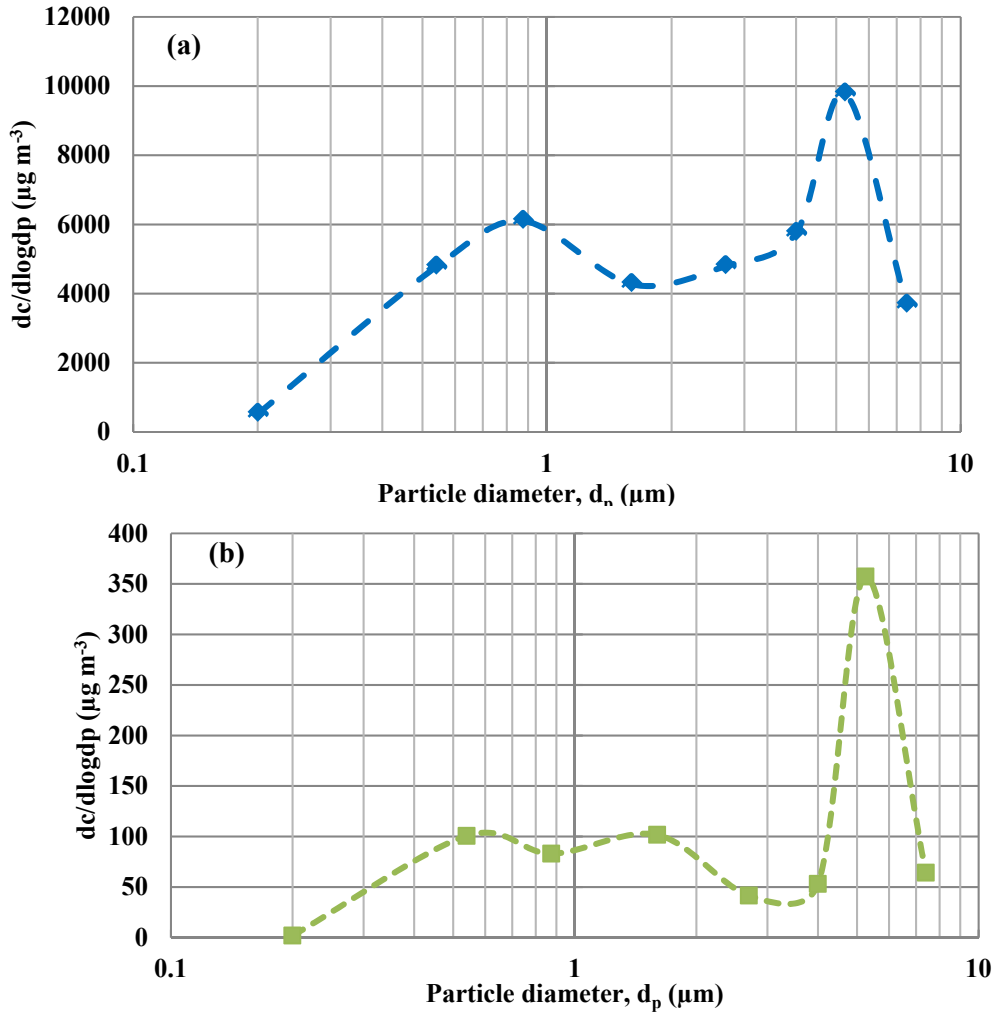

Figure 2. Size distributions of atmospheric aerosols during open burning of cable sheath (a) and during no burning activity (b)

3.2 Concentrations and size distributions of p-PAHs

Concentrations of 16 PAHs adsorbed on each particle size range during open burning of cable sheath are presented in Table 1. In this work, recovery efficiencies of 16 PAHs (n = 3) were ranged between 94.73 and 98.06 %. PAHs were likely generated from thermal degradation of PVC sheath through cracking and cross-linking processes of polymers [10]. The concentrations of total 16 PAH adsorbed on ultrafine, fine and coarse particles during burning of cable sheath were 717.86, 3,645.43 and 1,897.19 ng m^{-3}, respectively as shown in Figure 3. Total 16 PAHs were dominantly bound on fine particles (58.23% of the total PAHs) followed by coarse particles (30.30% of the total PAHs) and ultrafine particles (11.47% of the total PAHs). This is likely because p-PAHs in the accumulation mode were formed from condensation of vapor- phase PAHs as well as coagulation of their primary components. These results are similar to the findings of previous studies reporting that carcinogenic PAHs were likely attached on fine particles [21-23].

In this work, 16 PAHs attached on particles were divided into four groups, depending on the numbers of aromatic rings in their structures: 3-ring PAHs (Acy, Ace, Flu, Phe, Ant), 4-ring PAHs (Fla, Pyr, BaA, Chr), 5-ring PAHs (BbF, BkF, BaP, DbA) and 6-ring PAHs (InP, BgP). For 3-ring PAHs, distributions of Acy and Ace were bimodal with two peaks in accumulation mode whereas those of Flu, Phe and Ant were multimodal with peaks in accumulation and coarse modes as shown in Figure 4(a). For 4-ring PAHs, BaA had a unimodal distribution with a main peak in accumulation mode while Fla had a bimodal distribution with two peaks in accumulation mode. Multimodal distributions with peaks in accumulation and coarse modes were found in Pyr and Chr as shown in Figure 4(b). For 5-ring PAHs, distributions of BaP and DbA were unimodal with a main peak in accumulation mode while those of BbF and BkF were multimodal with peaks in accumulation and coarse modes as shown in Figure 4(c). For 6-ring PAHs, BgP had a unimodal distribution with a dominant peak in accumulation mode while InP was not detected (Figure 4(d)). These results indicate that most of less volatile PAHs preferentially condensed on fine particles, which is likely correlated with the previous work [14, 20]. However, burning parameters such as heat release rate, temperature, char length, afterburn time are required to be identified in future work.

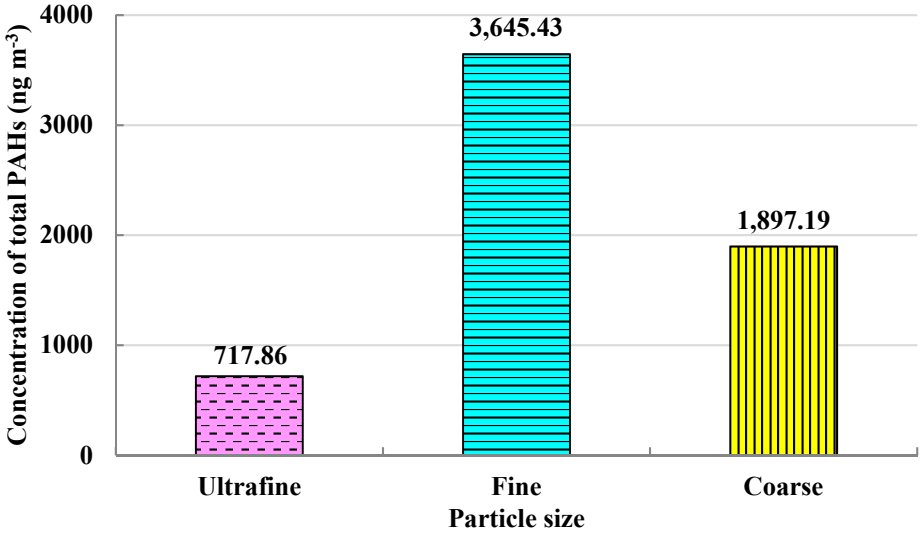

Figure 3. Concentrations of total 16 PAHs adsorbed on ultrafine, fine and coarse particles

Table 1. Concentrations of 16 PAHs adsorbed on each particle size range during open burning of cable sheath

Particle size (μm)	PAHs concentration (ng m^{-3})															
	Nap	**Acy**	**Ace**	**Flu**	**Phe**	**Ant**	**Fla**	**Pyr**	**BaA**	**Chr**	**BbF**	**BkF**	**BaP**	**InP**	**DbA**	**BgP**
<0.4	6.98	2.68	6.71	5.47	17.51	11.82	8.97	8.71	38.98	23.65	71.06	430.69	77.90	n.d.	n.d.	6.73
0.43-0.65	19.57	5.92	29.59	17.93	86.09	11.36	313.24	147.22	176.58	164.54	174.17	270.02	211.42	n.d.	n.d.	n.d.
0.65-1.1	7.33	4.54	16.13	9.76	29.91	10.70	207.03	16.06	16.30	39.89	n.d.	192.53	263.70	n.d.	37.94	19.13
1.1-2.1	11.22	2.68	16.41	4.47	385.14	14.82	277.64	71.40	n.d.	65.30	n.d.	211.58	n.d.	n.d.	86.17	n.d.
2.1-3.3	8.60	2.43	10.44	5.21	92.74	7.92	68.57	6.13	n.d.	10.59	14.91	371.76	72.63	n.d.	n.d.	n.d.
3.3-4.7	9.94	3.97	5.61	n.d.	15.73	3.62	5.18	2.55	n.d.	8.33	n.d.	181.50	44.59	n.d.	n.d.	n.d.
4.7-5.8	7.45	2.43	27.14	4.81	10.13	3.64	2.36	4.00	n.d.	3.89	n.d.	239.71	n.d.	n.d.	n.d.	n.d.
5.8-9.0	7.47	2.84	6.72	4.61	14.43	2.81	2.67	3.08	n.d.	n.d.	49.29	291.59	n.d.	n.d.	n.d.	n.d.
9.0-10.0	7.16	2.51	7.77	3.61	11.11	1.97	3.24	2.28	n.d.	n.d.	n.d.	213.52	n.d.	n.d.	n.d.	n.d.
Total	**85.72**	**30.00**	**126.52**	**55.87**	**662.79**	**68.67**	**888.88**	**261.43**	**231.86**	**316.19**	**309.43**	**2,402.90**	**670.24**	**n.d.**	**124.11**	**25.86**

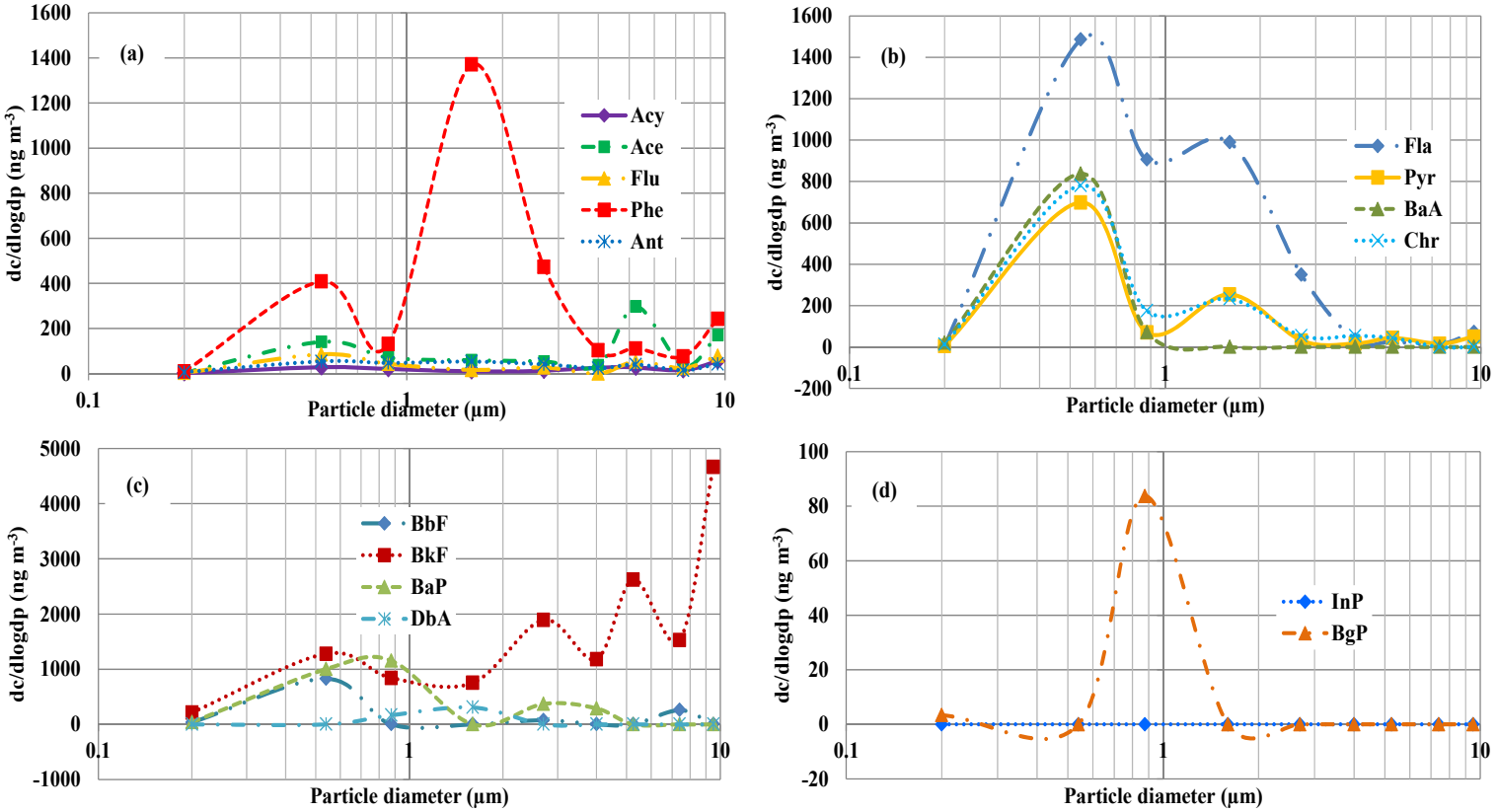

Figure 4. Size distributions of 3-6 ring PAHs adsorbed on particles during open burning of cable sheath (a) 3-ring PAHs, (b) 4-ring PAHs, (c) 5-ring PAHs and (d) 6-ring PAHs

3.3 Risk assessment

Figure 5 shows the ratios of 3-6 ring PAHs and carcinogenic PAHs adsorbed on particles during open burning of cable sheath. Ultrafine particles were composed of 2-ring PAHs (0.92% of total PAHs), 3-ring PAHs (5.84% of total PAHs), 4-ring PAHs (15.76% of total PAHs), 5-ring PAHs (76.59% of total PAHs) and 6-ring PAHs (0.89% of total PAHs). Fine particles contained 2-ring PAHs (1.05% of total PAHs), 3-ring PAHs (17.70% of total PAHs), 4-ring PAHs (41.01% of total PAHs), 5-ring PAHs (39.71% of total PAHs) and 6-ring PAHs (0.53% of total PAHs). Coarse particles comprised 2-ring PAHs (2.14% of total PAHs), 3-ring PAHs (13.40% of total PAHs), 4-ring PAHs (6.48% of total aPAHs) and 5-ring PAHs (77.98% of total PAHs). The inhalable particles (PM_{10}) were predominantly composed of 5-ring PAHs (55.67% of total PAHs) followed by 4-ring PAHs (27.58% of total PAHs) and 3-ring PAHs (14.98% of total PAHs) as shown in Figure 5(a). These results show that adsorption of low volatile PAHs onto particle surfaces was easier than that of high volatile ones due to their volatile property. This is closely related to the previous studies indicating that more than four aromatic rings readily adsorbed onto combustion aerosols [15-17]. However, only small amount of BgP, six-rings PAHs (0.41% of total PAHs) was observed. In this work, small amount of Nap attached on particles (1.36% of total PAHs) was detected even it is the most volatile PAHs. Several studies also found Nap in the particle phase [6, 36].

In this study, 16 PAHs were divided into four groups following the International Agency for Research on Cancer (IARC): BaP as carcinogenic to humans (Group 1), DbA as probably carcinogenic to humans (Group 2A), Nap, BaA, BbF, BkF, InP and Chr as possibly carcinogenic to humans (Group 2B), Acy, Ace, Flu, Phe, Ant, Fla, Pyr and BgP as not classifiable as to its carcinogenicity to humans (Group 3) [37]. The fraction of PAHs bound on ultrafine particles was mainly classified as Group 2B (79.59 % of the total mass), followed by Group 1 (10.85 % of the total mass), and Group 3 (9.56 % of the total mass) whereas Group 2A was not detected. The fraction of PAHs bound on fine particles was dominantly classified as Group 3 (46.56 % of the total mass) followed by Group 2B (37.01 % of the total mass), Group 1 (13.03% of the total mass), and Group 2A (3.40 % of the total mass), respectively. The fraction of PAHs bound on coarse particles was mainly classified as Group 2B (75.15 % of the total mass) followed by Group 3 (18.67 % of the total mass), Group 1 (6.18 % of the total mass) while Group 2A was not detected. The ratio of carcinogenic PAHs adsorbed on ultrafine particles was similar to that of coarse particles. The fraction of PAHs bound on the inhalable particles (PM_{10}) was primarily classified as Group 2B (53.45 % of the total mass) followed by Group 3 (33.86 % of the total mass), Group 1 (10.71 % of the total mass), and Group 2A (1.98 % of the total mass) as shown in Figure 5(b). The results reveal that some PAHs bound on particles during open burning of cable sheath were assessed as possible carcinogens to humans.

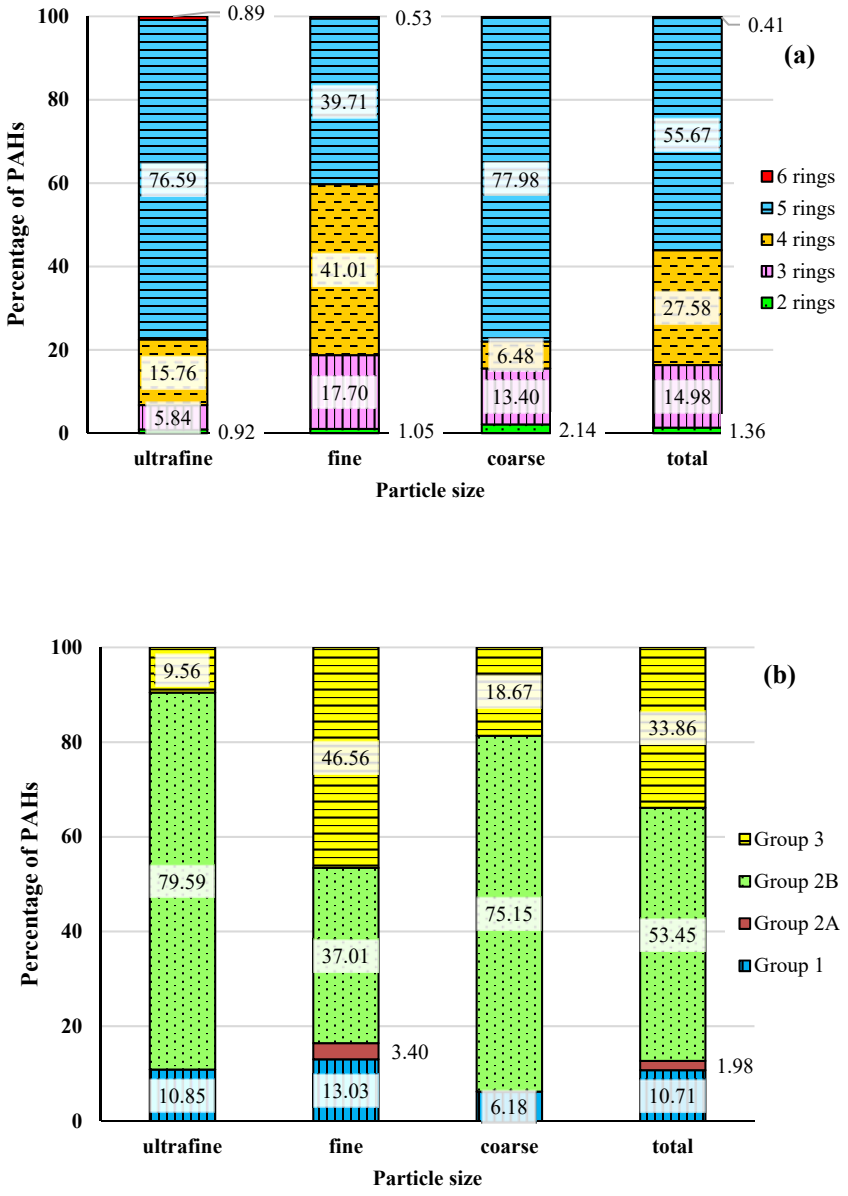

Figure 5. The ratios of 3-6 ring PAHs (a) and carcinogenic PAHs (b) adsorbed on particles during open burning of cable sheath

Table 2. Concentrations of 16 PAHs and B[a]P_{eq} adsorbed on particles

Compounds	TEF	Cable sheath burning	
		PAHs (ng m^{-3})	**B[a]P_{eq} (ng m^{-3})**
Nap	0.001*	85.71	0.08571
Acy	0.001*	29.99	0.02999
Ace	0.001*	126.54	0.12654
Flu	0.0005	55.88	0.02794
Phe	0.0005	662.78	0.33139
Ant	0.0005	68.67	0.03433
Fla	0.05	888.88	44.44423
Pyr	0.001	261.42	0.26142
BaA	0.005	231.86	1.15932
Chr	0.03	316.20	9.48589
BbF	0.1	309.43	30.94302
BkF	0.05	2,402.90	120.14512
BaP	1	670.24	670.23810
InP	0.1	n.d.	n.d.
DbA	1.1	124.11	136.52008
BgP	0.02	25.86	0.51719
Total		**6,260.47**	**1,014.35**
Lifetime lung cancer risk			**8.83E-02**

Note: TEFs derived from Larsen and Larsen [31] except TEFs* of Nap, Acy, Ace derived from Nisbet and Lagoy [30]
E-02 means additional cases per 100 people exposed.

Table 2 shows the concentrations of 16 PAHs bound on particles and BaP-equivalent during open burning of cable sheath. The concentrations of total PAHs and total B[a]P_{eq} during wire burning were 6,260.47 ng m^{-3} and 1,014.35 ng m^{-3}, respectively. The B[a]P_{eq} value during burning of cable sheath significantly exceeded 1 ng m^{-3} of the European Union's annual average standard [38]. The estimated lifetime cancer risk was 8.83E-02 (8.83 additional cases per 100 people exposed). The experimental results proposed that some PAHs released from open burning of cable sheath were established lung carcinogens resulting in high lung cancer risk, which is in consistent with the study of Wang *et al.* [19].

4. Conclusions

The ambient particles during open burning of cable sheath comprised coarse particles (49.59 % of the total mass) and fine particles (38.96 % of the total mass), and ultrafine particles (11.45 % of the total mass). The particle size distributions were bimodal with one major peak in the coarse mode (5.8-4.7 μm range) and another minor peak in the accumulation mode (1.1-0.65 μm range). Total PAHs were dominantly bound on fine particles (58.23% of the total PAHs) followed by coarse

particles (30.30% of the total PAHs) and ultrafine particles (11.47% of the total PAHs), respectively. The inhalable particles mainly contained 5-ring PAHs (55.67% of total PAHs) followed by 4-ring PAHs (27.58% of total PAHs) and 3-ring PAHs (14.98% of total PAHs), respectively. Some of the PAHs were determined as possibly carcinogenic to humans (Group 2B). The average concentrations of 16 PAHs and B[a]P_{eq} during open burning of cable sheath were 6,260.47 ng m^{-3} and 1,014.35 ng m^{-3}, respectively. The estimated lifetime lung cancer risk during wire burning was 8.83E-02 (8.83 additional cases per 100 people exposed). The exposure of PAHs adsorbed on particles during open burning of cable sheath was potentially high risk for developing lung cancer.

5. Acknowledgements

This research was supported by the Ratchadaphiseksomphot Endowment Fund 2013 of Chulalongkorn University (CU-56-855-SD). The authors are also grateful to Faculty of Science, King Mongkut's Institute of Technology Ladkrabang (KMITL) for support of this work through a studentship (Thidarat Keawhanu).

References

[1] Baldé, C.P., Forti, V., Gray, V., Kuehr, R. and Stegmann, P., 2017. *The global e-waste monitor–2017*. United Nations University (UNU), International Telecommunication Union (ITU) and International Solid Waste Association. Bonn, Geneva, Vienna.

[2] Li, L., Liu, G., Pan, D., Wang, W., Wu, Y. and Zuo, T., 2017. Overview of the recycling technology for copper-containing cables. *Resources, Conservation and Recycling*, 126, 132-140.

[3] Suresh, S.S., Mohanty, S. and Nayak, S.K., 2017. Composition analysis and characterization of waste polyvinyl chloride (PVC) recovered from data cables. *Waste Management*, 60, 100-111.

[4] Gangwar, C., Choudhari, R., Chauhan, A., Kumar, A., Singh, A. and Tripathi, A., 2019. Assessment of air pollution caused by illegal e-waste burning to evaluate the human health risk. *Environment International*, 125, 191-199.

[5] Nishimura, C., Horii, Y., Tanaka, S., Asante, K.A., Ballesteros, Jr. F., Viet, P.H., Itai, T., Takigami, H., Tanabe, S. and Fujimori, T., 2017. Occurrence, profiles, and toxic equivalents of chlorinated and brominated polycyclic aromatic hydrocarbons in E-waste open burning soils. *Environmental Pollution*, 225, 252-260.

[6] Lv, Y., Li, X., Xu, T.T., Cheng, T.T., Yang, X., Chen, J.M., Iinum, Y. and Herrmann, H., 2016. Size distribution of polycyclic aromatic hydrocarbons in urban atmosphere: sorption mechanism and source contributions to respiratory deposition. *Atmospheric Chemistry and Physics*, 16(5), 2971-2983.

[7] Ji, H., Zhang, D. and Shinohara, R., 2007. Size distribution and estimated carcinogenic potential of particulate polycyclic aromatic hydrocarbons collected at a downtown site in Kumamoto, Japan, in spring. *Journal of Health Science*, 53(6), 700-707.

[8] Schwartz, J. and Neas, L.M., 2000. Fine particles are more strongly associated than coarse particles with acute respiratory health effects in school children. *Epidemiology*, 11, 6-10.

[9] Meng, X., Ma, Y., Chen, R., Zhou, Z., Chen, B. and Kan, H., 2013. Size-fractionated particle number concentrations and daily mortality in a Chinese City. *Environmental Health Perspectives*, 121(10), 1174-1178.

[10] Yu, J., Sun, L., Ma, C., Qiao, Y. and Yao, H., 2016. Thermal degradation of PVC: a review. *Waste Management*, 48, 300-314.
[11] Richter, H. and Howard, J.B., 2000. Formation of polycyclic aromatic hydrocarbons and their growth to soot-a review of chemical reaction pathways. *Progress in Energy and Combustion Science*, 26, 565-608.
[12] Sitaras, I.E., Bakeas, E.B. and Siskos, P.A., 2004. Gas/particle partitioning of seven volatile polycyclic aromatic hydrocarbons in a heavy traffic urban area. *Science of the Total Environment*, 327(1-3), 249-264.
[13] Venkataraman, C., Thomas, S. and Kulkarni, P., 1999. Size distributions of polycyclic aromatic hydrocarbons-Gas/particle partitioning to urban aerosols. *Journal of Aerosol Science*, 30, 759-770.
[14] Allen, J.O., Dookeran, K.M., Smith, K.A., Sarofim, A.F., Taghizadeh, K. and Lafleur, A.L., 1996. Measurement of polycyclic aromatic hydrocarbons associated with size-segregated atmospheric aerosols in Massachusetts. *Environmental Science and Technology*, 30, 1023-1031.
[15] Cincinelli, A., Bubba, M.D., Martellini, T., Gambaro, A. and Lepri, L., 2007, Gas-particle concentration and distribution of n-alkanes and polycyclic aromatic hydrocarbons in the atmosphere of Prato (Italy). *Chemosphere*, 68, 472-478.
[16] Spezzano, P., Picini, P. and Cataldi, D., 2009. Gas-and particle-phase distribution of polycyclic aromatic hydrocarbons in two-stroke, 50-cm3 moped emissions. *Atmospheric Environment*, 43, 539-545.
[17] Harrison, R.M., Smith, D.J.T. and Luhana, L., 1996. Source apportionment of atmospheric polycyclic aromatic hydrocarbons collected from an urban location in Birmingham, UK. *Environmental Science and Technology*, 30(3), 825-832.
[18] IARC, 2010. *Monographs on the Evaluation of Carcinogenic Risk to Humans. Vol. 92, Some Non-Heterocyclic Polycyclic Aromatic Hydrocarbons and Some Related Exposures*. Lyon : International Agency for Research on Cancer.
[19] Wang, J., Chen, S., Tian, M., Zheng, X., Gonzales, L., Ohura, T., Mai, B. and Simonich, S.L.M., 2012. Inhalation cancer risk associated with exposure to complex polycyclic aromatic hydrocarbon mixtures in an electronic waste and urban area in south China. *Environmental Science and Technology*, 46, 745-9752.
[20] Keshtkar, H. and Ashbaugh, L.L., 2007. Size distribution of polycyclic aromatic hydrocarbon particulate emission factors from agricultural burning. *Atmospheric Environment*, 41, 2729-2739.
[21] Wu, D., Wang, Z., Chen, J., Kong, S., Fu, X., Deng, H., Shao, G. and Wu, G., 2014. Polycyclic aromatic hydrocarbons (PAHs) in atmospheric PM2.5 and PM10 at a coal-based industrial city: Implication for PAH control at industrial agglomeration regions, China. *Atmospheric Research*, 149, 217-229.
[22] Menichini, E., Monfredini, F. and Merli, F., 1999. The temporal variability of the profile of carcinogenic polycyclic aromatic hydrocarbons in urban air: study in a medium traffic area in Rome, 1993-1998. *Atmospheric Environment*, 33, 3739-3750.
[23] Lu, W., Yang, L., Chen, J., Wang, X., Li, H., Zhu, Y., Wen, L., Xu, C., Zhang, J., Zhu, T. and Wang, W., 2016. Identification of concentrations and sources of PM2.5-bound PAHs in North China during haze episodes in 2013. *Air Quality Atmosphere and Health*, 9, 823-833.
[24] Niu, J., Sun, P. and Schramm, K-W., 2007. Photolysis of polycyclic aromatic hydrocarbons associated with fly ash particles under simulated sunlight irradiation. *Journal of Photochemistry and Photobiology A: Chemistry*, 186, 93–98.

[25] Zheng, X., Huo, X., Zhang, Y., y Wang, Q., Zhang, Y. and Xu, X., 2019. Cardiovascular endothelial inflammation by chronic coexposure to lead (Pb) and polycyclic aromatic hydrocarbons from preschool children in an e-waste recycling area. *Environmental Pollution*, 246, 587-596.

[26] Zhang, K., Zhang, B.Z., Li, S.M., Wong, C.S. and Zeng, E.Y., 2012. Calculated respiratory exposure to indoor size-fractioned polycyclic aromatic hydrocarbons in an urban environment. *Science of the Total Environment*, 431, 245-251.

[27] US EPA, 1999. Office of Research and Development, National Center for Environmental Assessment, Washington Office, Washington DC, EPA/600/P-99/002.

[28] Phoothiwut, S. and Junyapoon, S., 2013. Size distribution of atmospheric particulates and particulate-bound polycyclic aromatic hydrocarbons and characteristics of PAHs during haze period in Lampang Province, northern Thailand. *Air Quality Atmosphere and Health*, 6, 397-405.

[29] US EPA, 1999. *Compendium Method TO-13A Determination of Polycyclic Aromatic Hydrocarbons (PAHs) in Ambient Air using Gas Chromatography/Mass Spectrometry (GC/MS)*. Cincinnati : Center for Environmental Research Information Office of Research and Development, U.S. Environmental Protection Agency.

[30] Nisbet, I.C.T. and LaGoy, P.K., 1992. Toxic equivalent factors (TEFs) for polycyclic aromatics hydrocarbons (PAHs). *Regulatory Toxicology and Pharmacology*, 16, 290-300.

[31] Larsen, J.C. and Larsen, P.B., 1998. Chemical carcinogens. In: R.E. Herster and R.M. Harrison, eds. *Air Pollution and Health*. Cambridge : Royal Society of Chemistry, pp 33-56.

[32] OEHHA, 1993. Benzo[a]pyrene as a toxic air contaminant. In: *Part B. Health Effects of Benzo [a] pyrene*. Berkeley : California Environmental Protection Agency, Office of Environmental Health Hazard Assessment, Air Toxicology and Epidemiology Section.

[33] OEHHA, 2005. Air toxics hot spots program risk assessment guidelines. In: *Part II. Technical Support Document for Describing Available Cancer Potency Factors*. Oakland : California Environmental Protection Agency, Office of Environmental Health Hazard Assessment, Air Toxicology and Epidemiology Section.

[34] WHO, 2000. Air quality guidelines for Europe. 2nd ed. In: *European Series, No. 91 WHO Regional Publication*. Copenhagen : World Health Organization Regional Office for Europe.

[35] Ramírez, N., Cuadras, A., Rovira, E., Marcé, R.M. and Borrull, F., 2011. Risk assessment related to atmospheric polycyclic aromatic hydrocarbons in gas and particle phases near industrial sites. *Environmental Health Perspectives*, 119(8), 1110-1116.

[36] Pooltawee, J., Pimpunchat, B. and Junyapoon, S., 2017. Size distribution, characterization and risk assessment of particle-bound polycyclic aromatic hydrocarbons during haze periods in Phayao Province, northern Thailand. *Air Quality Atmosphere and Health,* 10, 1097-1112.

[37] IARC, 2019. *List of Classifications, Volumes 1-123*. [online] Available at: https://monographs.iarc.fr/list-of-classifications-volumes/. Accessed in January 2019.

[38] EU, 2019. Air quality standards. [online] Available at: www.transportpolicy.net/standard/eu-air-quality-standards/. Accessed in January 2019.

Mathematical Model of Dengue Virus with Primary and Secondary Infection

Rattiya Sungchasit[1] and Puntani Pongsumpun[2*]

[1]Department of Mathematics, Faculty of Science and Technology,
Phuket Rajabhat University, Phuket, Thailand
[2]Department of Mathematics, Faculty of Science,
King Mongkut's Institute of Technology Ladkrabang, Bangkok, Thailand

Received: 22 January 2019, Revised: 7 May 2019, Accepted: 7 May 2019

Abstract

In this study, we analyzed SEIR model for human and SEI model for mosquitoes. We considered the development of dengue infection from dengue fever (DF) to dengue hemorrhagic fever (DHF). The stability of the endemic equilibrium and the disease-free equilibrium states are incurred by Routh-Hurwitz criteria. Numerical simulations for the model are used to solve a system of differential equations. It showed that the local stability for disease free states and endemic states depended on the basic reproductive rate of the disease. The results of this study is recommended as an effective control measure for reducing the transmission of dengue disease.

Keywords: dengue fever, SEIR model, SEI model
DOI 10.14456/cast.2019.14

1. Introduction

Dengue is a violent infectious disease that occurs in tropical and sub-tropical regions, being one of the average harsh arthropod borne viral disease in group of human death and morbidity [1-5]. Dengue occurs due to an infection of virus in the *Flaviviridae* Family. Four serotypes of the dengue virus, namely DENV-1, -2, -3 and -4 have been identified as the main causes of the infection. An infection with any type of these viruses may be asymptomatic or causing temperature sickness known as dengue fever (DF). Such epidemic occurs due to atmosphere change and limited understanding of the degenerate native of the dengue disease. The World Health Organization (WHO) has reported approximately 50 -100 million cases globally, including 50,000 cases infected with dengue hemorrhagic fever (DHF) or dengue shock syndrome (DSS) annually [1, 6-12]. The main prevalence of this epidemic disease is in Central America, Southeast Asia and South Asia [11-16].

*Corresponding author: Tel.: 662-329-8000 Ext. 6196 Fax: 662-329-8412
E-mail: kppuntan@kmitl.ac.th

Since preliminary symptoms of the DFF/DSS and DF are similar, a relatively short period of infection further complicates the diagnosis of the disease, as well as of the possible person having the capacity of spreading severe transpiration, DHF represents a separate pathophysiological procedure or is only the opposite end of a continuation of identical diseases. DF follows a change from the normal but rather a danger self-inclined course. DHF may show as a relatively mild infection at first but can quickly develop into life-menacing disease as fever reduces. DHF can mainly be distinguished from the usual dengue fever due to three predictable classification phrases [4, 13].

WHO classifies the type of DF based on the severity of illness. Classic dengue fever "break bone fever" is identified by beginning of a high fever. The symptom appears 3 to 14 days after the biting of infected mosquitoes. The characteristics of DF are myalgia, headache, rash and arthralgias. As the fever begins to subside 3 to 7 days after first appearance of the symptom, the patient may have complete resolution of symptoms, or go on to develop DHF. It assorts dengue virus as with or without forewarning covenant (aching belly, retaining, severe vomiting, mucosal hemorrhage, nausea and sleepiness, high hematocrit with low thrombocytes) and violent dengue (violent plasma puncture, violent hemorrhage, or stalk naught) [9, 13-18]. Cases of DHF are defined by four characteristics: recent history of any hemorrhagic manifestation fever, thrombocytopenia and evidence of increased vascular permeability. Cases of dengue shock syndrome meet the four criteria for DHF but also show signs of circulatory failure, rapid, narrow pulse pressure such as a weak pulse or hypotension. The risk of progression to DHF or DSS is increased in secondary infection when the individual has been infected previously by a different virus serotype [16-21].

Many researches have applied mathematical model to describe the transmission of dengue fever. The work of Sungchasit and Pongsumpun [8] used SEIR model to describe the transmission of dengue disease between human and mosquito in each season. SIR model was used to study the transmission of dengue infection with two types of mosquitoes such as *Aedes aegypti* and *Aedes albopictus* mosquitoes [22]. Changal *et al*. [17] studied about the clinical course and IgG/IgM ratio was used to separate the difference between primary and secondary infections. Esteva and Vargas [7] used SIR model for describing the transmission of dengue fever in a constant human population and variable vector population. Syafruddin and Noorani [14] studied the system of differential equations for the dynamics of SEIR model for DF. For more detailed prediction of the epidemic, it is necessary to examine the higher order moments, namely the variance of the number of infected. The predictability of mean-field models depends on the variations around the mean [22-25]. In this work, we focus on the mathematical model of dengue disease with the development of dengue infection from DF to DHF.

2. Mathematical Model

We use mathematical model to formulate the dynamical equations between human and mosquito populations. The development of dengue infection from DF to DHF is considered. We separate the human population into 4 groups, namely Susceptible group (S), Exposed group (E), Infectious group (I) and Recovered group (R). The infectious group is further subdivided into two subclasses; those infected with DF and those whose disease has morphed into DHF. The mosquito populations are subdivided into 3 groups, namely Susceptible group (S), Exposed group (E) and Infectious group (I) because the mosquitoes do not recover from infection. The basis of evidence is that all human population and mosquito population possess fixed rate sizes [6-8, 15, 17]. The characteristics of dengue fever transmission can be described through a state transition diagram as shown in Figures 1-2 [7, 17, 21]. The variables and parameters for model is explained in Table 1.

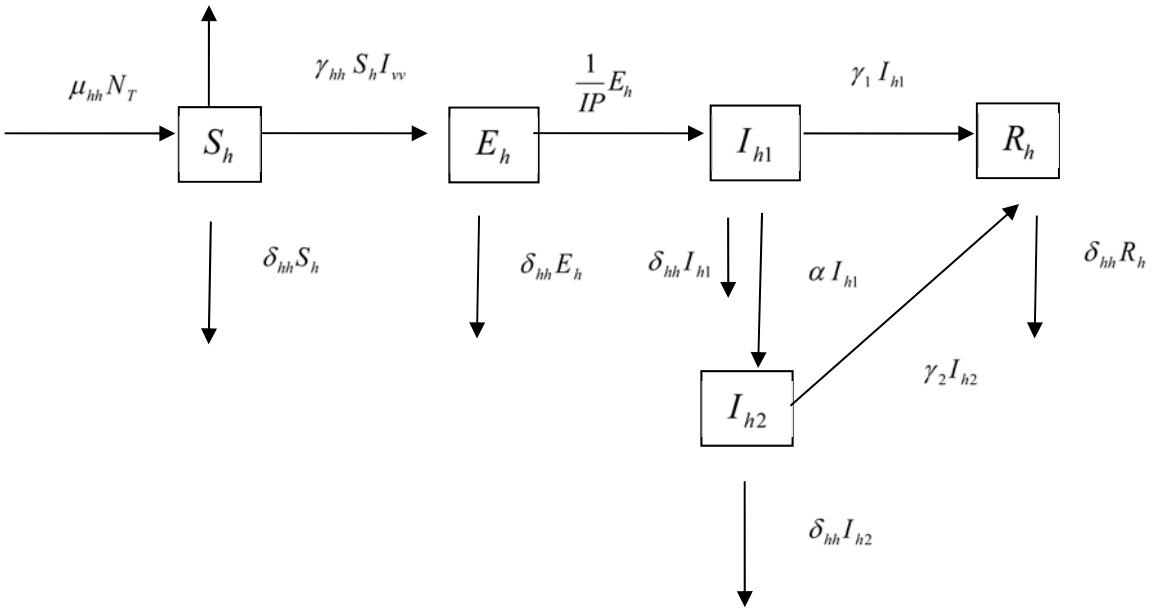

Figure 1. The state transition diagram for the human population

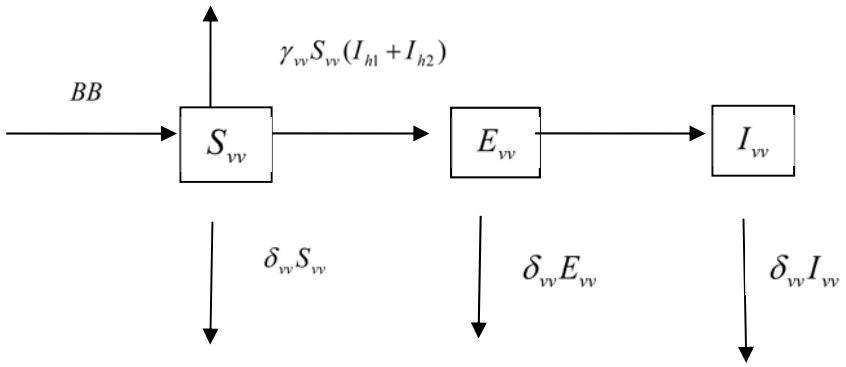

Figure 2. The state transition diagram for the mosquito population

Table 1. The variables and parameters in model

Variables/ parameters	Description
S_h	The number of susceptible human population
E_h	The number of exposed human population (infected but not yet transmit the dengue virus)
I_{h1}	The number of DF patients
I_{h2}	The number of DHF patients
R_h	The number of recovery human population
S_{vv}	The number of susceptible mosquito population
E_{vv}	The number of exposed mosquito population (infected but not yet transmit the dengue virus)
I_{vv}	The number of infectious mosquito population
μ_{hh}	The birth rate of human population
δ_{hh}	The death rate of human population
N_T	The total human population
γ_{hh}	The transmission probability of dengue virus from mosquito to human
$\frac{1}{IP}$	Incubation rate of dengue virus in human population
γ_1	The recovery rate of DF cases
γ_2	The recovery rate of DHF cases
γ_{vv}	The transmission probability of dengue disease from human to mosquitoes
α	The rates of change from DF cases to DHF cases
BB	The recruitment rate of mosquitoes
N_v	The total mosquitoes
δ_{vv}	The death rate of mosquitoes
$\frac{1}{EP}$	The incubation rate of dengue virus in mosquito population

From the state transition diagram of Figure 1, the following system of differential equations is written for the human population.

$$\frac{dS_h}{dt} = \mu_{hh} N_T - \gamma_{hh} S_h I_{vv} - \delta_{hh} S_h \quad (1)$$

$$\frac{dE_h}{dt} = \gamma_{hh} S_h I_{vv} - \delta_{hh} E_h - \frac{1}{IP} E_h \quad (2)$$

$$\frac{dI_{h1}}{dt} = \frac{1}{IP} E_h - \delta_{hh} I_{h1} - \gamma_1 I_{h1} - \alpha I_{h1} \quad (3)$$

$$\frac{dI_{h2}}{dt} = \alpha I_{h1} - \delta_{hh} I_{h2} - \gamma_2 I_{h2} \quad (4)$$

$$\frac{dR_h}{dt} = \gamma_1 I_{h1} + \gamma_2 I_{h2} - \delta_{hh} R_h \quad (5)$$

Similarly, the state transition diagram of Figure 2 admits the following system of differential equations for the mosquito population.

$$\frac{dS_{vv}}{dt} = BB - \gamma_{vv} S_{vv} (I_{h1} + I_{h2}) - \delta_{vv} S_{vv} \quad (6)$$

$$\frac{dE_{vv}}{dt} = \gamma_{vv} S_{vv} (I_{h1} + I_{h2}) - \delta_{vv} E_{vv} - \frac{1}{EP} E_{vv} \quad (7)$$

$$\frac{dI_{vv}}{dt} = \frac{1}{EP} E_{vv} - \delta_{vv} I_{vv} \quad (8)$$

Therefore, the rate of changes for total human and mosquito populations is equal to zero. From Setting $\frac{dN_{vv}}{dt} = 0$ and $\frac{dN_T}{dt} = 0$, we can have $\mu_{hh} = \delta_{hh}$. Birth rates and death rates are equivalent for human population. For mosquito population, we have $\mu_{vv} = BB$.

We introduce the normalized variables

$S'_h = \frac{S_h}{N_T}, E'_h = \frac{E_h}{N_T}, I'_{h1} = \frac{I_{h1}}{N_T}, I'_{h2} = \frac{I_{h2}}{N_T}, R'_h = \frac{R_h}{N_T}$ and

$S'_{vv} = \frac{S_{vv}}{N_{vv}}, E'_{vv} = \frac{E_{vv}}{N_{vv}}, I'_{vv} = \frac{I_{vv}}{N_{vv}}$, then the reduced equations become

$$\frac{dS'_h}{dt} = \mu_{hh} - \gamma_{hh} S'_h I'_{vv} N_{vv} - \delta_{hh} S'_h \quad (9)$$

$$\frac{dE'_h}{dt} = \gamma_{hh} S'_h I'_{hv} N_{vv} - \delta_{hh} E'_h - \frac{1}{IP} E'_h \quad (10)$$

$$\frac{dI'_{h1}}{dt} = \frac{1}{IP} E'_h - \delta_{hh} I'_{h1} - \gamma_1 I'_{h1} - \alpha I'_{h1} \quad (11)$$

$$\frac{dI'_{h2}}{dt} = \alpha I'_{h1} - \delta_{hh} I'_{h2} - \gamma_2 I'_{h2} \quad (12)$$

$$\frac{dE'_{vv}}{dt} = \gamma_{vv}(1-E'_{vv}-I'_{vv})(I'_{h1}N_T + I'_{h2}N_T) - \delta_{vv}E'_{vv} - \frac{1}{EP}E'_{vv} \quad (13)$$

$$\frac{dI'_{vv}}{dt} = \frac{1}{EP}E'_{vv} - \delta_{vv}I'_{vv} \quad (14)$$

with the conditions $S'_h + E'_h + I'_{h1} + I'_{h2} + R'_h = 1$ and $S'_{vv} + E'_{vv} + I'_{vv} = 1$.

3. Analysis of Mathematical Model

We analyze the formulated model and described the variant region and the positive of solutions. The feasible solution set of systems enters the region with the initial conditions as follows:

$$\Omega = \{(S_h, E_h, I_{h1}, I_{h2}, E_{vv}, I_{vv}) : 0 \le S_h + E_h + I_{h1} + I_{h2} \le 1; E_{vv} + I_{vv} \le 1\}.$$

We will just define the conditions for local stability through an analysis of the boundaries of the areas where the equilibrium points are in Ω [22].

3.1 Equilibrium points

The equilibrium points are incurred by setting the righthand side of equations (9)-(14) equal to zero. We obtained the equilibrium points as follows: [7, 22]
Disease free equilibrium point:

$$P_0 = (\frac{\mu_{hh}}{\delta_{hh}}, 0, 0, 0, 0, 0)$$

Endemic equilibrium point:

$$P_1 = (S_h^*, E_h^*, I_{h1}^*, I_{h2}^*, E_{vv}^*, I_{vv}^*)$$

Where:

$$S_h^* = \frac{\mu_{hh}}{\delta_{hh} + I_{vv}^* N_{vv}\gamma_{hh}},$$

$$E_h^* = \frac{IP\, I_{vv}^* N_{vv}\gamma_{hh}\mu_{hh}}{(1+\delta_{hh}\, IP)(\delta_{hh} + I_{vv}^* N_{vv}\gamma_{hh})},$$

$$I_{h1}^* = \frac{I_{vv}^* N_{vv}\gamma_{hh}\mu_{hh}}{(1+\delta_{hh}\, IP)(\delta_{hh}+\alpha+\gamma_1)(\delta_{hh} + I_{vv}^* N_{vv}\gamma_{hh})},$$

$$I_{h2}^* = \frac{I_{vv}^* N_{vv}\gamma_{hh}\mu_{hh}\alpha}{(1+\delta_{hh}\, IP)(\delta_{hh}+\alpha+\gamma_1)(\delta_{hh} + I_{vv}^* N_{vv}\gamma_{hh})(\delta_{hh}+\gamma_2)}, \quad E_{vv}^* = \frac{EP(I_{h1}^* + I_{h2}^*)(-1+I_{vv}^*)N_T\gamma_{vv}}{1+EP((I_{h1}^* + I_{h2}^*)N_T\gamma_{vv} + \mu_{vv}}},$$

$$I_{vv}^* = \frac{(N_T N_{vv}(\delta_{hh}+\alpha+\gamma_2)\gamma_{hh}\gamma_v\mu_{hh} - \delta_{hh}(1+\delta_{hh}IP)(\delta_{hh}+\alpha+\gamma_1)(\delta_{hh}+\gamma_2)\mu_{vv} - \delta_{hh}EP(1+\delta_{hh}IP)(\delta_{hh}+\alpha+\gamma_1)(\delta_{hh}+\gamma_2)\mu_{vv}^2)}{N_{vv}\gamma_{hh}(1+EP\mu_{vv})(N_T(\delta_{hh}+\alpha+\gamma_2)\gamma_{vv}\mu_{hh} + (1+\delta_{hh}IP)(\delta_{hh}+\alpha+\gamma_1)(\delta_{hh}+\gamma_2)\mu_{vv}}$$

3.2 Stability analysis

Theorem 3.2.1 Disease free equilibrium point of the method is locally asymptotically stable if $R_0 < 1$ and unstable if $R_0 > 1$.

Proof: We consider the equations

$$S_h = \mu_{hh} - \gamma_{hh} S'_h I'_{vv} N_{vv} - \delta_{hh} S'_h \tag{15}$$

$$E_h = \gamma_{hh} S'_h I'_{vv} N_{vv} - \delta_{hh} E'_h - \frac{1}{IP} E'_h \tag{16}$$

$$I_{h1} = \frac{1}{IP} E'_h - \delta_{hh} I'_{h1} - \gamma_1 I'_{h1} - \alpha I'_{h1} \tag{17}$$

$$I_{h2} = \alpha I'_{h1} - \delta_{hh} I'_{h2} - \gamma_2 I'_{h2} \tag{18}$$

$$E_{vv} = \gamma_{vv}(1 - E'_{vv} - I'_{vv})(I'_{h1} N_T + I'_{h2} N_T) - \delta_{vv} E'_{vv} - \frac{1}{EP} E'_{vv} \tag{19}$$

$$I_{vv} = \frac{1}{EP} E'_{vv} - \delta_{vv} I'_{vv} \tag{20}$$

The eigenvalues are computed from the solutions of the characteristic equation $|S - \lambda I| = 0$, where S is the Jacobian matrix at the equilibrium point and I is the identity matrix of dimension 6x6. If all the eigenvalues have negative real parts, then the equilibrium point is locally stable [7].

The Jacobian matrix evaluated at $P_0 = (\frac{\mu_{hh}}{\delta_{hh}}, 0, 0, 0, 0, 0)$ is given as

$$S_0 = \begin{pmatrix} -(\delta_{hh}) & 0 & 0 & 0 & 0 & -\gamma_{hh}(\frac{\mu_{hh}}{\delta_{hh}}) N_w \\ 0 & -(\delta_{hh} + \frac{1}{IP}) & 0 & 0 & 0 & \gamma_{hh}(\frac{\mu_{hh}}{\delta_{hh}}) N_w \\ 0 & \frac{1}{IP} & -(\delta_{hh} + \gamma_1) & \alpha & 0 & 0 \\ 0 & 0 & 0 & -(\delta_{hh} + \gamma_2) & 0 & 0 \\ 0 & 0 & \gamma_w(N_T) & \gamma_w(N_T) & -\mu_w - ((1/EP)) & -((0)+(0)) N_T \gamma_w \\ 0 & 0 & 0 & 0 & \frac{1}{EP} & -\mu_w \end{pmatrix}.$$

The characteristic equation is given as

$$\lambda^6 + A_1\lambda^5 + A_2\lambda^4 + A_3\lambda^3 + A_4\lambda^2 + A_5\lambda^1 + A_6 = 0,$$

Where:

$$A_1 = 4\delta_{hh} + \frac{1}{EP} + \frac{1}{IP} + 2\left(\gamma_1 + \gamma_2 + 2\mu_{vv}\right) \tag{21}$$

$$A_2 = \frac{1}{EP\,IP}(1 + 6\delta_{hh}{}^2\, EP\,IP + IP(\gamma_1 + \gamma_2 + \mu_{vv}) + EP(\gamma_1 + \gamma_2 + IP\gamma_1\gamma_2 + 2(1 + IP(\gamma_1 + \gamma_2))\mu_{vv} + IP\,\mu_{vv}{}^2) + \delta_{hh}(4IP + EP(3 + 3IP(\gamma_1 + \gamma_2) + 8\,IP\mu_{vv}))) \tag{22}$$

$$A_3 = \frac{1}{EP\,IP}(4\delta_{hh}{}^3 EP\,IP + \gamma_1 + \gamma_2 + (EP + IP)\gamma_1\gamma_2 + \mu_{vv} + (IP(\gamma_1 + \gamma_2) + 2EP(\gamma_1 + \gamma_2 + IP\gamma_1\gamma_2))\mu_{vv} + EP(1 + IP(\gamma_1 + \gamma_2))\mu_{vv}{}^2 + \delta_{hh}(3 + 3IP(\gamma_1 + \gamma_2) + 4\,IP\mu_{vv} + 2EP(\gamma_1 + \gamma_2 + IP\gamma_1\gamma_2 + 3(1 + IP(\gamma_1 + \gamma_2))\mu_{vv} + 2IP\mu_{vv}{}^2)) + 3\delta_{hh}{}^2(2IP + EP(1 + IP(\gamma_1 + \gamma_2 + 4\mu_{vv})))) \tag{23}$$

$$A_4 = \frac{1}{EP\,IP}(-N_T N_{vv}\gamma_{hh}\gamma_{vv}\mu_{hh} + \delta_{hh}(\delta_{hh}{}^4 EP\,IP + \gamma_1\gamma_2 + (\gamma_1 + \gamma_2 + (2EP + IP)\gamma_1\gamma_2)\mu_{vv} + EP(\gamma_1 + \gamma_2 + IP\gamma_1\gamma_2)\,\mu_{vv}{}^2 + \delta_{hh}(2\gamma_1 + 2\gamma_2 + EP\gamma_1\gamma_2 + 2IP\gamma_1\gamma_2 + (3 + 3IP(\gamma_1 + \gamma_2) + 4EP(\gamma_1 + \gamma_2 + IP\gamma_1\gamma_2))\,\mu_{vv} + 3EP(1 + IP(\gamma_1 + \gamma_2))\mu_{vv}{}^2) + \delta_{hh}{}^2(3 + 3IP(\gamma_1 + \gamma_2 + 2\mu_{vv}) EP(\gamma_1 + \gamma_2 + IP\gamma_1\gamma_2 + 6(1 + IP(\gamma_1 + \gamma_2))\mu_v + 6IP\mu_{vv}{}^2)) + \delta_{hh}{}^3(4IP + EP(1 + IP(\gamma_1 + \gamma_2 + 8\mu_{vv}))))) \tag{24}$$

$$A_5 = \frac{1}{EP\,IP}(-N_T N_{vv}\gamma_{hh}\gamma_{vv}\mu_{hh} + \delta_{hh}(\delta_{hh}{}^4 EP\,IP + \gamma_1\gamma_2 + (\gamma_1 + \gamma_2 + (2EP + IP)\gamma_1\gamma_2)\mu_{vv} + EP(\gamma_1 + \gamma_2 + IP\gamma_1\gamma_2)\,\mu_{vv}{}^2 + \delta_{hh}(2\gamma_1 + 2\gamma_2 + EP\gamma_1\gamma_2 + 2IP\gamma_1\gamma_2 + (3 + 3IP(\gamma_1 + \gamma_2) + 4EP(\gamma_1 + \gamma_2 + IP\gamma_1\gamma_2))\,\mu_{vv} + 3EP(1 + IP(\gamma_1 + \gamma_2))\mu_{vv}{}^2) + \delta_{hh}{}^2(3 + 3IP(\gamma_1 + \gamma_2 + 2\mu_{vv}) EP(\gamma_1 + \gamma_2 + IP\gamma_1\gamma_2 + 6(1 + IP(\gamma_1 + \gamma_2))\mu_{vv} + 6IP\mu_{vv}{}^2)) + \delta_{hh}{}^3(4IP + EP(1 + IP(\gamma_1 + \gamma_2 + 8\mu_{vv}))))) \tag{25}$$

$$A_6 = \frac{(\delta_{hh} + \gamma_2)(-N_T N_{vv}\gamma_{hh}\gamma_{vv}\mu_{hh} + \delta_{hh}(1 + \delta_{hh}IP)(\delta_{hh} + \gamma_1)\mu_{vv}(1 + EP\mu_{vv}))}{EP\,IP} \tag{26}$$

All six eigenvalues possess negative real parts if they satisfy the Routh-Hurwitz criteria. Hence, the equilibrium point is locally asymptotically stable if the following conditions are satisfied [7-9, 11, 13, 19].

$$A_1 A_2 > A_3 \tag{27}$$

$$A_1 A_2 A_3 > A_3^2 + A_1^2 A_4 \tag{28}$$

$$A_2 A_3\, A_5 + A_1 A_4 (A_2 A_3 + A_5) > A_4 (A_3^2 + A_1^2 A_4) + A_1 A_2^2 A_5 \tag{29}$$

$$A_2 A_3\, A_5^2 + A_1 A_4 A_5\, (A_2 A_3 + 2A_5) + A_3^3 A_6 + A_1^2 (A_3 A_4 + 2A_2 A_5) A_6 > A_5 (A_4 (A_3^2 + A_1^2 A_4) + A_1 A_2^2 A_5 + A_5^2) + A_1 A_3 (A_2 A_3 + 3A_5) A_6 + A_1^3 A_6^2 \tag{30}$$

The conditions of equations (27)-(30) are investigated numerically. Figure 3 plots the results of this investigation. It is evident that if $R_0 < 1$, the Routh-Hurwitz criteria is satisfied.

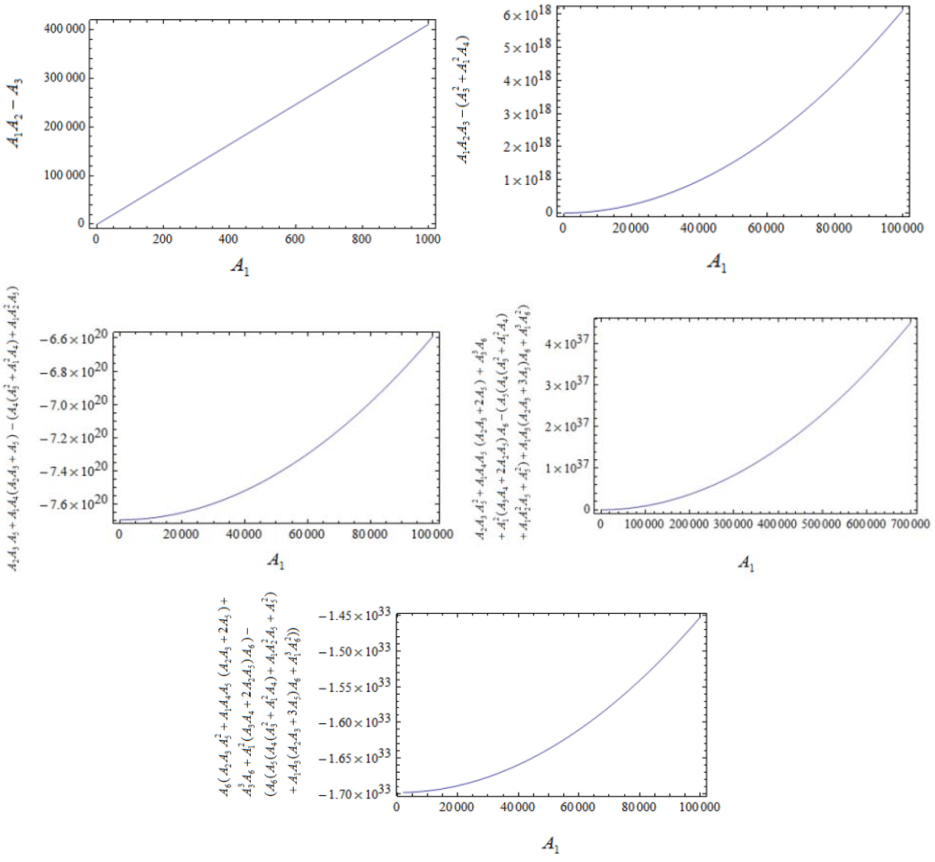

Figure 3. The parameter spaces of disease-free equilibrium point that influences the Routh-Hurwitz criteria with the value of parameters; $\gamma_1 = 0.178$, $\delta_{hh} = 1/(365*74)$, $\gamma_{hh} = 0.5$, $\gamma_{vv} = 0.8$, $\gamma_2 = 0.4$, $EP = 0.87$, $\alpha = 0.001$, $IP = 0.09$, $N_T = 100{,}000$, $N_{vv} = 5{,}000$

Each subfigures of Figure 3 shows the values for each condition of equations (27)- (30) where the parameter A_1 is changed and the other parameters are kept fixed. It is evident that the Routh-Hurwitz situations are satisfied for the case of $R_0 < 1$.

Theorem 3.2.2 If $R_0 > 1$, the endemic equilibrium stable P_1 is locally asymptotically stable.

Proof: The Jacobian matrix is evaluated on the endemic equilibrium point $P_1 = (S_h^*, E_h^*, I_{h1}^*, I_{h2}^*, E_{vv}^*, I_{vv}^*)$ as given by

$$S_1 = \begin{pmatrix} -(\gamma_{hl} I^*_{vv} N_{vv} + \delta_{hh}) & 0 & 0 & 0 & 0 & -\gamma_{hh} S^*_h N_{vv} \\ \gamma_{hl} I^*_{vv} N_{vv} & -(\delta_{hh} + \frac{1}{IP}) & 0 & 0 & 0 & \gamma_{hh} S^*_h N_{vv} \\ 0 & \frac{1}{IP} & -(\delta_{hh} + \gamma_1) & \alpha & 0 & 0 \\ 0 & 0 & 0 & -(\delta_{hh} + \gamma_2) & 0 & 0 \\ 0 & 0 & \gamma_{vv}(1 - E'_{vv} - I'_{vv})(N_T) & \gamma_{vv}(1 - E'_{vv} - I'_{vv})(N_T) & (-(I^*_{hl} + I^*_{h2}) N_t \gamma_{vv} - \mu_{vv} - ((1/EP))) & -(I^*_{hl} + I^*_{h2}) N_T \gamma_{vv} \\ 0 & 0 & 0 & 0 & \frac{1}{EP} & -\mu_{vv} \end{pmatrix}$$

The six eigenvalues are again found from solving the characteristic equation.

$$\lambda^6 + D_1\lambda^5 + D_2\lambda^4 + D_3\lambda^3 + D_4\lambda^2 + D_5\lambda^1 + D_6 = 0 \tag{31}$$

The solution of equation (31) will yield negative real parts if the Routh-Hurwitz criteria is satisfied, i.e. the conditions of equations (27)-(30) are satisfied with $A_i = D_i$, i = 1, 2, 3, 4, 5 and 6.

To simplify the computations, numerical analysis into conditions laid out in equations (27)-(30) was conducted in similar fashion to the disease-free case. Figure 4 plots the results of the investigations. It is seen that the Routh-Hurwitz criteria will be satisfied for $R_0 > 1$.

From Figure 4, the Routh-Hurwitz conditions are satisfied in the case of $R_0 > 1$. Each Figure shows the values for each condition when there is the variation of the parameter A_1. We can see that the Routh Hurwitz criteria of equations (27)-(30) are again satisfied.

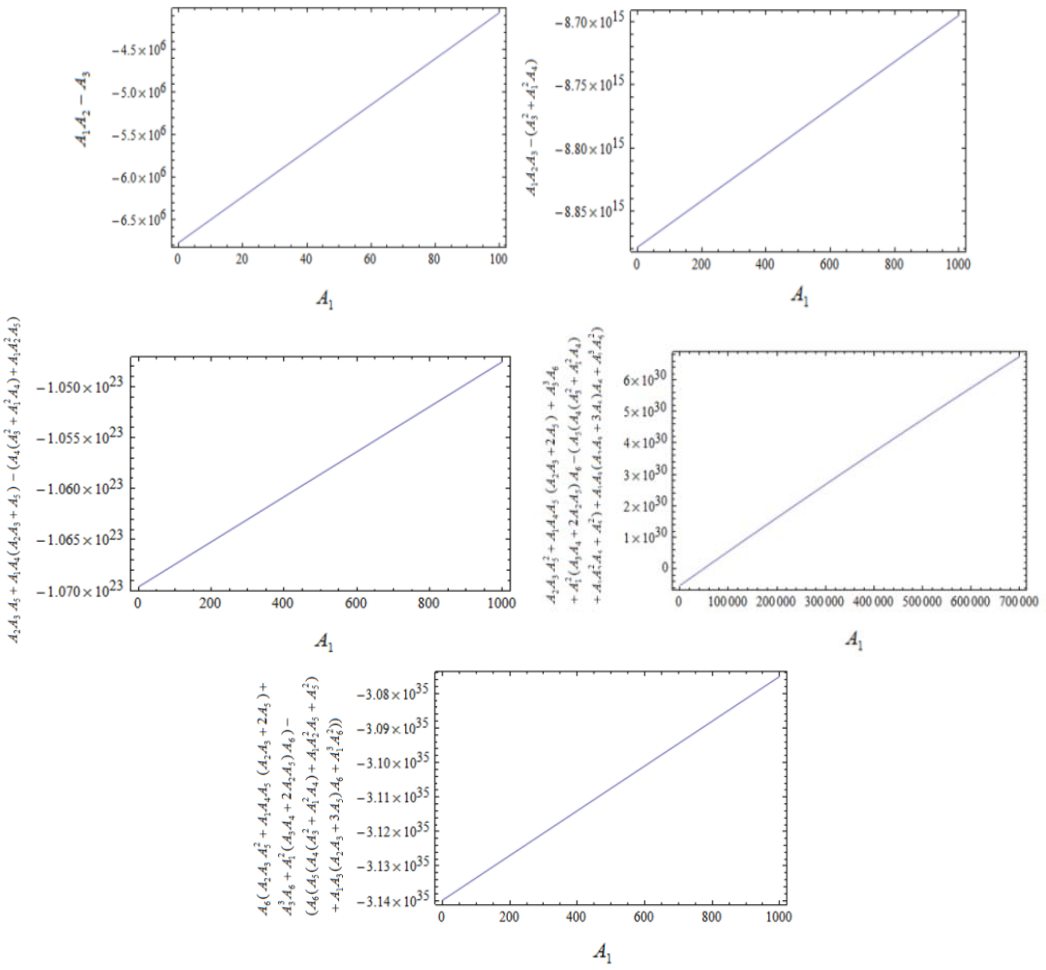

Figure 4. The parameter spaces in support of endemic equilibrium point which convinces the Routh - Hurwitz criteria with the values of parameters; $\gamma_1 = 0.178, \delta_{hh} = 1/(365*74), \gamma_{hh} = 0.5$, $\gamma_{vv} = 0.8, \gamma_2 = 0.4, EP = 0.87, \alpha = 0.006, IP = 0.09, N_T = 600{,}000, N_{vv} = 30{,}000$

3.3 Numerical Simulation

From practical point of view, numerical results are very important for any analysis. In our study, we suggested the mathematical model in support of dengue disease considering the development of dengue disease from DF to DHF. We also performed the numerical solutions by using set of parameter values. We considered the dynamics of our model for both disease-free and endemic states. The parameter values used in this study are given in Table 2. The numerical results are shown in Figures 5-7 [6, 8, 11, 13, 15, 17].

Table 2. Parameters used in simulations for secondary dengue fever.

Parameter	Biological meaning	Values
μ_{hh}	The birth rate of human population	$\frac{1}{(365*74)}$ per day
δ_{hh}	The death rate of human population	$\frac{1}{(365*74)}$ per day
N_T	The total human population	300,000 per day
γ_{hh}	The transmission probability of dengue virus from mosquito to human	0.01 – 0.009
$\frac{1}{IP}$	The incubation rate of dengue virus in human population	0.01 – 0.000009 per day
γ_1	The recovery rate of DF cases	0.1 – 0.09 per day
γ_2	The recovery rate of DHF cases	0.1 – 0.9 per day
γ_{vv}	The transmission probability of dengue disease from human to mosquito	0.1 – 0.99
BB	The recruitment rate of mosquitoes	0.1 – 0.9 per day
N_{vv}	The total mosquitoes	200 - 100,000 per day
δ_{vv}	The death rate of mosquitoes	0.1 – 0.0007 per day
$\frac{1}{EP}$	The incubation rate of dengue virus in mosquito population	0.01 – 0.0087 per day
α	The rates of change from DF cases to DHF cases	0.1 - 0.9 per day

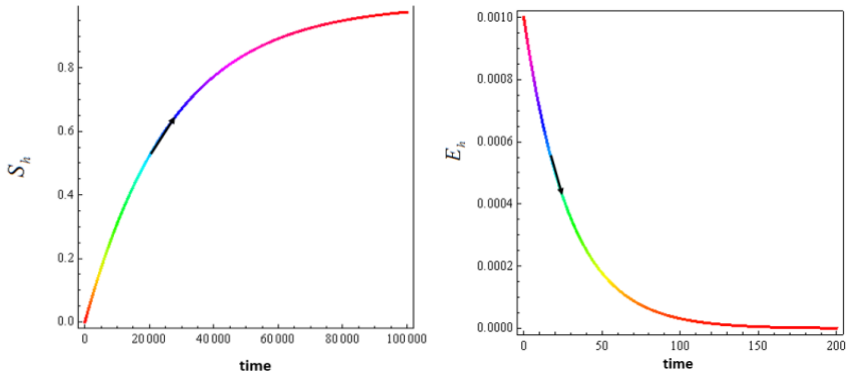

(aa) (ab)

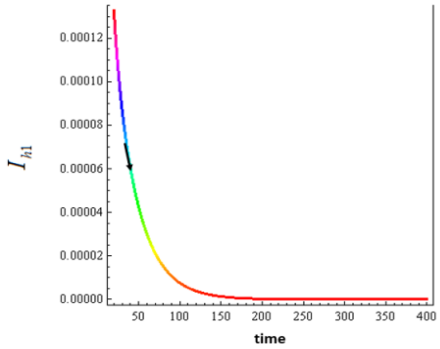

(ac)

Figure 5. The time series of each population group

(aa) The time rate of change for the susceptible human population,
(ab) The time rate of change for the exposed population (infected but not yet transmit the dengue virus) at time,
(ac) The time rate of change for the DF patients,
(ad) The time rate of change for the DHF patients,
(af) The time rate of change for the exposed mosquitoes (infected but not yet transmit the dengue virus) at time,
(ae) The time rate of change for the infectious mosquitoes

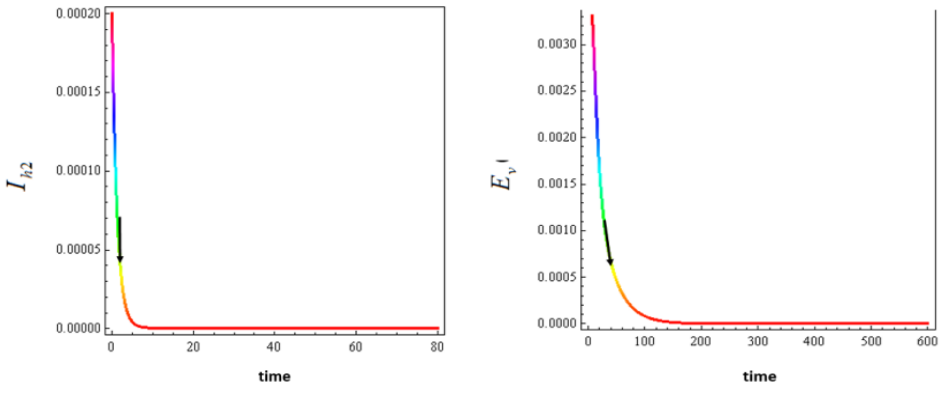

(ad) (ae)

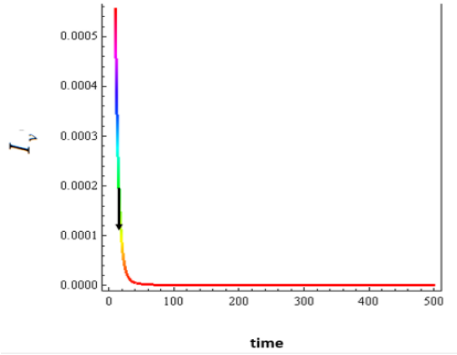

(af)

Figure 5. (cont.) The time series of each population group

The disease-free equilibrium is locally stable in support of the choice of parameter values within Table 2. The parameters used to generate the plots of Figure 5 are $\gamma_1 = 0.178$, $\delta_{hh} = 1/(365*74)$, $\gamma_{hh} = 0.005$, $\gamma_{vv} = 0.009$, $\gamma_2 = 0.8$, $EP = 0.87$, $\alpha = 0.04$, $IP = 0.09$, $N_T = 100{,}000$, $N_{vv} = 3{,}000$, respectively.

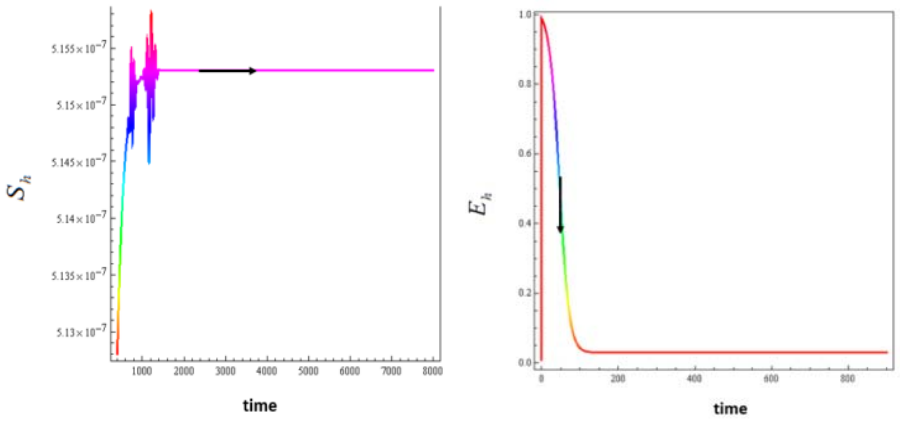

(a) (b)

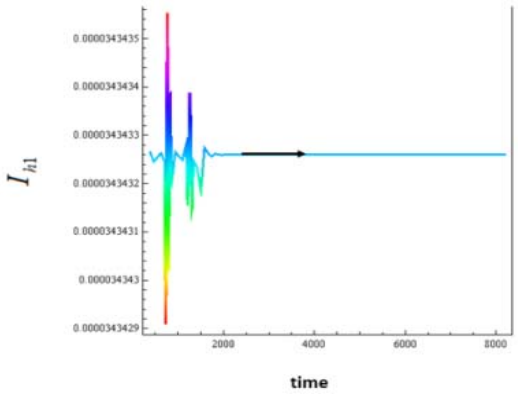

(c)

Figure 6. The time series of each population group

(a) The time rate of change for the susceptible human population,
(b) The time rate of change for the exposed population (infected but not yet transmit the dengue virus) at time,
(c) The time rate of change for the DF patients,
(d) The time rate of change for the DHF patients,
(f) The time rate of change for the exposed mosquitoes (infected but not yet transmit the dengue virus) at time,
(g) The time rate of change for the infectious mosquitoes.

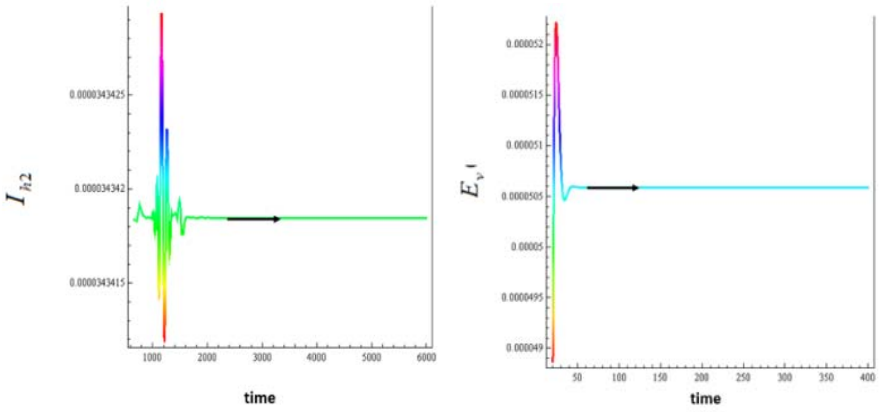

(e) (f)

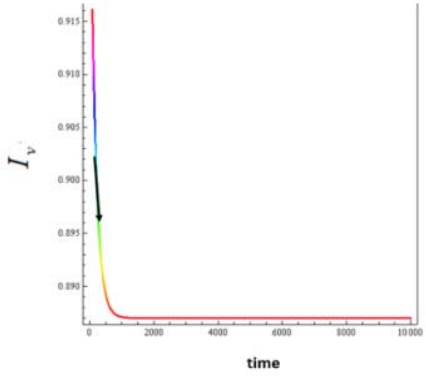

(g)

Figure 6. (cont.) The time series of each population group

The endemic equilibrium is locally stable within support of the choice for parameter values within Table 2. The parameters used to generate the plots of Figure 6 are $\gamma_1 = 0.178$, $\delta_{hh} = 1/(365*74)$, $\gamma_{hh} = 0.009$, $\gamma_{vv} = 0.0008$, $\gamma_2 = 0.9$, $EP = 0.87$, $\alpha = 0.9$, $IP = 0.0006$, $N_T = 100{,}000$, $N_{vv} = 3{,}000$, respectively.

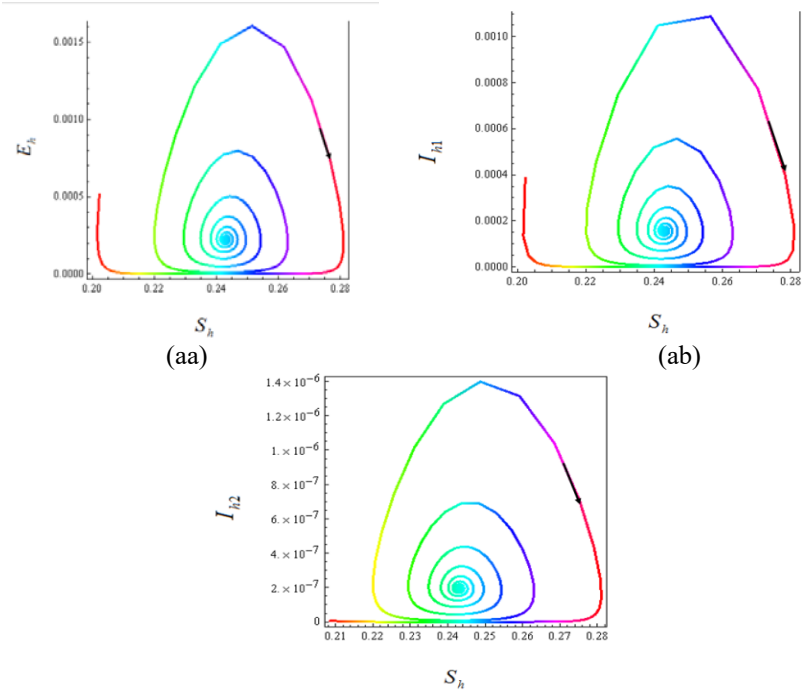

(aa) (ab)

(ac)

Figure 7. Numerical solution of (15)-(20) demonstrates the solution trajectory for each pair of population group(aa) The solutions projected onto the coordinates (S_h, E_h)
(ab) The solutions projected onto the coordinates (S_h, I_{h1})
(ac) The solutions projected onto the coordinates (S_h, I_{h2})
(ad) The solutions projected onto the coordinates (S_h, E_v)
(ae) The solutions projected onto the coordinates (S_h, I_v)
(af) The solutions projected onto the coordinates (E_h, I_{h1})
(ag) The solutions projected onto the coordinates (E_h, I_{h2})
(ah) The solutions projected onto the coordinates (E_h, E_v)
(ai) The solutions projected onto the coordinates (E_h , I_v)

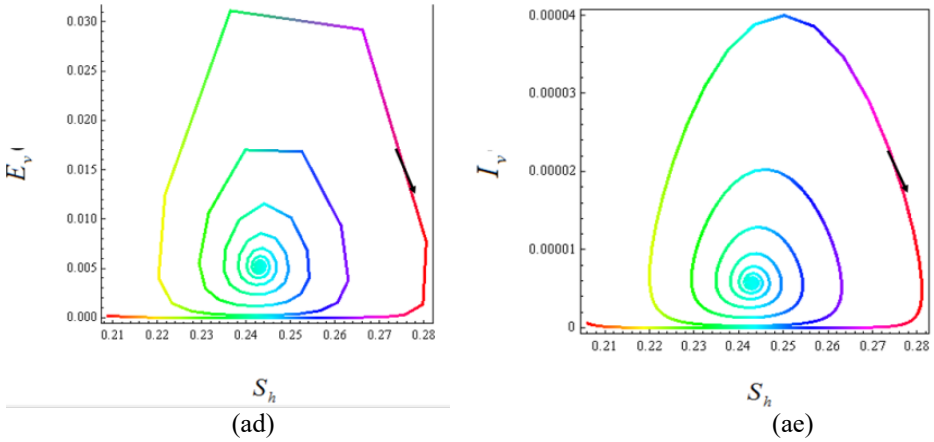

(ad) (ae)

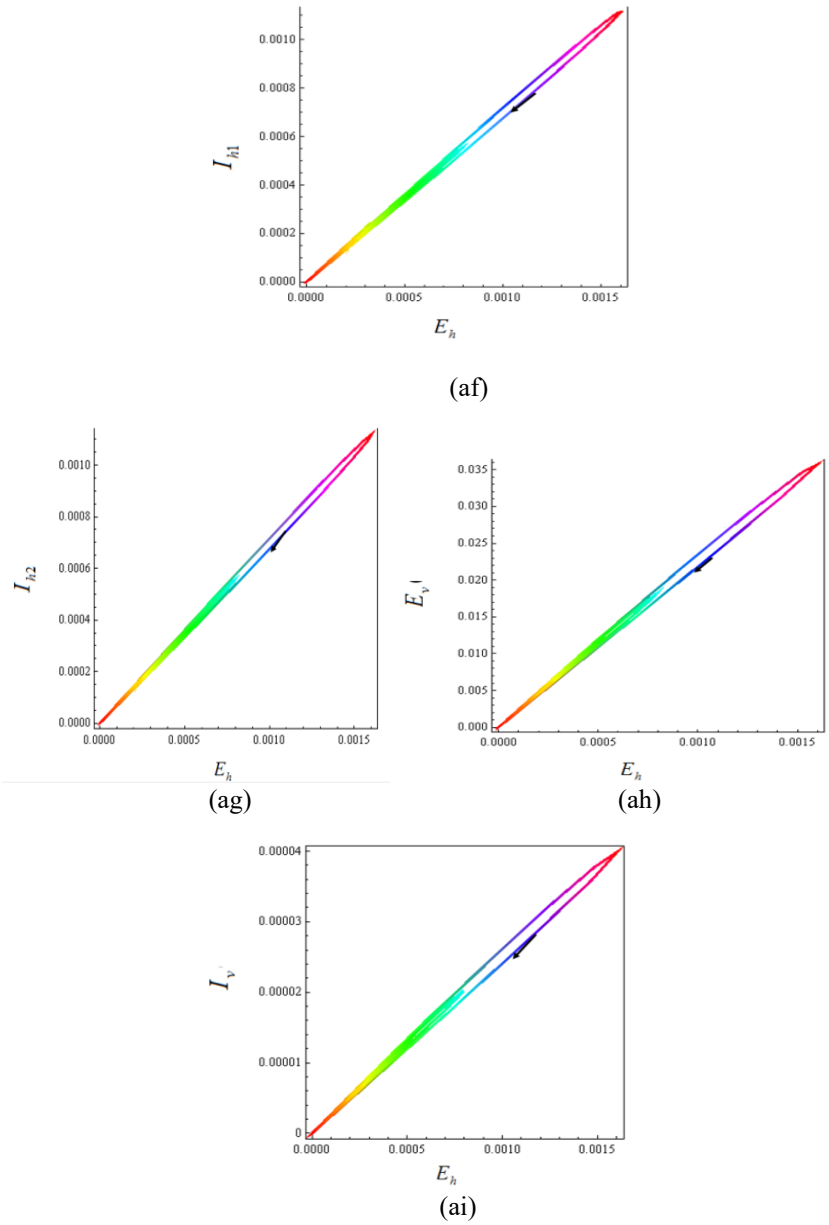

Figure 7. (cont.) Numerical solution of (15)-(20) demonstrates the solution trajectory for each pair of population group

The endemic equilibrium is locally stable in support of the choice for parameter values within Table 2. The parameters used to generate the plots of Figure 7 are $\gamma_1 = 0.178$, $\delta_{hh} = 1/(365*74)$, $\gamma_{hh} = 0.009$, $\gamma_{vv} = 0.0008$, $\gamma_2 = 0.9$, $EP = 0.87$, $\alpha = 0.9$, $IP = 0.0006$ $N_T = 100{,}000$, $N_{vv} = 3{,}000$, respectively.

4. Conclusions

In this paper, we analyzed the SEIR model for human populations and SEI model for mosquito population. The model is considered by taking infection times (primary and secondary infections) into account. The results are to predict the developing tendency of disease and recovery. The model equations were solved analytically. We obtained the basic reproductive number R_0, when $R_0 < 1$. The trajectory approaches the disease-free equilibrium point such as indicated within Figure 5. The trajectory solutions approached to the endemic equilibrium point as shown in Figure 6. The R_0 is given as follows:

$$R_0 = \frac{N_T N_{vv} (\delta_{hh} + \alpha + \gamma_2) \gamma_{hh} \gamma_{vv} \mu_{hh}}{\delta_{hh}(1+\delta_{hh} IP)(\delta_{hh} + \alpha + \gamma_1)(\delta_{hh} + \gamma_2)\mu_{vv}(1+EP\mu_{vv})} \tag{32}$$

Based on the epidemiological data, we estimated R_0 for the dengue sequential infection in Thailand. The implication of this point is to feasible defect for the model.

Next, we compare the behavior solutions of each population group between SEIR and SIR model for human population. The basic SIR model is derived simply by removing the exposed human population compartment E_h. Specifically, equations (1)-(5) are now rewritten as follows:

$$\frac{dS_h}{dt} = \mu_{hh} N_T - \gamma_{hh} S_h I_{vv} - \delta_{hh} S_h \tag{33}$$

$$\frac{dI_{h1}}{dt} = \gamma_{hh} S_h I_v - \delta_{hh} I_{h1} - \gamma_1 I_{h1} - \alpha I_{h1} \tag{34}$$

$$\frac{dI_{h2}}{dt} = \alpha I_{h1} - \delta_{hh} I_{h2} - \gamma_2 I_{h2} \tag{35}$$

$$\frac{dR_h}{dt} = \gamma_1 I_{h1} + \gamma_2 I_{h2} - \delta_{hh} R_h \tag{36}$$

The parameters used to compute the behavior solutions of equations (33)-(36) are kept the same as the SEIR model. Figure 8 (i) plots the responses of the SEIR model, while Figure 8 (ii) plots the responses of the SIR model of equations (33)-(36). We can see that the solutions of SEIR model converge to the equilibrium states faster than SIR model. The parameters of SIR model are the same as in SEIR model.

For the simulation seen in Figure 8 (iii) for SEIR model and (iv) for SIR model, the existing only in the imagination part of the complex roots is roughly 0.002698 and 0.014759. Thus, we can forecast the period with the oscillations as they approach P_1 by method of the solutions of the linearized system, acquiring $2\pi / 0.002698 \approx 6.38$ years and $2\pi / 0.014759 \approx 1.17$ years, respectively.

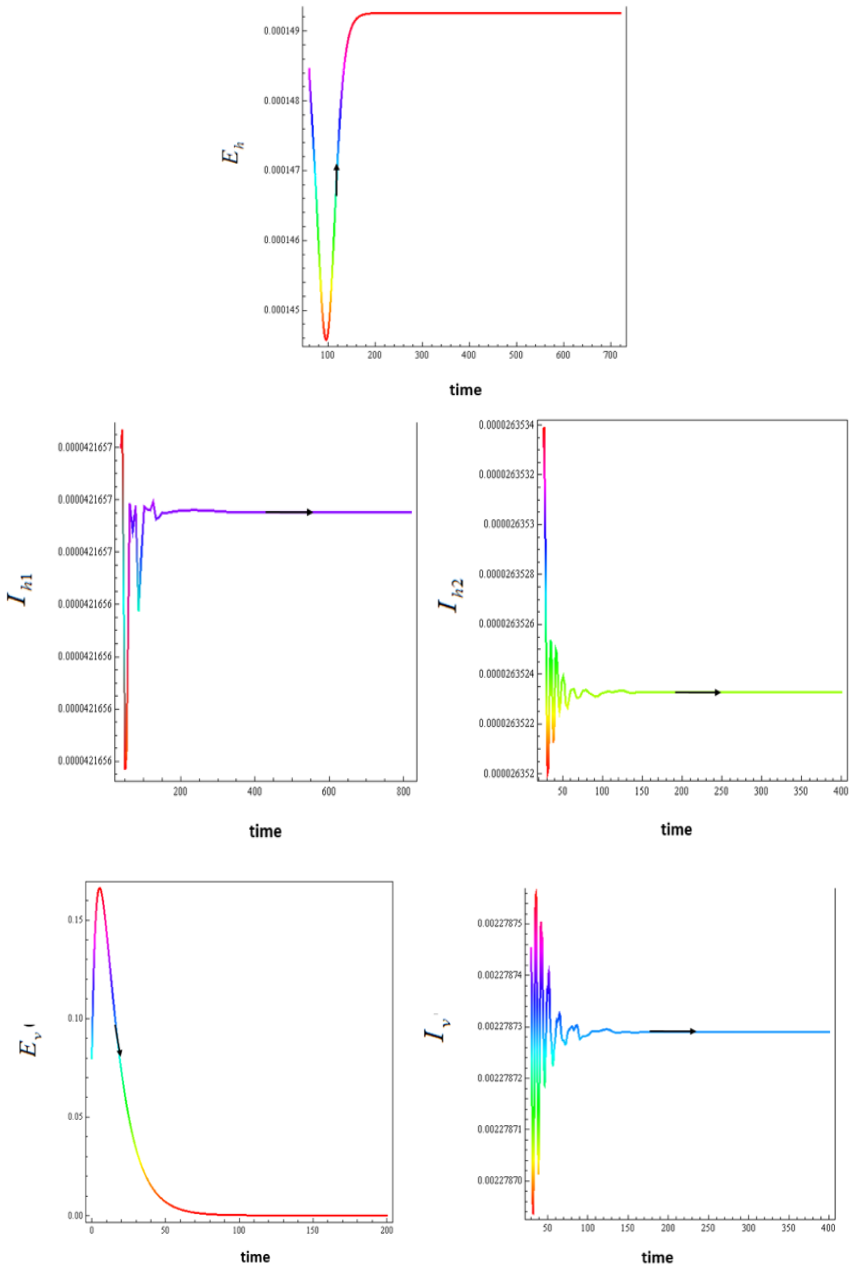

(i) Behavior in structured SEIR model

Figure 8. Plot of number of susceptible and infected humans in SEIR model and SIR model

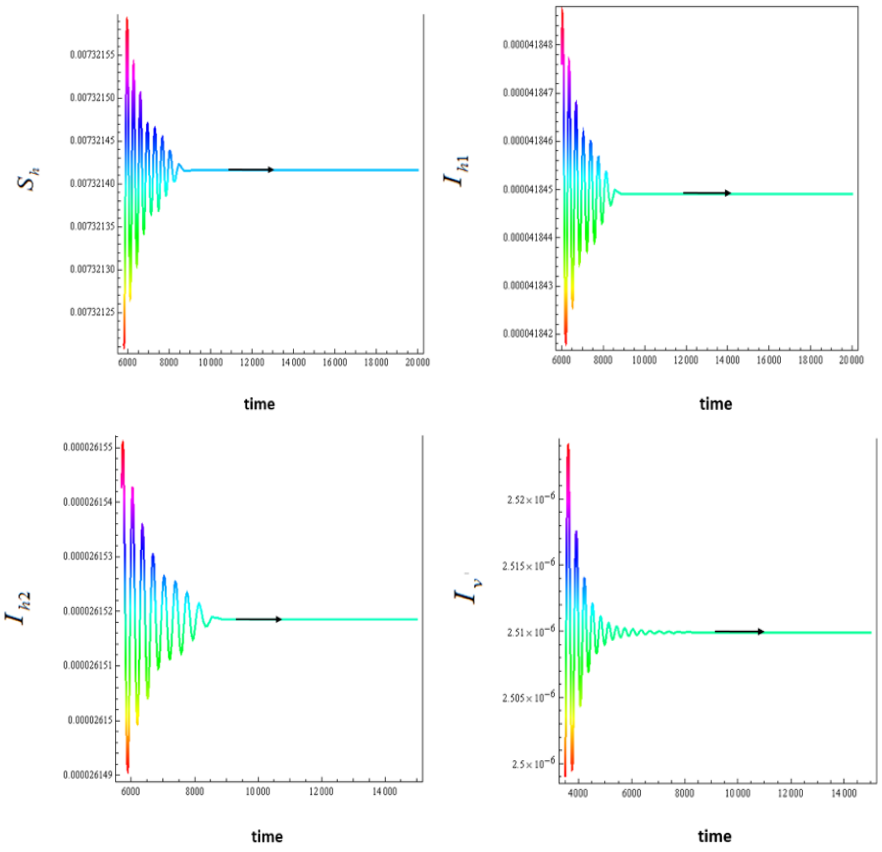

(ii) Behavior in structured SIR model

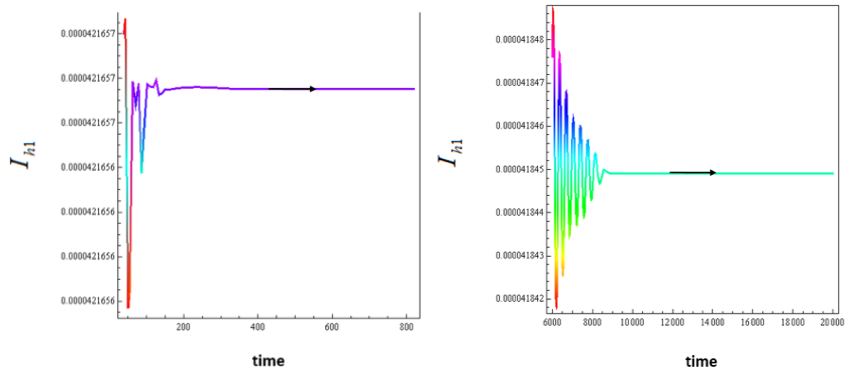

Figure 8. (cont.) Plot of number of susceptible and infected humans in SEIR model and SIR model

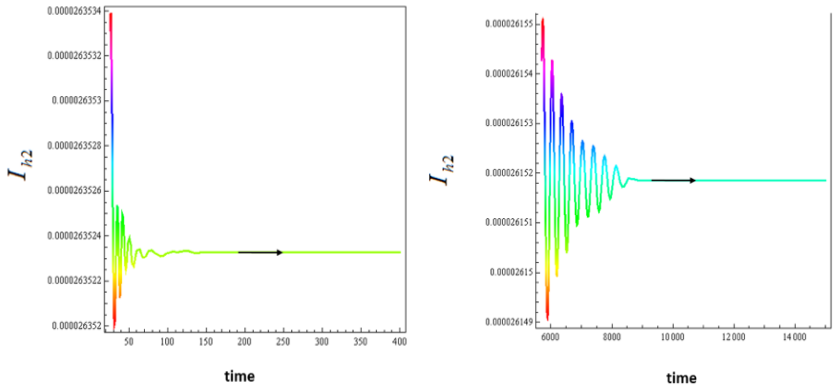

(iii) Behavior in I_{h1} and I_{h2} structured SEIR model (iv) Behavior in I_{h1} and I_{h2} structured SIR model

Figure 8. (cont.) Plot of number of susceptible and infected humans in SEIR model and SIR model

(i) The time series for each of population group for the SEIR model. The parameters are $\gamma_1 = 0.178$, $\delta_{hh} = 1/(365*74)$, $\gamma_{hh} = 0.007$, $\gamma_{vv} = 0.0003$, $\gamma_2 = 0.8$, $\alpha = 0.5$, $N_T = 100,000$, $N_{vv} = 5,000$, $EP = 0.09$, $IP = 0.0008$ and $R_0 = 15.47$. The solutions converge in support of the endemic disease state (0.0000455,0.15546, 0.0000979, 0.000002448, 0.36766, 0.004406). It is seen that the solutions oscillate to the endemic disease state.

(ii) The time series of each population group for the SIR model. The parameters are $\gamma_1 = 0.178$, $\delta_{hh} = 1/(365*74)$, $\gamma_{hh} = 0.007$, $\gamma_{vv} = 0.0003$, $\gamma_2 = 0.8$, $\alpha = 0.5$, $N_T = 100,000$, $N_{vv} = 5,000$ and $R_0 = 19.17$. This model has no E_{hh} and E_{vv}. The solutions approach to the endemic disease state (145.95425, 0.0299943, 0.00003742, 0.001838). We can see that the responses oscillate to the endemic disease state.

5. Acknowledgements

The authors would like to thank Research and Development Institute, Faculty of Science and Technology, Phuket Rajabhat University and Faculty of Science, King Mongkut's Institute of Technology Ladkrabang.

References

[1] Bureau of Epidemiology, 2017. Department of Disease Control, Ministry of Public Health, Thailand. [online] Available at: http://www.boe.moph.go.th/fact/ Dengue_ Haemorrhagic_ Fever.htm

[2] Hanson, J.L. and Fischer, P.R., 2017. Ready for Dengue in the United States? [online] Available at: https:// www.ahcmedia. com /articles/140960-ready-for-dengue-in-the-united-states

[3] Wikipedia, 2017. Dengue Virus. [online] Available at: https://en.wikipedia.org/wiki/ Dengue_virus.

[4] Structure of Dengue Virus, 2017. BioInteractive. [online] Available at: https://www.hhmi.org/biointeractive/structure-dengue-virus.

[5] Immunization, Vaccines and Biologicals, Word Health Organization, 2017. [online] Available at: https://www.who.int/immunization/research/development/dengue_vaccines/en/.

[6] Kongnuy, R. and Pongsumpun, P., 2010. Mathematical Modeling for Dengue Transmission with the Effect of Season. *International Journal of Biological and Medical Sciences*, 5(2), 74 -78.
[7] Esteva, L. and Vargas, C., 1998. Analysis of a dengue disease transmission model. *Mathematical Bioscience*, 150, 131-151.
[8] Sungchasit, R. and Pongsumpun, P., 2012. Dengue transmission model with the different incubation rate for each season. *1st Mae FahLuang University International Conference 2012*, Chiangrai, 1-12.
[9] Nikin, B.R. and Ciupe, S.M., 2017. Modelling original antigenic sin in dengue viral infection. *Mathematical Medicine and Biology*, 35(2), 1-16.
[10] Pongsumpun, P. and Tang, I.M., 2003. A realistic age structured transmission model for dengue hemorrhagic fever in Thailand. *Mathematical and Computer Modelling 32*, 336-340.
[11] Thavara, U., Tawastsin, A., Chansang C., Kong-ngamsuk, W., Paosriwong, S., Boon-Long, J., Rongsriyam, Y., Komalamisra, N., 2001. Larval occurrence, oviposition behavior and biting activity of potential mosquito vectors of dengue on Samui Island, Thailand. *Journal of Vector Ecology*, 26(2), 172-180.
[12] World Health Organization, 2009. *Dengue: Guidelines for Diagnosis, Treatment. Prevention and Control.* Geneva: World Health Organization and the Special Programme for Research and Training in Tropical Diseases.
[13] Guidance Clinical, 2017. Centers for Disease Control and Prevention. [online] Available at: https://www.cdc.gov/dengue/clinicallab/clinical.html.
[14] Syafruddin, S. and Noorani, M., 2012. SEIR model for transmission of dengue fever in Selangor Malaysia. *International Journal of Modern Physic: Conference Series*, 9, 380- 389.
[15] Kerdpanich, A., Watanaveeradej, V., Samakoses, R., Chumnanvanakij, S., Chulyamitporn, T., Sumeksri, P., Vuthiwong, C., Kounruang, C., Nisalak, A. and Endy, T., 2001. Perinatal dengue infection, *Southeast Asian Journal of Tropical Medicine and Public Health*, 32(3), 488-493.
[16] Ferguson, N., Donnelly, C. and Anderson, R., 1999. Transmission dynamics and epidemiology of dengue: insights from age-stratified sero-prevalence surveys. *Philosophical Transactions of the Royal Society London B. Biological Science*, 354, 757-768.
[17] Changal, K., Raina, A.B., Raina, A., Raina, M., Bashir, R., Latief, M., Mir, T. and Changal, Q., 2016. Differentiating secondary from primary dengue using IgG to IgM ratio in early dengue: an observational hospital based clinico-serological study from North India. *BMC Infectious Diseases*,16(1),715-721.
[18] Guzman, M.G., Mayling, A. and Halstead, S.B., 2013. Secondary infection as a risk factor for dengue hemorrhagic fever/dengue shock syndrome: an historical perspective and role of antibody-dependent enhancement of infection. *Archives of Virology*, 158(7), 1445-1459.
[19] Diekmann, D. and Heesterbeek, J., 2000. *Mathematical Epidemiology of Infectious Disease: Model Building, Analysis and Interpretation*. Chichester: John Wiley and Sons Ltd.
[20] Adams, B., Holmes, E.C., Zhang, C., Mammen, M.P., Nimmannitya, S., Kalayanarooj S. and Boots, M., 2006. Cross-protective immunity can account for the alternating epidemic pattern of dengue virus serotypes circulating in Bangkok. *Proceedings of the National Academy of Sciences*, 103(38), 14234-14239.
[21] Annual Epidemiological Surveillance Report, 1992-2012. Division of Epidemiology, Ministry of Public Health, Royal Thai Government.
[22] Sungchasit, R., Pongsumpun, P. and Tang, I.M., 2015. SIR transmission model of dengue virus taking into account two species of mosquitoes and an age structure in the human population. *American Journal of Applied Sciences*, 12(6), 426-443.
[23] Cheah, W.K., Ng, K.S., Marzilawati, A.-R. and Lum, L.C.S., 2014. A review of dengue research in Malaysia. *Medical Journal of Malaysia*, 69 (Supplement A), 59-67.
[24] Pongsumpun, P. and Tang, I.M., 2003. Transmission of dengue hemorrhagic fever in an age structured population. *Mathematical and Computer Modelling*, 37, 949-961.
[25] Omic, J. and Van Mieghe, P., 2016. Epidemic spreading in networks-variance of the number of infected nodes. [online] Available at: https://www.nas.ewi.tudelft.nl/people/Piet/papers/VirusSpread_VarianceTUDReport20090707.pdf

Review article

Assessing Status of Life Cycle Assessment Studies in Egypt

Dalia M. M. Yacout*

Department of Chemistry, Umea University, Umea, Sweden

Received: 4 January 2019, Revised: 9 May 2019, Accepted: 22 May 2019

Abstract

One of the tools used worldwide nowadays for achieving sustainable development is "Life cycle assessment." This tool is being used to assess and compare environmental impacts of products or services through their entire lifetime. Researchers and environmental experts in both academia and industry are using Life cycle assessment (LCA) as it presents a quantitated and qualitative tool that reflects the environmental impacts. In spite of this, it was noted that limited studies employed this important tool in Egyptian cases. The goal of this review paper was to identify potential usage of LCA in Egypt. This was done by evaluating the conducted studies concerning this area in Egypt and main gaps and challenges were determinined, accordingly. Improvement options and future requirements for using LCA in Egypt would then be recommended.

In order to assess the statues of the LCA studies in Egypt, the published documents by both national and international scholars related to LCA cases conducted in Egypt during the period of 2006 till 2019 were collected and reviewed. It was found that 39 documents were published concerning this area. The published documents covered seven main area of studies namely; building and construction materials, aquaculture farming, energy, industrial manufacturing, transportation, water treatment and waste handling. Top publications were in the building and construction materials field accounting for 44% of the total publications followed by energy, aquaculture farming, waste handling strategies, and industrial manufacturing of textile and packing materials (13%, 13%, 13 and 8% of the total publications, respectively). The main benefits as well as gaps of the conducted studies were discussed for each area. Current concerns, need of future studies as well as related recommendation and suggestions were also presented.

Keywords: Life cycle assessment, sustainable development, Egypt
DOI 10.14456/cast.2019.15

1. Introduction

In view of the increasing awareness concerning environmental issues worldwide, several techniques were developed to assess the environmental impacts and assist in mitigating and minimizing the negative impacts. Life cycle assessment (LCA) is one of techniques developed for these issues. LCA is employed to estimate the environmental impacts of products, services or systems considering all inputs from raw materials, water, energy and outputs from end product, air emissions, liquid discharge and solid wastes. LCA studies are used to identify the main points of

*Corresponding author: E-mail: Dalia.abdelfattah@umu.se

environmental concern in a product or service life cycle to improve them. They can also assist decision makers in the industrial sector as well as policy makers in setting priorities, strategic planning and product design [1].

LCA methodology was introduced for the first time to the research community in the late 1960s, then developed by many countries [2]. International standards on "Environmental management of life cycle assessment" were developed for understanding and frame working usage of this important tool. ISO 14041:1998 [3] was the first developed standard and it clarifies what is meant by LCA goal and scope. In addition, it explains how to design the system model, the inventory analysis and data collection. It was followed up in 2000 with ISO 14042: 2000 [4] which served as a guide to understand the life cycle impact assessment phase and its relation to other phases and ISO 14043 [5] was established to help explain the results and data obtained from previous phases. Furthermore, ISO14040: 2006 [1] describes the principles and frameworks of life cycle assessment including its four main phases; the goal and scope, life cycle inventory, impact assessment, and data interpretation. As presented in Figure (1), ISO14044: 2006 [6] is the last version of the standards. This ISO combines the three previous ones [3 - 5] and in combination with IISO 14044 [1] and replace them by presenting the requirements and guidelines for conducting LCA study.

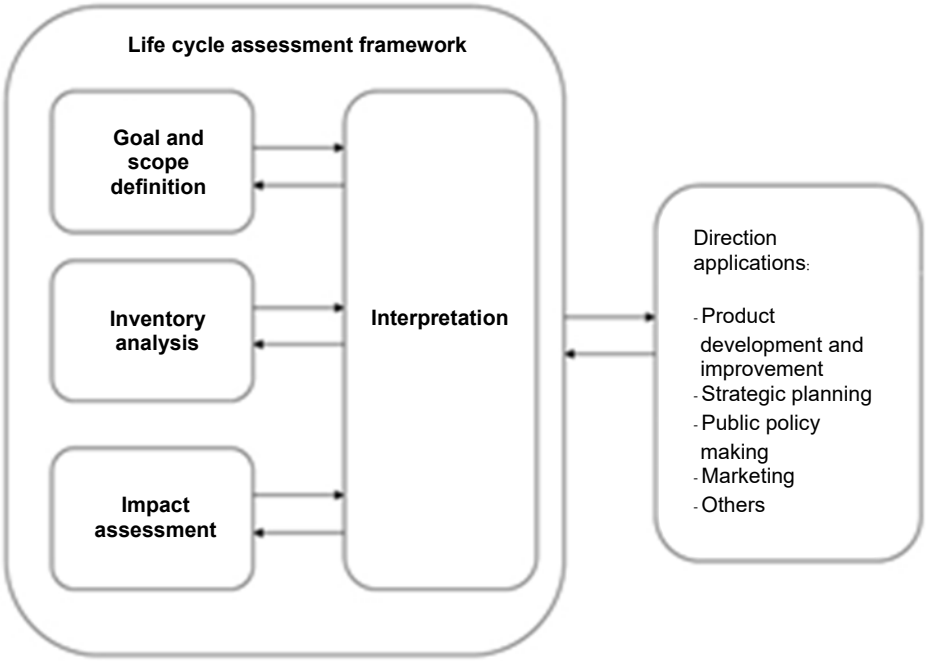

Figure 1. Conceptual framework on LCA [1]

Nowadays many organizations have adopted the life cycle thinking and LCA studies are being conducted worldwide by researchers in universities, research centers and industrial plants. In Egypt, in spite of the increasing awareness and concern about environmental issues, there are limited studies on the use of LCA as a tool for environmental sustainability.

This review article will attempt to evaluate the current status of LCA studies conducted in Egypt and to identify potential usage of LCA in future investigation. The main objectives are to

identify conducted LCA studies in Egypt, determine main gaps and challenges in conducted LCA studies in Egypt and recommend improvement options and future requirements for using LCA in Egypt.

Data Assessment

In order to assess the conducted LCA studies in Egypt, the published literature was collected, classified and evaluated following the adopted methodology by various researchers [7- 9] as shown in Figure 2. The methodology consists of the following steps:

a) Setting a time frame of required data. Data were collected from published documents related to LCA in Egypt from 2006 when the final international standard of LCA [1] was released till date 2019.

b) Framing questions, three main questions were taken into consideration; How many documents were published related to LCA in Egypt?, What type of documents? and Which topics were covered?

c) Identifying search criteria and conducting search. Search was done on "ISI Web of Science", Science direct", " Scopus", " Google", " Google scholar" and " Research gate" using the keywords " Egypt", "Life cycle assessment" and "LCA".

d) Screening records, classification and evaluation of collected data. The classification and evaluation would consider published documents such as "research papers" and "review papers" published in local journals, international journals or conference proceedings. Documents should be related to LCA in Egypt published during the period from 2006-2019.

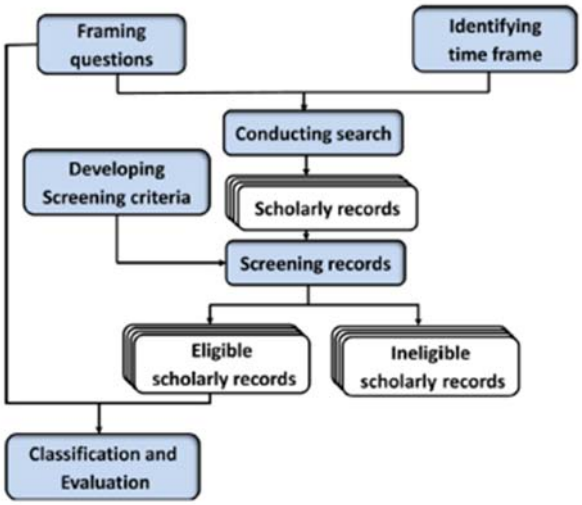

Figure 2. Data collection and evaluation methodology [7-9]

Overview on LCA Publications Related to Egypt

Summary of the published documents related to LCA in Egypt is presented in Tables 1 and 2. It was found that 39 publications were concerned on LCA studies in Egypt. Thirty-three papers were case study investigations using LCA as an environmental assessment tool and the rest were working papers or review papers. Most of the documents (85%) were published in international peer-

reviewed journals, a few in conference proceedings (13 %) and only one (3%) in a national paper. Most of the conducted studies were done by national universities and research centers and only one research study by one holding company. This reflects the need to promote LCA as an environmental and sustainable tool within the private sector in Egypt.

Table 1. Summary of local LCA studies in Egypt published during 2006 -2019

Area of study	Aim of study	Reference	Publication Type	Affiliation
Aquaculture	Analyze the environmental impact of tilapia production in different production systems	[10], [11], [12]	International paper	Stockholm Resilience Center / WorldFish
		[13], [14]	International paper	Alexandria University
Building and construction materials	Assessing the environmental impacts of residential buildings and construction materials	[15]	Local paper	Tanta University
		[16], [24], [25], [26]	Conference paper	Egypt-Japan University of Science and Technology (E-JUST)
		[17], [18], [19], [20], [21], [22], [23], [27], [28]	International paper	
		[29]	International paper	Cairo University
		[30]	International paper	Menoufia University
	A framework for incorporation of green building materials	[31]	International paper	Housing and Building National Research Center
Transportation	Estimating the environmental impacts of vehicles tires	[32]	International paper	E-JUST
Water treatment	Assessing the environmental impacts of water systems	[33]	International paper	Technische Universität Berlin, Germany
Waste handling	Assessing the sewage sludge treatment process	[34]	International paper	National Water Research Center
		[35]	Conference paper	Technische Universität Braunschweig, Germany
		[36]	International paper	Mansoura University
	Comparing the waste handling scenarios of synthetic fiber waste	[37]	International paper	Alexandria University

Table 1. (cont.) Summary of local LCA studies in Egypt published during 2006 -2019

Area of study	Aim of study	Reference	Publication Type	Affiliation
	Assessing the potential use of some agricultural and industrial wastes as building materials	[38]	International paper	National Research Center
	Identifying the impacts of different waste management strategies for recovery of used lubricating oil	[39]	International paper	Alexandria Petroleum Company (APC)
Industrial manufacturing	LCA of aluminum foil packaging material	[40]	International paper	Alexandria University
	Evaluating the environmental impact of textile materials	[41]	International paper	
		[42]	International paper	Università Politecnica delle Marche, Italy
Energy	Evaluating energy infrastructure and their impacts	[43]	International paper	School of Engineering, Kyushu University, Japan
		[44]	International paper	University of Hamburg, Germany
		[45]	International paper	E-JUST
		[46]	International paper	Beni-Suef University
	Assessing the environmental impact of renewable energy materials	[47]	International paper	Riga Technical University, Latvia
Others	The interplay of environmental assessment methods; and characterizing the institutional background in Egypt	[48]	International paper	The British University in Egypt (BUE)

Table 2. Summary of local LCA studies in Egypt per type and affiliation

Affiliation		International Journal	National Journal	Conference proceedings	Total	%
Name	**Country**					
Alexandria University	Egypt	5			5	12.8
Egypt-Japan University of Science and Technology (E-JUST)		11		4	15	38.5
Menoufia University		1			1	2.6
Mansoura University		1			1	2.6
Alexandria Petroleum Company (APC)		1			1	2.6
Cairo University		1			1	2.6
National Research Center (NRC)		1			1	2.6
Environment and Climate changes Research Institute National Water Research Center		1			1	2.6
Tanta University			1		1	2.6
Beni-Suef University		1			1	2.6
British University in Egypt (BUE)		1			1	2.6
Housing and Building National Research Center		1			1	2.6
Technische Universität Braunschweig,	Germany			1	1	2.6
Technische Universität Berlin		1			1	2.6
University of Hamburg		1			1	2.6
Stockholm Resilience Center / WorldFish	Sweden	3			3	7.7
Riga Technical University	Latvia			1	1	2.6
Università Politecnica delle Marche	Italy	1			1	2.6
School of Engineering, Kyushu University	Japan	1			1	2.6
Total (Number)		32	1	6	39	100.0

As per the covered topics, Table 3 summarizes the number and percentage of publications per area of studies. Seven areas of studies were addressed in this study namely; aquaculture, industrial manufacturing, building and construction materials, transportation, energy, water treatment and waste handling.

Table 3. Number of local LCA publications per covered area of studies

Area of study	Number of Publications	%
Aquaculture	5	13%
Industrial manufacturing	3	8%
Building and construction materials	17	44%
Transportation	1	3%
Water treatment	1	3%
Waste handling	6	15%
Energy	5	13%
Other	1	3%
Total	39	100%

Cover Areas of Study, Related Challenges and Gaps

1) Building and construction materials

LCA publications related to building and construction materials were the major area of publications, accounting for 44% of the total published documents. Publications in this area include assessments in several case study that aimed to estimate the carbon emissions or evaluate the environmental impacts of local building construction in several locations across Egypt [19, 24, 29] when the environmental impacts of various construction materials such as cement, bricks [16, 18, 21-23, 25-26], sidewalk pavement [27, 30] and pile foundation [28] were compared. One study employed LCA as a support decision tool in green building design [20]. The concerns about the impacts of the building and construction sector on the environment have arisen recently due to the continued expansions and constructions by both private and public sectors in different areas across Egypt. However, the conducted LCA studies in this area until now have focused only on modeling the environmental impacts of the cases in question without taking the cost analysis or social impacts into consideration. Thus, the sustainability of this expanding sector should be taken into consideration.

Furthermore, the development or usage of green building materials as an ecofriendly alternative to conventional building materials was not addressed properly. The only study in this area was conducted by Garas *et al*. [28] who investigated the impacts of using some agricultural and industrial waste, i.e. rice straw cementitious bricks, rice straw bales, and concrete mix with granite waste building materials as building materials for the construction industry. Based on their results they found that used waste for developing new eco-friendly building materials can significantly reduce the negative environmental impact of the construction industry. However, the related impacts differ for each case study. In agreement with Ay-Eldeen *et al.* [28] and Azouz [31], there is a need for database on alternatives for eco-friendly building. The usage of agricultural and industrial wastes as building materials will reduce the waste handling problems, reduce production costs and minimize negative environmental impacts of the construction industry. Future LCA studies in the area of building and construction materials should address this issue with more focus on other agricultural and industrial wastes for different construction application (buildings and roads).

2) Energy

Due to the energy crisis worldwide and global interest in replacing the dependence on fossil fuels and ongoing attempts to replace it by renewable energy sources, LCA studies related to energy are gaining more and more importance. The published documents related to this topic and Egypt represents 13% of the total publications, these studies were done at different levels. The studies conducted by Aly and Managi [43] and Shaaban *et al*. [44] employed LCA to assist the policy decisions making by assessing the energy infrastructure and their impacts on societies' capital assets. The studies highlighted the positive potential of using different energy and renewable energy systems.

Technology oriented studies presenting the potential impacts of applying different energy sources were conducted by Armanuos *et al*. [45] and Menoufi *et al*. [46]. Armanuos *et al*. [45] compared between the environmental impacts of running an irrigation system for rice cultivation by diesel fuel pumps verses solar pumps. They declared that the usage of solar pumps was more ecofriendly and reduced the overall impacts. Their study took the cost analysis factor which would be of most importance when introducing such a technology. Menoufi *et al*. [46] compared between the potential impacts and energy performance of two photovoltaic systems "Building Added Concentrating Photovoltaic (BACPV)" and a "conventional Building Integrated Photovoltaic (BIPV)". They presented the novel design related environmental impacts and payback. Their study reflected the potential usage of novel solar energy systems and promoted its employment, which seems a promising solution for using renewable energy in Egypt.

The potential impacts of using novel materials for biodiesel production was addressed by only one study [47]. Fawzy *et al*. [47] conducted LCA study to model a novel Egyptian system for biodiesel production from Jatropha using waste water in unused desert land. Their results showed the environmental benefit of using Jatropha for biodiesel production. However, the cost analysis and social impacts were not addressed in this study. Similar studies using other novel materials including agricultural and industrial waste materials for biofuel production are strongly recommended for future studies. Using hybrid systems of biomass and solar energy can be a potential area of future studies as well.

3) Aquaculture

Egypt is considered as the top producer of farmed tilapia in Africa and one of the top ten worldwide [13-14]. Aquaculture farming is a very important industry in Egypt that has been expanding over the last few years [13-14]. Published LCA studies related to aquaculture in Egypt represented 13% of the total. Aquaculture farming of tilapia and environmental assessment of its production systems were the main concern of the studies in this area. "Nile tilapia" is considered as one of the most important sources of cheap protein in Egypt. The author of the studies [10 - 14] agreed that both energy consumption for fish feed production and aeration of aquaculture farming ponds together with the production of fish feed were the main contributors to the environmental impacts of this industry. In order to reduce the negative environmental impacts, they suggested to adopt energy saving practices by better energy management of the aquaculture farm to reduce the overall energy consumption. In addition, they emphasized on the need to use novel fish feed formulas and new ingredients. In agreement with researchers [10 - 14], the use of local ingredients for fish feed will reduce the overall footprint of the aquaculture production cycle. The cost benefits as well as the impacts on the surrounding society has to be taken into consideration since it will be an opportunity for jobs' creation.

4) Water, wastewater treatment and waste handling

Mahgoub *et al*. [33] conducted LCA study on the environmental impacts of water systems in Egypt. For wastewater treatment, comparative studies for different handling strategies at industrial and city levels were covered by 15% of total LCA publications related to Egypt. At city level, the conducted

studies evaluated the environmental impacts of wastewater treatment processes in Alexandria city [35], and the different treatment technologies in relation to cost analysis were compared [34, 36]. The possibility of using new technologies can be considered in future studies.

At the industrial level, one study aimed to identify the preferable waste handling strategy for hazardous solid waste in synthetic textile industry [37], different waste management strategies for recovery of used lubricating oil were evaluated by Hassanain *et al.* [39]. Garas *et al.* [38] used some agricultural and industrial waste materials for production of building materials. The number of LCA studies related to waste handling is low in comparison to the number of industrial applications in Egypt. Further waste management options for different products can be evaluated for achieving a more eco- friendly and sustainable industry. Waste management strategies for handling different types of waste at city level can also be addressed. These waste management strategies can address the preferable options for handling municipal solid waste and household waste by landfill, incineration, recycle or reuse.

5) Industrial manufacturing

Topics related to industrial manufacturing represented 8% of the total publications. The conducted studies addressed the environmental impacts of textile production [41, 42] and packing materials manufacturing [40]. The studies suggested means for the improvement of current production process in order to obtain a more ecofriendly production, however, cost analysis and social impacts were not considered by any of these studies. Egypt is a major industrial country in the MENA region with many manufacturing facilities to meet the local demand and for exportation. The conducted studies only addressed the production of synthetic fabrics, cotton yarn and foil packing material, future LCA studies should focus on other products such as equipment manufacturing, different textile materials, food and dairy products, cement industry and so on.

6) Transportation

In spite of the important rule of transportation sector, huge impacts on environment and especially on energy consumption and climate change affected the society. Only one LCA related to this sector in Egypt was conducted [32]. Elkafoury and Negm [32] assessed the life cycle of vehicles tyres on Egyptian road network in order to estimate the environmental impacts of their production and consumption phases.

With only one conducted LCA study in this sector the area is open for further studies. The potential of reducing greenhouse gases (GHG) emissions and mitigating related climate change impacts using alternative routes and methods for products transportation can be addressed [49]. Furthermore, the potential of reducing fossil fuels consumption by using alternative renewable energies is a rich area for investigation as well.

Towards Promoting LCA Studies in Egypt

LCA proved to be an efficient tool for researchers, engineers who design products and decision-makers in the industry as well as policy makers [6]. This important tool should be employed in Egyptian studies more frequently. Main gaps of each area of study and related improvement and future need of studies were illustrated in the previous section. The main challenges that face further usage of LCA as a tool for sustainability in Egypt are the lack of local experts and the awareness about this important tool limits its utilization [49]. In agreement with Yacout [49], capacity building workshops and scientific events such as conferences can be organized to promote benefits of this tool on how to employ it and to connect between international experts in this area and national researchers.

Data limitations, in terms of unavailability of recent local data for conducting the research and for benchmarking of results is a challenging point for consideration. The availability of data is a key factor for conducting any LCA [50]. In this case, data has to be collected from case studies by the research group that could be subjected to some uncertainty. In order to minimize bias, data analysis for uncertainty has to be taken into consideration [51]. Additionally, the absence of a local database, a National Egyptian Life Cycle Inventory (NELCI) database is required to standardize LCA research studies in Egypt. In Agreement with various researchers [17, 31, 41, 50-51], the development of a NELCI is a must to obtain more accurate results concerning LCA studies in Egypt.

2. Conclusions

Life cycle assessment is an efficient tool for environmental sustainability worldwide. However, limited investigations employed LCA in Egyptian studies. The current status of LCA studies conducted in Egypt was evaluated for potential usage of LCA in future investigations. Conducted LCA studies in Egypt were identified. Determination of main gaps and challenges and recommend improvement options and future requirements for using LCA in Egypt were also analysed by reviewing the published documents concerning LCA in Egypt. The covered areas of study were identified as well as the main gaps and challenges. Areas of concern and topic to be addressed were suggested for future studies in each study area. Improvement options for promoting LCA usage as a tool for sustainable development in Egypt were presented as well.

References

[1] ISO 14040, 2006. *Environmental Management - Life Cycle Assessment-Principles and Frameworks*. Geneva : International Organization for Standardizations.

[2] Udo de Haes, H.A., 1993. Applications of life cycle assessment : expectations, drawbacks and perspectives. *Journal of Cleaner Production* 1(3-4), 131-137.

[3] ISO 14041, 1998. *Environmental Management - Life cycle Assessment - Goal and Scope Definition and Inventory Analysis*. Geneva : International Organization for Standardizations.

[4] ISO 14042, 2000. *Environmental Management - Life cycle Assessment* - Life Cycle Impact Assessment. Geneva : International Organization for Standardizations.

[5] ISO 14043, 2000. Environmental Management - Life Cycle Assessment - Life cycle Interpretation. Geneva : International Organization for Standardizations.

[6] ISO 14044, 2006. Environmental Management - Life Cycle Assessment - Requirements and Guidelines. Geneva : International Organization for Standardizations.

[7] Hassaan, M.A., 2018. Using scholarly big data in assessing contribution of national expertise to climate change knowledge; case study: Egypt. *Journal of Data Analysis and Information Processing*, 6, 67-78.

[8] Akoka, J., Comyn-Wattiau, I. and Laoufi, N., 2017. Research on big data-a systematic mapping study. *Computer Standards and Interfaces*, 54, 105-115.

[9] Cohen, M., 2017. A systematic review of urban sustainability assessment literature. *Sustainability*, 9, 2048. https://doi.org/10.3390/su9112048

[10] Henriksson, P.J.G., Dickson, M.W., Nasr-allah, A.M., Al-Kenawy, D.A.R. and Phillips, M., 2015. *Life Cycle Assessment of Egyptian Tilapia Productio*n. [online] Avilable at : https://www.researchgate.net/publication/288486017_Life_cycle_assessment_of_Egyptian_tilapia_production

[11] Henriksson, P.J.G., Dickson, M., Nasr-Allah, A.M., Al-Kenawy, D.A.R. and Phillips, M., 2017. Benchmarking the environmental performance of best management practice and genetic improvements in Egyptian aquaculture using life cycle assessment. *Aquaculture*, 468 (1), 53-59.

[12] Dickson, M. and Henriksson, P., 2016. *A Life Cycle Assessment of the Environmental Impacts in the Egyptian Aquaculture Value Chain*. [online] Avilable at : https://cgspace.cgiar.org/handle/10568/78477

[13] Soliman, N.F. and Yacout, D.M.M., 2015. The prospects of analysing the environmental impacts of Egyptian aquaculture using cycle life assessment. *International Journal of Aquaculture*, 5(37), 1-9.

[14] Yacout, D.M.M., Soliman, N.F. and Yacout, M.M., 2016. Comparative life cycle assessment (LCA) of tilapia in two production systems. *The International Journal of Life Cycle Assessment*, 21(6), 806-819.

[15] AbdElghaffar, M.A.E., 2007. Life cycle assessment tools for maintenance management and resource conservation. *Assiut Universit Bullitin for Environmental Research,* 10(1) 73-83.

[16] Ali, A.A.M. and Negm, A.M., 2014. Environmental impacts assessment of the Egyptian brick types using life cycle assessment tool. *Energy Procedia*, 54, 260-269.

[17] Ali, A.A.M., Negm, A.M., Bady, F. and Ibrahim, M.G.E., 2014. Moving towards an Egyptian national life cycle inventory database. *The International Journal of Life Cycle Assessment*, 19 (8), 1551-1558.

[18] Ali, A.A.M., Negm, A., Bady, M. and Ibrahim, M.G.E., 2014. Towards an integrated tool to estimate carbon emissions from life cycle assessment of building materials in Egypt. *International Journal of Research in Engineering and Technology,* 2(3), 81-92.

[19] Ali, A.A.M., Negm, A., Bady, A. and Ibrahim, M.A.G., 2015. Environmental life cycle assessment of residential building in Egypt : a case study. *Procedia Technology*, 19, 349-356.

[20] Elshafei, G. and Negm, A., 2015. Life cycle assessment as a decision making for window performance comparison in green building design. *International Journal of Architectural and Environmental Engineering*, 9 (9), 1155-1163.

[21] Ali, A.A.M., Negm, A.M., Bady, A.F. and Ibrahim, A.G., 2016. Environmental impact assessment of the Egyptian cement industry based on a life-cycle assessment approach : a comparative study between Egyptian and Swiss plants. *Clean Technologies and Environmental Policy*, 18(4), 1053-1068.

[22] Ibrahim M., and Ali, A.A.M. 2017. Practical case study for life cycle assessment of the Egyptian brick industry: A comparative analysis of the Japanese industry. *(unpublished data).*

[23] Sharaan, M. and Negm, A., 2017. Life cycle assessment of dredged materials placement strategies: case study, Damietta port, Egypt. *Procedia Engineering*, 181, 102-108.

[24] Ali, A.A.M., Negm, A.M., Bady, M. and Ibrahim, M.G.E., 2014. Framework for application of life cycle assessment approach on Egyptian residential building case study : new Assiut city, Egypt. In: *ICIME 2014: International Conference in Integrated Management of Environment*, Hammamet, Tunisia.

[25] Ali, A.A.M., Negm, A.M., Bady, M. and Ibrahim, M.G.E., 2014. Effect of fuel type on the life cycle of Egyptian cement industry: environmental impact assessment approach. In: *The Asian Conference on Sustainability, Energy & the Environment,* Vol. 4. Osaka, Japan. https://doi.org/10.13140/2.1.4741.2801

[26] Ali, A.A.M., Negm, A.M. and Bady, M., 2014. Estimating carbon emissions from industrial process by using life cycle assessment tool. In: *IAC 2014: International Conference on Industry Academia Collaboration*, Cairo, Egypt.

[27] Elboshy, B., Negm, A., Gamaleldin, M. and Abdel-Fattah, S., 2017. Life cycle assessment for sidewalk pavement types, case study: extension of new Borg El-Arab city. *Procedia Engineering,* 181, 370-377.

[28] Ay-Eldeen, M.K. and Negm, A.M., 2015. Global warming potential impact due to pile foundation construction using life cycle assessment. *Engineering,* 20(12), 4413-4421.
[29] Marzouk, M. and Azab, S., 2017. Analyzing sustainability in low-income housing projects using system dynamics. Energy and Buildings, 134, 143-153.
[30] Younes, M., Huang, Y. and Hashim, I., 2016. Towards an integrated tool of a life cycle assessment for construction of asphalt pavements in Egypt. *Journal of Earth Sciences and Geotechnical Engineering*, 6(4), 377-388
[31] Azouz M., 2018. The future of green building materials in Egypt: A framework for action. *Proceedings of Science and Technolgy*, 1(1), 1-13. doi : 10.21625/resourceeedings.vlil.180.
[32] Elkafoury, A. and Negm, A., 2016. Assessment approach of life cycle of vehicles tyres on Egyptian road network. Periodica Polytechnica Transportation Engineering, 44(2), 75-79.
[33] Mahgoub, M.E.M., van der Steen, N.P., Abu-Zeid, K., and Vairavamoorthy, K., 2010. Towards sustainability in urban water: a life cycle analysis of the urban water system of Alexandria City, Egypt. Journal of Cleaner Production, 18 (10/11), 1100-1106.
[34] Roushdi M., El-Hawary, A. and Mahgoub, M., 2012. Environmental improvement of Alexandria's wastewater treatment plants using life cycle assessment approach. Global NEST Journal, 14(4), 450-459. https://doi.org/10.30955/gnj.000831
[35] Ghazy, M.R., Dockhorn, T. and Dichtl, N., 2011. Economic and environmental assessment of sewage sludge treatment processes applications in Egypt. International Water Technology, 1(2), 1-17.
[36] Awad, H., Alalm, M.G. and El-Etriby, H. Kh., 2019. Environmental and cost life cycle assessment of different alternatives for improvement of wastewater treatment plants in developing countries. *Science of the Total Environment*, 660 (10), 57-68.
[37] Yacout, D.M.M. and Hassouna, M.S., 2016. Identifying potential environmental impacts of waste handling strategies in textile industry. Environmental Monitoring and Assessment, 188, 445. https://doi.org/10.1007/s10661-016-5443-8
[38] Garas, G., Bakhoum, E. and Allam, M., 2016. Optimal use of selected waste materials in buildings. *Ecology, Environment and Conservation*, 22(3), 1129-1136.
[39] Hassanain, E.M., Yacout, D.M.M., Metwally, M.A. and Hassouna, M.S., 2017. Life cycle assessment of waste strategies for used lubricating oil. The International Journal of Life Cycle Assessment, 22, 232-1240.
[40] El Sebaie, O., Ahmed, M., Hussein, A., El Sharkawy, F. and Samy, M., 2006. Life cycle analysis of aluminum foil packaging material. *Journal of the Egyptian Public Health Association*, 81(3-4), 199-222.
[41] Yacout, D.M.M., Abd El-Kawi, M.A. and Hassouna, M.S., 2016. Cradle to gate environmental impact assessment of acrylic fiber manufacturing. *International Journal of Life Cycle Assessment*, 21(3), 326-336.
[42] Bevilacqua, M., Ciarapica, F. E., Mazzuto, G. and Paciarotti, C., 2014. Environmental analysis of a cotton yarn supply chain. *Journal of Cleaner Production*, 82, 154-165.
[43] Aly, E. A. and Managi, S., 2018. Energy infrastructure and their impacts on societies' capital assets: a hybrid simulation approach to inclusive wealth. *Energy Policy*, 121, 1-12.
[44] Shaaban, M., Scheffran, J., Böhner, J. and Elsobki, S.M., 2018. Sustainability assessment of electricity generation technologies in Egypt using multi-criteria decision analysis. *Energies*, 11(5), 1117. https://doi.org/10.3390/en11051117
[45] Armanuos, A.M., Negm, A. and Tahan, A. H. M. H. El. (2016). Life cycle Assessment of diesel fuel and solar pumps in operation stage for rice cultivation in Tanta, Nile Delta, Egypt. *Procedia Technology*, 22, 478-485.
[46] Menoufi, K., Chemisana, D. and Rosell, J.I. 2017. Life cycle assessment of a building added concentrating photovoltaic system (BACPV). *Energy Procedia*, 128, 194-201.

[47] Fawzy, M.M. and Romagnoli, F., 2016. Environmental life cycle assessment for Jatropha biodiesel in Egypt. *Energy Procedia*, 95, 124-131.
[48] Ismaeel, W.S.E. and Elsayed, M.A., 2018. The interplay of environmental assessment methods; characterising the institutional background in Egypt. *Journal of Environmental Assessment Policy and Management*, 20 (1). https://doi.org/10.1142/S1464333218500035
[49] Yacout, D.M.M., 2018. *Potential Applications of Life Cycle Assessment in Climate Change Arena*. ARCA Working Paper No. 7.
[50] McManus, M.C. and Taylor, C.M., 2015. The changing nature of life cycle assessment. *Biomass Bioenergy*, 82, 13-26.
[51] Baker, J.W. and Lepech, M., 2009. Treatment of uncertainties in life cycle assessment. *Proceedings of the 10th International Conference on Structural Safety and Reliability*, Osaka, Japan, September 13-17, 2009.

Mean and Variance Adjustment of the Average Control Chart by Shape Parameter Using Bayesian Estimation of the Inverse Gaussian Distribution

Kittisak Jangphanish*

Department of Mathematics, Faculty of Liberal Art, Rajamangala University of Technology Rattanakosin, Salaya Campus, Nakhon Pathom, Thailand

Received: 20 November 2018, Revised: 8 May 2019, Accepted: 25 May 2019

Abstract

This research aims to develop the average control chart ($\bar{x}-chart$) using the shape parameter of the Inverse Gaussian Distribution by Bayesian Estimation for estimating mean and variance, and to compare the process potential capability (C_p) and the actual process capability index (C_{pk}) for Monte Carlo simulation with $10{,}000$ replications assuming that the specification is ± 0.001. The result shows that the process potential capability (C_p) and the actual process capability index (C_{pk}) of the Adjusted $\bar{x}-chart$ using Bayesian Estimation of the shape parameter of the Inverse Gaussian Distribution for estimating mean and variance have more capability than the $\bar{x}-chart$ under the normal distribution when the sample size is less than 30. For the sample size of 30, the two control charts have the indifferent capability process.

Keywords: Adjusted $\bar{x}-chart$, Bayesian Estimation, shape parameter, Inverse Gaussian Distribution
DOI 10.14456/cast.2019.16

1. Introduction

Statistical Process Control is a critical tool in maintaining the quality of products and services in the new manufacturing process to meet the standards that manufacturers and consumers require. It is the highest satisfaction for the products and services in order to maximize profits in the long run. This will result in the company to be able to continue its quality control. Statistical methods are used to calculate and apply the results for decision-making in relation to the quality of products in various areas such as the development of products to meet the standards of the manufacturer itself and the development of product standards to have equivalent level to other manufacturers in the market [1].

The most widely used instrument for statistical quality control is a control chart that applies the attribute data such as p- chart and np- chart to estimate mean and variance under assumption of the data with Binomial distribution. For the variable data, the control charts, like

*Corresponding author: Tel.: 02-4416083, 0863623508
E-mail: kittisak.jang@rmutr.ac.th, kittisakaj1986@gmail.com

$\bar{x}-chart$, R-chart are used. Estimating mean and variance under the assumptions have a normal distribution [2-3].

The attribute control chart has broadly been developed. Quesenberry [4] proposed a Q Chart for binomial random variables for controlling the proportion of waste in the process. Khoo [5] offered a control chart for moving averages. De Oliveira *et al*. [6] and Ryand and Schwertman [7] proposed beta control chart. Their results showed that the Q control chart has more efficiency than the control chart controlling the proportion of waste in the process.

Moreover, Rungruang [8] compared the efficiency of 3 control charts which are beta, moving average and the queue control chart. When the data has a binomial distribution in the parameters n and p, the criteria used to compare the efficiency of the control chart is the average run length (ARL) of 240 simulating situations with replication of 10,000 times by Monte Carlo technique. It was found that when the process was under the moving averages and queue control charts, it was equally efficient without process control. For the beta control charts, it was more efficient in case of less number of waste with small variation. On the other hand, the moving average control chart was more efficient in case of large number of waste with large variation at all levels of sample size.

For the variable data, the widely used control charts are $\bar{x}-chart$, R-chart to estimate mean and variance under the assumption of normal distribution. If the data is not normal distribution, the normal distribution in estimating mean and variance for controlling in the upper limit (UCL) and lower limit (LCL) will lead to high error of the estimations. So, we apply the shape parameter (α) of the Inverse Gaussian Distribution by Bayesian estimation for adjusted mean and variation in average control chart ($\bar{x}-chart$). Moreover, we compare the process potential capability (C_p) and the actual process capability index (C_{pk}) for Monte Carlo simulation with 10,000 replications.

2. Materials and Methods

The Inverse Gaussian Distribution has right distribution (Figure 1). The probability density function is:

$$f_{IG}(x:\alpha,\beta)=\sqrt{\frac{\beta}{2\pi}}x^{-\frac{3}{2}}\exp\{\frac{\beta(x-\alpha)^2}{2\alpha^2 x}\},\ x>0 \tag{1}$$

where α is the shape parameter ($E(X)=\alpha$) and β is the scale parameter [9].

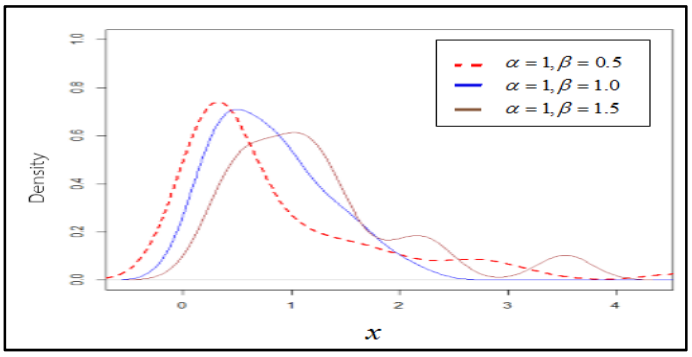

Figure 1 Probability density function of the Inverse Gaussian

The estimation of the shape parameter (α) of the Inverse Gaussian Distribution by Bayesian estimation using Weibull as prior distribution can be derived as:

$$h_{WB}(\alpha,\beta \mid x_1,x_2,...,x_n) = \frac{L_{IG}(x:\alpha,\beta)g_{WB}(\alpha,\beta)}{\int_0^\infty\int_0^\infty L_{IG}(x:\alpha,\beta)g_{WB}(\alpha,\beta)d\alpha d\beta} \quad (2)$$

Where $h_{WB}(\alpha,\beta \mid x_1,x_2,...,x_n)$ is posterior distribution,

$L_{IG}(x:\alpha,\beta)$ is likelihood function,

$g(\alpha,\beta)$ is Weibull prior distribution, The probability density function is as:

$$g_{WB}(\alpha,\beta) = \alpha\beta x^{\alpha-1}e^{\{-\beta x^\alpha\}},\ x>0,\alpha>0,\beta>0 \quad (3)$$

The expectation of the parameter α is as:

$$\hat{\alpha}_{WB} = E(\alpha \mid x_1,...,x_n) \quad (4)$$

$$\hat{\alpha}_{WB} = \int_0^\infty \alpha.h_{WB}(\alpha,\beta \mid x_1,x_2,...,x_n)d\alpha \text{ [10].} \quad (5)$$

The (5) equation is not integral in close form so we cannot find the posterior distribution. We use Lindley's Approximation [11] within square error loss, the equation for approximation is as:

$$\hat{\alpha}_{WB} = \hat{\alpha}_{MLE} + \frac{1}{2}(\theta_2 + 2\theta_1\rho_1)\sigma^2 + \frac{1}{2}l_3\theta_1\sigma^4 \quad (6)$$

Where θ_1 is the first Derivative of α by α

θ_2 is the second Derivative of α by α

ρ is natural Logarithm of Weibull Prior Distribution

ρ_1 is the first Derivative of ρ by α

l is natural Logarithm of Inverse Gaussian Distribution Function by α

l_2 is the second Derivative of l Function by α

l_3 is the third Derivative of l Function by α

$\sigma^2 = \frac{(-1)}{l_2}$,

So

$$\hat{\alpha}_{WB} \approx \hat{\alpha}_{MLE} + \rho_1\sigma^2 + \frac{1}{2}l_3\sigma^4\hat{\alpha}_{WB} \quad (7)$$

$$\hat{\alpha}_{WB} \approx \hat{\alpha}_{MLE} + \left(\frac{1}{\frac{3\hat{\beta}_{MLE}\sum_{i=1}^{n} x_i}{(\hat{\alpha}_{MLE})^4} - \frac{2n\hat{\beta}_{MLE}}{(\hat{\alpha}_{MLE})^3}}\right)\left(\left(\frac{n}{\hat{\alpha}_{MLE}} + \sum_{i=1}^{n}\ln x_i - \hat{\beta}_{MLE}\sum_{i=1}^{n} x^{\alpha}\ln x_i\right) + \left(\frac{6\hat{\beta}_{MLE}\sum_{i=1}^{n} x_i}{(\hat{\alpha}_{MLE})^5}\right.\right. \tag{8}$$

$$\left.\left. - \frac{3n\hat{\beta}_{MLE}}{(\hat{\alpha}_{MLE})^4}\right)\left(\frac{1}{\frac{3\hat{\beta}_{MLE}\sum_{i=1}^{n} x_i}{(\hat{\alpha}_{MLE})^4} - \frac{2n\hat{\beta}_{MLE}}{(\hat{\alpha}_{MLE})^3}}\right)\right)$$

where $\hat{\alpha}_{MLE} = \overline{X}$ and $\hat{\beta}_{MLE} = \frac{n}{\sum_{i=1}^{n}\left(\frac{1}{X_i} - \frac{1}{\overline{X}}\right)}$ [12]

The variance of the shape parameter (α) has the following formula

$$Var(\hat{\alpha}_{WB}) = \frac{\sum_{i=1}^{n}(\hat{\alpha}_{(WB)_i} - \overline{\alpha}_{WB})^2}{n-1} \tag{9}$$

We obtained the estimator of mean and variance of the shape parameter in the Inverse Gaussian Distribution. We adjusted mean and variance of the formula of average control chart ($\overline{x}-chart$). The formula of $\overline{x}-chart$ is as:

$$UCL = \overline{\overline{X}} + 3\frac{\sigma}{\sqrt{n}} \tag{10}$$

$$CL = \overline{\overline{X}} \tag{11}$$

$$LCL = \overline{\overline{X}} - 3\frac{\sigma}{\sqrt{n}} \tag{12}$$

When $\overline{\overline{X}} = \frac{\sum_{i=1}^{n} X_i}{n}$ and $\sigma = \sqrt{\frac{\sum_{i=1}^{N}(X-\mu)^2}{N}}$

Then, we replaced $\overline{\overline{X}} = \hat{\alpha}_{WB}$ and $\sigma = \sqrt{Var(\hat{\alpha}_{WB})}$

The formula of the adjusted $\overline{x}-chart$ is as :

$$UCL = \hat{\alpha}_{WB} + 3\frac{\sqrt{Var(\hat{\alpha}_{WB})}}{\sqrt{n}} \tag{13}$$

$$CL = \hat{\alpha}_{WB} \tag{14}$$

$$LCL = \hat{\alpha}_{WB} - 3\frac{\sqrt{Var(\hat{\alpha}_{WB})}}{\sqrt{n}} \tag{15}$$

So, we calculate the process potential capability (C_p) and actual process capability index (C_{pk}) with in assume that the specification is ± 0.001. The formula of the process potential capability (C_p) is as :

$$C_p = \frac{USL - LSL}{UCL - LCL} \tag{16}$$

where $USL =$ upper specification limit
$LSL = lower$ specification limit

For the actual process capability index (C_{pk}) the formula is as :

$$C_{pk} = \min(C_{pu}, C_{pl}) \tag{17}$$

Where $C_{pu} = \frac{USL - \overline{\overline{X}}}{3\sigma}$,

$C_{pl} = \frac{\overline{\overline{X}} - LSL}{3\sigma}$ [13].

C_p = Process Capability. A simple and straightforward indicator of process capability.
C_{pk} = Process Capability Index. Adjustment of C_p for the effect of non-centered distribution.

Afterwards, simulation in R program was implemented supposing that $\alpha = 0.01, 0.02, 0.03, 0.04, 0.05$ (the Copper plating process in Gravure Printing was stopped when the values exceed), $n = 5, 10, 15, 20, 25, 30$ for 10,000 replications and calculating the process potential capability (C_p) and the actual process capability index (C_{pk}), assuming that specification is ± 0.001 because this can be accepted by customers. The criteria of C_p and C_{pk} are not less than 1 for the process ability to be accepted (ISO/TS 16949).

3. Results

The simulation was computed by Monte Carlo from 30 situations (α = 0.01, 0.02, 0.03, 0.04, 0.05 and n = 5, 10, 15, 20, 25, 30) with R Program of 10,000 replications in specification ± 0.001. Furthermore, the process potential capability (C_p) and the actual process capability index (C_{pk}) of the average control chart ($\bar{x} - chart$) under normal distribution and adjusted

average control chart (Adjusted $\bar{x}-chart$) under Inverse Gaussian Distribution with shape parameter (α) were calculated. The results were as follows:

In case of $n=5$, the Adjusted $\bar{x}-chart$ has more capability in process than the $\bar{x}-chart$ in customer requirement in parameter $\alpha=0.04$ ($C_p=1.63$, $C_{pk}=1.47$) and $\alpha=0.05$ ($C_p=1.76$, $C_{pk}=1.22$) but the $\bar{x}-chart$ has no capability in process for customer requirement.

In case of $n=10$, the Adjusted $\bar{x}-chart$ has more capability in process than the $\bar{x}-chart$ in customer requirement in parameter $\alpha=0.01,0.02,0.03,0.04,0.05$ (all situations) and the $\bar{x}-chart$ has capability in process for customer requirement in parameter $\alpha=0.01$ ($C_p=1.53$, $C_{pk}=1.25$) but the other case of the $\bar{x}-chart$ has no capability in process for customer requirement.

In case of $n=15$, the Adjusted $\bar{x}-chart$ has more capability in process than the $\bar{x}-chart$ for customer requirement in parameter $\alpha=0.01$ ($C_p=1.30$, $C_{pk}=1.23$), $\alpha=0.02$ ($C_p=1.45$, $C_{pk}=1.32$) and $\alpha=0.03$ ($C_p=1.73$, $C_{pk}=1.34$) but the $\bar{x}-chart$ has capability in process for customer requirement in parameter $\alpha=0.01$ $C_p=1.25$, $C_{pk}=1.13$) and $\alpha=0.02$ ($C_p=1.78$, $C_{pk}=1.56$).

In case of $n=20$, the Adjusted $\bar{x}-chart$ has more capability in process than the $\bar{x}-chart$ for customer requirement in parameter $\alpha=0.01,0.02,0.03,0.04,0.05$ (all situations), but the $\bar{x}-chart$ has capability in process for customer requirement in parameter $\alpha=0.01$ ($C_p=1.17$, $C_{pk}=1.01$), $\alpha=0.03$ ($C_p=1.79$, $C_{pk}=1.35$) and $\alpha=0.04$ ($C_p=1.87$, $C_{pk}=1.42$).

In case of $n=25$, the Adjusted $\bar{x}-chart$ has more capability in process than the $\bar{x}-chart$ for customer requirement in parameter $\alpha=0.01$ ($C_p=1.70$, $C_{pk}=1.35$) and $\alpha=0.02$ ($C_p=1.76$, $C_{pk}=1.36$) but the $\bar{x}-chart$ has capability in process for customer requirement in parameter $\alpha=0.04$ ($C_p=1.80$, $C_{pk}=1.55$) and $\alpha=0.05$ ($C_p=1.89$, $C_{pk}=1.40$).

In case of $n=30$, the Adjusted $\bar{x}-chart$ and the $\bar{x}-chart$ have capability in process for customer requirement in all situations (Table 1 and Figure 2).

Table 1. Situations for comparing C_p, C_{pk} in $\bar{x}-chart$ and Adjusted $\bar{x}-chart$.

Situations		Type of Control Chart			
		$\bar{x}-chart$		Adjusted $\bar{x}-chart$	
n	α	C_p	C_{pk}	C_p	C_{pk}
5	0.01	0.85	0.72	0.82	0.97
	0.02	0.87	0.73	0.78	0.88
	0.03	0.75	0.66	0.78	0.67
	0.04	0.93	0.85	1.63**	1.47**
	0.05	0.98	0.86	1.76**	1.22**
10	0.01	1.53**	1.25**	1.84**	1.47**
	0.02	0.98	0.87	1.75**	1.39**
	0.03	0.79	0.75	1.85**	1.42**
	0.04	0.87	0.82	1.77**	1.32**
	0.05	0.98	0.85	1.89**	1.38**
15	0.01	1.25**	1.13**	1.30**	1.23**
	0.02	1.78**	1.56**	1.45**	1.32**
	0.03	0.99	0.92	1.73**	1.34**
	0.04	0.87	0.75	0.85	0.76
	0.05	0.78	0.63	0.94	0.75
20	0.01	1.17**	1.01**	1.87**	1.47**
	0.02	0.96	0.88	1.95**	1.52**
	0.03	1.79**	1.35**	1.89**	1.49**
	0.04	1.87**	1.42**	1.67**	1.34**
	0.05	1.88**	1.39**	1.60**	1.32**
25	0.01	0.68	0.40	1.70**	1.35**
	0.02	0.76	0.55	1.76**	1.36**
	0.03	0.79	0.60	0.89	0.45
	0.04	1.80**	1.55**	0.93	0.56
	0.05	1.89**	1.40**	0.78	0.44
30	0.01	1.87**	1.45**	1.79**	1.45**
	0.02	1.95**	1.37**	1.70**	1.44**
	0.03	1.88**	1.36**	1.95**	1.67**
	0.04	1.75**	1.32**	1.99**	1.70**
	0.05	1.78**	1.36**	1.59**	1.23**

** $C_p, C_{pk} > 1$, the capability in process is in customer requirement (ISO/TS 16949)

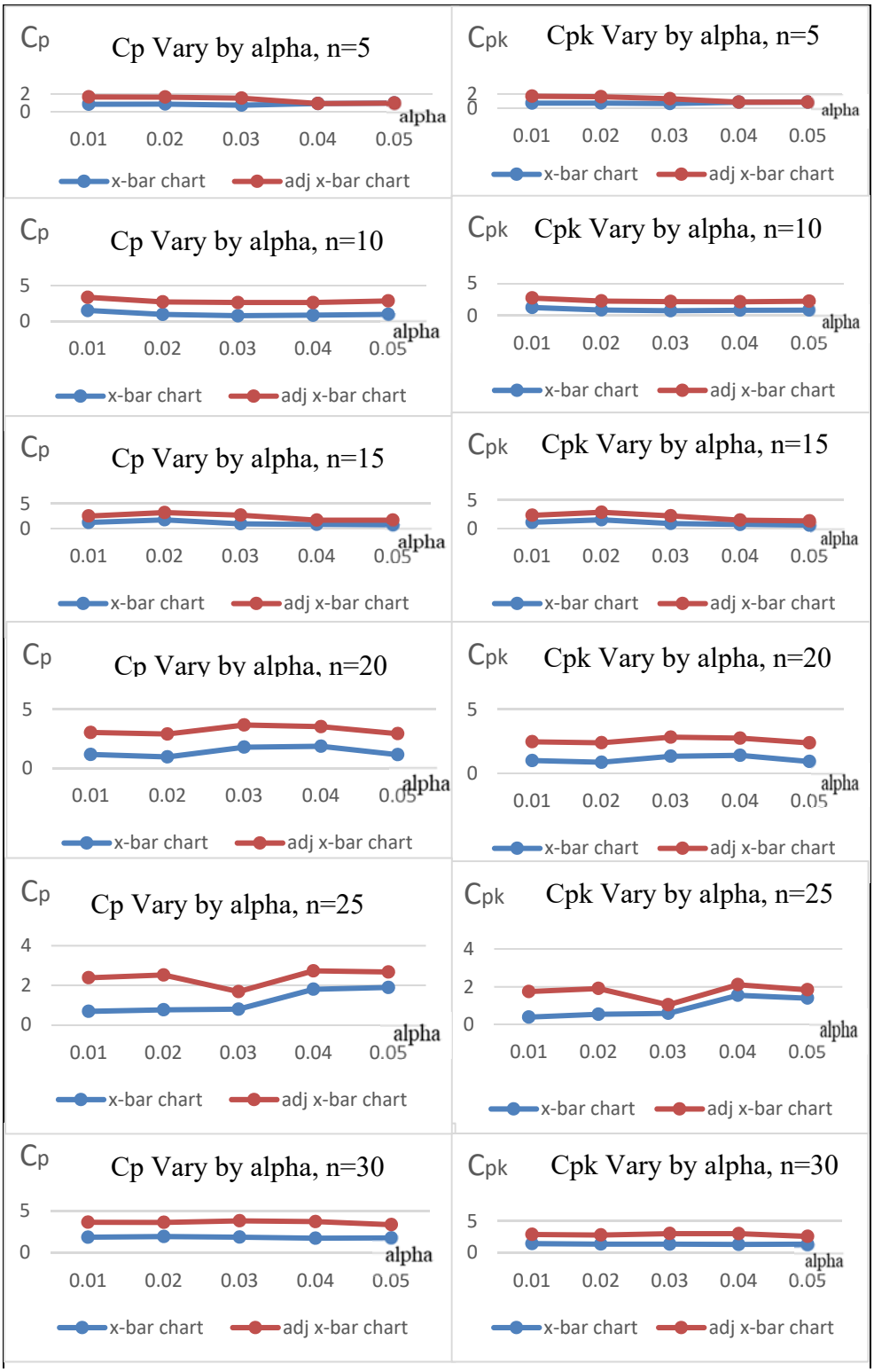

Figure 2. C_p, C_{pk}, $\alpha = 0.01, 0.02, 0.03, 0.04, 0.05$ and $n = 5, 10, 15, 20, 25, 30$

4. Conclusions

The process potential capability (C_p) and the actual process capability index (C_{pk}) of the average control chart ($\bar{x}-chart$) and the Adjusted control chart (Adjusted $\bar{x}-chart$) show that when the sample size is 5-25, the process potential capability (C_p) and actual process capability index (C_{pk}) of the Adjusted control chart (Adjusted $\bar{x}-chart$) have more capability in process for customer requirement than the average control chart ($\bar{x}-chart$). Moreover, when the sample size is 30, the process for customer requirement is capable of both control charts. For the shape parameter supposing that the simulation for Copper plating process in Gravure Printing (α = 0.01, 0.02, 0.03, 0.04, 0.05), it was found that the parameter is small. Further investigation shoud be done by Adjusted $\bar{x}-chart$ in situations of the big shape parameter. For the shape parameter (α), the Bayesian estimated in the Inverse Gaussian Distribution using the Weibull as prior distribution was more efficient when the sample size was small. The approximation of the shape parameters is impossible to find the formulas in the form of closed form. Therefore, Lindley's Approximation technique is consistent [10]. It can be concluded that the shape parameter of the Inverse Gaussian using Weibull as prior distribution has more efficiency than using Gamma as prior distribution in case of small sample size.

5. Acknowledgements

We would like to thank Rajamangala University of Technology Rattanakosin for financial support.

References

[1] Sant'Anna, Â.M.O. and ten Caten, C.S., 2012. Beta control charts for monitoring fraction data. *Expert Systems with Applications*, 39(11), 10236-10243.
[2] Cooper, R. And Van Vliet, B., 2012. Whole distribution statistical process control in high frequency trading. *Journal of Trading*, 7(2). 1-23.
[3] Hoyle, D., 2017. *ISO 9000 Quality Systems Handbook-updated for the ISO 9001: 2015 Standard: Increasing the Quality of an Organization's Outputs*. London: Routledge.
[4] Quesenberry, C.P.,1997. *SPC Methods for Quality Improvement*. New York : Wiley.
[5] Khoo, M.B., 2004. A moving average control chart for monitoring the fraction non-conforming. *Quality and Reliability Engineering International*, 20(6), 617-635.
[6] De Oliveira, G.S., Knautz, J.S., Sherwani, S. and McCarthy, R.J., 2012. Systemic magnesium to reduce postoperative arrhythmias after coronary artery bypass graft surgery: a meta-analysis of randomized controlled trials. *Journal of Cardiothoracic and Vascular Anesthesia*, 26(4), 643-650.
[7] Ryan, T.P. and Schwertman, N.C., 1997. Optimal limits for attributes control charts. *Journal of Quality Technology*, 29(1), 86-98.
[8] Rungruang, S., 2013. An efficiency comparison of fraction nonconforming control charts. *Veridian E-Journal*, 6(3), 860-876.
[9] Chhikara, R.S. and Folks, J.L., 1977. The Inverse Gaussian distribution as a lifetime model. *Technometrics*, 19(4), 461-468.

[10] Samaniego, F.J. , 2010. *A Comparison of the Bayesian and Frequentist Approaches to Estimation*. New York: Springer Science & Business Media.
[11] Lindley, D.V. , 1980. Approximate Bayesian methods. *Trabajos de Estadística Y de Investigación Operativa*, 31(1), 223-245.
[12] Jangphanish, K. and Kornpetpranee, S. , 2016. Monte Carlo simulation for comparing the parameters Inverse Gaussian Distributions estimated by Bayesian Estimation using Gamma and Weibull Prior Distribution. *KKU Science Journal*,45(1), 200-213.
[13] AIAG, 2005. *Statistical Process Control*. 2nd ed. (Thai Edition). Daimler Chrysler, Ford Motor Company and General Motors Corporation, pp. 72-102.

Instructions for Authors

Current Applied Science and Technology journal contains research reports, articles concerning development work, reviews of the literature and research activities. The objectives are to publish and promote research contributions and innovative work in fields associated with applied science and technology. An electronic journal is provided on the website (https://www.tci-thaijo.org/index.php/cast/index). The Editors reserve the right to require revision of the submitted manuscript as a condition for final acceptance.

The institute and the editorial board claim no responsibility for the contents or views expressed by the authors of individual articles. Copying is allowed provided that acknowledgement is made. All articles submitted for publication will be assessed by a group of distinguished.

Ethics:

The journal is committed to maintaining the high level of integrity in the content published and has a Conflict of Interest policy in place. The journal uses plagiarism detection software to screen the submissions. If plagiarism is found, the COPE guidelines on plagiarism will be followed. For more details, please see https://www.tci-thaijo.org/index.php/cast/navigationMenu/view/Publication_Ethics.

Page Charge: Free

Submission of Manuscripts:

Manuscripts must be written in English and submitted online. Manuscripts are to be reviewed (double blinded) by at least 3 referees specializing in relevant fields. Revised manuscripts have to be sent online.

All manuscripts should be submitted to: https://www.tci-thaijo.org/index.php/cast/index

Contact:

Editor of Current Applied Science and Technology
King Mongkut's Institute of Technology Ladkrabang
1 Soi Chalongkrung 1, Ladkrabang District,
Bangkok 10520, Thailand
Tel: 662-329-8136
Fax: 662-329-8221
Email: cast@kmitl.ac.th

Manuscript Preparation Guide:

General: Manuscripts must be typewritten using *Microsoft Word for Windows,* single-spaced with margin set-up (in page set up menu) as follows (see also the document template):

Top Margin 1.5"	Bottom Margin 1.5"
Left Margin 1.5"	Right Margin 1.5"

Good quality printouts using A4 paper size are required. Format should be a single column. Times New Roman font type is required. Font sizes for various text functions are as follows:

Text functions	Size *	Typeface
Title	14 (CT)	Bold
Author and co-authors	11 (CT)	Normal
Address for correspondence	11 (CT)	Normal
Abstract and main text	10 (LJ)	Normal
Section heading and number including "Abstract", "Acknowledgement", "References"	12 (CT)	Bold
Subsection heading and number	11 (LJ)	Bold

* CT = Center Text, LJ = Left Justified.

The corresponding author should be noted (included a Fax number and E-mail address) and indicated with an asterisk. Full postal addresses must be given for all co-authors, keyed to names (if required) by superscripted Arabic numbers.

Paper Length: Should not normally exceed 10 pages including figures and tables
Spelling: American English
Abstract: Should not exceed 250 words
Keywords: Should not exceed 8 keywords
Text: Authors are requested to use the following order when typing:-

All research reports (Full Length or Short Reports): Title, Authors, Affiliations, Abstract, Keywords, Introduction (in reserch papers this must be confined to relevant matters, and must not be a general review of cognate literature), Materials and Methods, Results and Discussion, Conclusions, Acknowledgements, References.

Reviews and Discussion Papers will be considered in any format appropriate to the purposes of the authors, although adherence to the general guidelines described above is encouraged.

Line Art Figures: Figures can be drawn using several packages such as Win Draw®, Auto CAD®, Corel Draw®, VISIO® etc.

Photographs: Actual size photographs are acceptable. However, they can also be put into a text stream using a good-resolution scanner. All photographs must be clear when printed in monochrome.

Graphs: Several packages available today can produce attractive and professional graph presentation. Some also provide curve-fitting function, which can be useful. However, two-dimensional bar charts are preferred. All graphs must be clear in monochrome printing.
Equations and complex expressions: Math CAD®, Math Writer® and Equation Editor® (included in Microsoft Word®) are acceptable for presentation of this type of material.

Citations: Citations in the text should be denoted by numbers between square brackets (i.e. [1, 2], [1-3], [1, 3-8]…) *in the order of first appearance in the text.*

References: References should be numbered to correspond with the text citations. References must be arranged as follows:

Books

Authors, Initials., Year. *Title of Book.* Edition. (only include this if not the first edition) Place: Publisher.

Example:

[1] Barker, R., Kirk, J. and Munday, R.J., 1988. *Narrative Analysis*. 3rd ed. Bloomington: Indiana University Press.

Chapters of edited books

Chapter authors' surname(s), initials., Year of book. Title of chapter. In**:** Book editor(s) initials. surnames, ed. or eds. *Title of Book*. Place of publication: Publisher. Chapter number or first and last page numbers.

Example:

[2] Samson, C., 1970. Problems of information studies in history. In: S. Stone, ed. *Humanities Information Research*. Sheffield: CRUS, pp. 44-68.

E-books

Author, Year, *Title of Book*. [e-book] Place of publication: Publisher. Available through: include e-book source/database, web address or URL.

Example:

[3] Carlsen, J. and Charters, S., eds. 2007. *Global Wine Tourism*.[e-book] Wallingford: CABI Pub. Available through: Anglia Ruskin University Library website <www.libweb.anglia.ac.uk>.

Journal articles

Author, Initials., Year. Title of article. *Full Title of Journal,* Volume number (Issue number), Page numbers.

Example:

[4] Ross, A.B., Junyapoon, S., Jones, J.M., Williams, A. and Bartle, K.D., 2005. A study of different soots using pyrolysis–GC–MS and comparison with solvent extractable material. *Journal of Analytical and Applied Pyrolysis*, 74(1-2), 494-501.

Proceedings

Author, Initials., Year. Title of article. *Full Title of Proceedings*, Place of Conference, Date, page

Example:

[5] Thanaboripat, D., Ruangrattanametee, V. and Srikitkademwat, K., 2010. Control of growth and aflatoxin production of aflatoxin producing fungi in corn by salts. *Proceeding of the 8th International Symposium on Biocontrol and Biotechnology*, Pattaya, Thailand, October 4-6, 2010, 283-289.

Patent

Inventor name, Initial(s)., Assignee., Year. *Title*. Place. Patent number (status, if an application).

Example:

[6] Leonard, Y., Super Sports Limited., 2008. *Tin Can Manufacture and Method of Sealing*. Canada. Pat. 12,789, 675.

Dissertation
Author, Year of publication. *Title of Dissertation*. Level. Official name of University.
Example:
[7] Richmond, J., 2005. *Customer Expectations in the World of Electronic Banking: a Case Study of the Bank of Britain.* Ph.D. Anglia Ruskin University.

Websites
Authorship or Source, Year. *Title of document*. [online] Available at: include web site address/URL (Uniform Resource Locator).
Example:
[8] NHS Evidence, 2003. *National Library of Guidelines*. [online] Available at: http://www.library.nhs.uk/guidelines

Acknowledgements: These should be as brief as possible.

Proofs:

Proofs will be sent to the corresponding author and *must* be returned as soon as possible. Corrections should be restricted to typesetting errors.

Copyright:

The author(s) transfer(s) the copyright of the article to Current Applied Science and Technology effective if and when the article is accepted for publication.

Page Numbering:

All pages must be sequentially numbered, preferably by using the automatic page numbering function on your computer.

Copyright Material:

It is the authors' responsibility to obtain written permission from the copyright holder (usually the book or journal publisher) to use copyright material, and to send a copy of this consent with the manuscript. This consent is not normally denied but it is an international legal requirement that it be obtained.

Note:

Please note that authors are urged to check their proofs carefully before returning, since the inclusion of late corrections cannot be guaranteed.

Author(s) are responsible for ensuring that the submitted manuscript fully meets the requirements specified in the above Instructions. Manuscripts which fail to do so will be returned unedited to the Author(s) for correction in accordance with the above requirements, before they can be submitted to the processes of Referee evaluation.

1.5 ”

TEMPLATE

Enter title here (14 PT type size, Title Case, Bold, Centered)

Author Information entered here:
Name (in full)

Affiliation
City
Country
(11 pt type size, upper and lower case, centered under the title)

How to Use This Document Template

Insert the information in your document in place of the text here. For the body of your document, use Times New Roman 10 pt. Font, upper and lower case, double-spaced. Allow an extra half space above a line containing superscripts and/or below a line containing subscripts. The whole text should be left-justified. The headings should be 12 pt size, uppercase, bold and centered.

1.5” **Abstract (12pt)** 1.5”

Maximum 250 words here. (10 pt)

.....
.....
.....
.....
.....

Keywords: (10 pt)

Maximum of 8 words

*Corresponding author: Tel.: ……..... Fax: …….
E-mail: ……

1. Introduction (12 pt)

Clearly explain the nature of the problem, previous work, purpose, and contribution of the paper (10 pt).

.....
.....
.....
.....
.....

2. Materials and Methods (12 pt)

.....
.....
.....
.....

3. Results and Discussion (12 pt)

.....
.....…

4. Conclusions (12 pt)

Clearly indicate advantages, limitations and possible applications (10 pt).

.....
.....

5. Acknowledgements (12 pt)

A brief acknowledgement section may be included here (10 pt).

.....
.....

References (12 pt)

References must be numbered in the order cited in the manuscript and indicated in the text by a number in square brackets (e.g. [1, 2]) (10 pt).

Example of References must be arranged as follows:

[1] Barker, R. Kirk, J. and Munday, R.J., 1988. *Narrative Analysis*. 3rd ed. Bloomington: Indiana University Press.

[2] Samson, C., 1970. Problems of information studies in history. In: S. Stone, ed. *Humanities Information Research*. Sheffield: CRUS, pp. 44-68.

[3] Carlsen, J. and Charters, S., 2007. *Global Wine Tourism*. [e-book] Wallingford: CABI Pub. Available through: Anglia Ruskin University Library website <www.libweb.anglia.ac.uk>.

[4] Ross, A.B., Junyapoon, S., Jones, J.M., Williams, A. and Bartle, K.D., 2005. A study of different soots using pyrolysis–GC–MS and comparison with solvent extractable material. *Journal of Analytical and Applied Pyrolysis*, 74(1-2), 494-501.

[5] Thanaboripat, D., Ruangrattanametee, V. and Srikitkademwat, K., 2010. Control of growth and aflatoxin production of aflatoxin producing fungi in corn by salts. *Proceeding of the 8th International Symposium on Biocontrol and Biotechnology*, Pattaya, Thailand, October 4-6, 2010, 283-289.

[6] Leonard, Y., Super Sports Limited., 2008. *Tin Can Manufacture and Method of Sealing*. Canada. Pat. 12,789, 675.

[7] Richmond, J., 2005. *Customer Expectations in the World of Electronic Banking: a Case Study of the Bank of Britain*. Ph.D. Anglia Ruskin University.

[8] NHS Evidence, 2003. *National Library of Guidelines*. [online] Available at: http://www.library.nhs.uk/guidelines

Note:

Tables and Graphs: Minimum of 10 pt type size, all captions should be upper and lower case, centered. Each table and figure must be on a separate page (or pages if required), ***and must be embedded in the text.***

Illustrations and Photographs: Halftones, minimum of 10 pt type size, bold, captions should be in upper and lower case, centered. Images must be computer-designed with clearly visibility.

Contact

Editor of Current Applied Science and Technology
King Mongkut's Institute of Technology Ladkrabang
1 Soi Chalongkrung 1, Ladkrabang District
Bangkok 10520, Thailand
Tel: 662-329-8136 Fax: 662-329-8221
E-mail: cast@kmitl.ac.th
Website: https://www.tci-thaijo.org/index.php/cast/index

KING MONGKUT'S INSTITUTE OF TECHNOLOGY LADKRABANG
1 Soi Chalongkrung 1, Ladkrabang District Bangkok 10520, Thailand
Tel: 662-329-8136 Fax: 662-329-8221
E-mail: cast@kmitl.ac.th
Website: https://www.tci-thaijo.org/index.php/cast/index